

ACCURACY AND STABILITY IMPROVEMENTS IN  
ELECTROMAGNETIC SIMULATIONS  
OF POWER TRANSMISSION LINES AND CABLES

by

H.M.J.S.P. DE SILVA

A thesis  
presented to the University of Manitoba  
in fulfillment of the  
thesis requirement for the degree of  
Doctor of Philosophy

The Department of Electrical and Computer Engineering  
University of Manitoba  
Winnipeg, Manitoba, Canada

©(Jeewantha) 2008

**THE UNIVERSITY OF MANITOBA**  
**FACULTY OF GRADUATE STUDIES**  
\*\*\*\*\*  
**COPYRIGHT PERMISSION**

**Accuracy and Stability Improvements in the Electromagnetic Simulations of Power  
Transmission Lines and Cables**

**BY**

**H.M.J.S.P. De Silva**

**A Thesis/Practicum submitted to the Faculty of Graduate Studies of The University of**

**Manitoba in partial fulfillment of the requirement of the degree**

**Of**

**Doctor of Philosophy**

**H.M.J.S.P. De Silva © 2008**

**Permission has been granted to the University of Manitoba Libraries to lend a copy of this  
thesis/practicum, to Library and Archives Canada (LAC) to lend a copy of this  
thesis/practicum, and to LAC's agent (UMI/ProQuest) to microfilm, sell copies and to  
publish an abstract of this thesis/practicum.**

**This reproduction or copy of this thesis has been made available by authority of the  
copyright owner solely for the purpose of private study and research, and may only be  
reproduced and copied as permitted by copyright laws or with express written  
authorization from the copyright owner.**

## **Author's Declaration**

I hereby declare that I am the sole author of this thesis. This is a true copy of the thesis, including any required final revisions, as accepted by my examiners. I understand that my thesis may be made electronically available to the public.

## Abstract

This report proposes several techniques to improve the accuracy and the stability of electromagnetic transient simulations of transmission lines. An improved transmission line model (mesh domain model) is proposed to simulate transients in underground cable systems accurately considering frequency dependent effects. One advantage of this approach is that the resulting transformation matrix between phase and mesh domain is frequency independent. The mesh currents and voltages in co-axial cables are naturally decoupled at high frequencies hence the propagation function shows relatively smooth behaviour. Compared with basic phase domain methods, the rational function approximation and transportation delay estimation are relatively easier in mesh domain method. Two approaches are introduced to enhance the accuracy at low frequencies for HVDC overhead lines and underground cables by modifying the form of the fitted function. In the first approach, a suitable low frequency pole is added to the existing fitted function. The pole is carefully selected such that the resulting function gives correct dc value and the other high frequency response is changed insignificantly. In the second approach (Modified Functional Form method), the functional form of the fitted function is reformulated so that the modified function gives theoretical dc values at zero Hertz. A robust passivity enforcement algorithm is proposed to impose passivity on a non-passive transmission line model. The proposed, two-step method can be applied to detailed phase domain models, such as the Universal Line Model. This enforcement algorithm first uses a modified functional form method to remove large passivity violations, which are usually present at low frequencies. Then a constrained least squares method is employed to perturb diagonal elements of the propagation matrix or characteristic admittance eliminating any small passivity violations. The time domain simulations were validated using Numerical Inverse Laplace Transform method.



## **Acknowledgements**

I am grateful to Dr. Ani Gole for being my supervisor, his encouragement and his expert ideas in this research work. I would like to express my sincere gratitude to Prof. Wedepohl for his immense support given to me in understanding and developing accurate time domain cable model. Also I would like to thank John Nordstrom, Rohitha Jayasinghe at MHVDC Research centre and Garth Irwin at Electranix Corporation for their invaluable support.

## **Dedication**

**This thesis is dedicated to my parents for their love, endless support and encouragement.**

## Table of Contents

Author's Declaration.....	ii
Abstract.....	iii
Acknowledgements.....	iv
Dedication.....	v
Table of Contents.....	vi
List of Figures.....	ix
List of Tables.....	xi
Chapter 1 Introduction.....	1
1.1 Overview of the report.....	4
Chapter 2 Review of Multi-Conductor Transmission Line Modelling.....	6
2.1 Single conductor transmission line model.....	6
2.2 Multi-conductor Transmission lines and Cables.....	18
2.3 Modal Domain Methods.....	19
2.4 Direct Phase Domain Models.....	24
2.4.1 Basic Concept of Phase Domain Models.....	24
2.4.2 Phase Domain Models in literature.....	28
2.5 Method for validity determination of time domain implementation.....	33
2.6 Chapter Summary.....	35
Chapter 3 Modelling of Co-axial Cables in the Mesh Domain.....	36
3.1 Introduction.....	36
3.2 Development of the Mesh Domain Model.....	36
3.2.1 Basic Mesh-Domain Equations.....	37
3.2.2 Shunt admittance and series impedance matrices in mesh domain.....	39
3.2.3 Transformation Matrices.....	44
3.3 Equivalent Circuit in Time Domain.....	47
3.4 Mesh Domain Modelling for Multi-cable Systems.....	50
3.4.1 Rational Function Approximation of $Y_c$ and $A$ .....	53
3.5 Application Example.....	54
3.6 Chapter Summary.....	61
Chapter 4 Improving the asymptotic fitting of TL and cable models.....	62
4.1 Introduction.....	62

4.2 Asymptotic behavior of transmission line parameters.....	64
4.2.1 Overhead Transmission Lines.....	64
4.2.2 Underground Cables .....	71
4.3 Issues with fitting of the transfer matrices at low frequency .....	73
4.4 Methods for dc correction for the Universal Line Model .....	77
4.4.1 Dc correction by adding series resistance in each phase .....	78
4.4.2 Dc Correction by Adding a Pole and Residue .....	80
4.4.3 Dc correction by Modified Functional Form method .....	82
4.5 Application Example- Voltage Sourced HVDC with Underground Cables.....	86
4.6 Chapter Summary .....	89
Chapter 5 Robust Passivity Enforcement Scheme for Multi-Conductor Transmission Lines and Cables .....	90
5.1 Introduction.....	90
5.2 Passivity criteria for multi-conductor transmission lines.....	93
5.3 Identification of passivity violated regions.....	98
5.3.1 State variable approach.....	98
5.3.2 Frequency sweep method.....	101
5.4 Proposed Passivity Enforcement Scheme.....	102
5.5 Eliminating large passivity violations using the Modified Functional Form method.....	103
5.5.1 Selection of shunt conductance value.....	107
5.6 Elimination of small passivity violations using perturbation method.....	107
5.6.1 Implementation using perturbation of propagation matrix, $A(s)$ .....	108
5.6.2 Implementation using perturbation of admittance matrix, $Y_c(s)$ .....	110
5.6.3 Comment on the usage of Method 1 (perturbation of $A(s)$ ) and Method 2 (perturbation of $Y_c(s)$ ).....	111
5.7 Simulation example .....	112
5.8 Passivity enforcement using state variable approach.....	117
5.9 Chapter summary .....	117
Chapter 6 Conclusions and Recommendations.....	119
6.1 Contributions towards improvements in accuracy and stability of transmission lines .....	120
6.1.1 New cable model for accurate simulation of coaxial underground cables.....	120

6.1.2 Improvement in accuracy of TL models at low frequencies.....	120
6.1.3 Passivity enforcement scheme for multi-conductor transmission line models .....	121
6.2 Directions for future research .....	123
6.2.1 Identifying exact locations of passivity violations without frequency sampling .....	123
6.2.2 Passivity enforcement scheme for detailed models based on state variable approach.....	123
Appendix A Modal Domain Equations.....	124
Appendix B Cable Impedances and Admittances.....	126
Appendix C Time Delay Calculation.....	132
Appendix D Rational function approximation using Vector Fitting.....	137
Appendix E Recursive Convolution .....	140
Appendix F Numerical Inverse Laplace Transform .....	143
Appendix G Constrained Least Squares Method.....	155
Appendix H Modified Functional Form method in ULM .....	160
Appendix I Passivity identification using state variable approach .....	165
Appendix J Matrix formulation in passivity enforcement .....	181
References.....	187

## List of Figures

Figure 2.1: Small section of the transmission line.....	6
Figure 2.2: Actual and fitted frequency responses of $Y_c$ .....	13
Figure 2.3: Propagation function after and before unwinding.....	16
Figure 2.4: Actual and fitted frequency responses of $A_{uw}$ .....	16
Figure 2.5: Time domain equivalent circuit.....	17
Figure 2.6: Magnitude plots of elements of a column of A matrix for 6 conductor case .....	18
Figure 2.7: Shows the phenomena of eigenvalue switching.....	22
Figure 2.8: Magnitude plots of normalized eigenvalues of YZ matrix, if NR method is used.....	23
Figure 2.9: Voltages and currents at sending-end and receiving-end of a TL .....	25
Figure 3.1: Phase voltages and currents in a coaxial cable system.....	37
Figure 3.2: Mesh voltages and currents in a cable.....	38
Figure 3.3: Equivalent circuits for unit length admittance and impedance .....	40
Figure 3.4: Time domain equivalent circuit.....	50
Figure 3.5: Equivalent circuit for unit length impedance .....	52
Figure 3.6: Three cable system .....	55
Figure 3.7: First column of the phase propagation matrix.....	56
Figure 3.8: First column of the mesh propagation matrix .....	57
Figure 3.9: Actual and fitted mesh propagation functions.....	58
Figure 3.10: Sending-end current .....	59
Figure 3.11: Induced voltage in the inner conductor of the cable 2 .....	60
Figure 4.1: Actual height and the effective height of a conductor in the transmission line. ..	66
Figure 4.2 : Conductor internal impedance.....	67
Figure 4.3 : Aerial & ground return impedance.....	67
Figure 4.4 : Series impedance function.....	68
Figure 4.5: Typical plot of propagation function, A.....	70
Figure 4.6: Typical plot of characteristic admittance function, $Y_c$ .....	70
Figure 4.7: Typical plots of sheath and conductor impedances.....	71
Figure 4.8: Typical plot of earth return impedance .....	72
Figure 4.9: Simple Cable System: 3 single-core coaxial cables. ....	75
Figure 4.10: Magnitude of A(1,1) after Vector Fitting over [1Hz, 1 MHz] .....	76
Figure 4.11: Sending-end current of the first conductor under short circuit conditions with different lower bounds considered for fitting .....	77
Figure 4.12: Sending-end current for conductor "A" with Series Resistance Compensation .....	79
Figure 4.13: Sending-end current for conductor "A" with Series Resistance Compensation .....	79
Figure 4.14: Magnitude of A(1,1) after and before addition of pole and residue.....	80
Figure 4.15: Sending-end current of first conductor with different poles selected (pole- residue method).....	82
Figure 4.16: Actual and fitted magnitudes of A(1,1), A(2,1) and A(3,1) with Functional Form method.....	84
Figure 4.17: Sending-end current of first conductor with and without correction .....	85
Figure 4.18: Induced voltage on middle conductor "B" under open circuit conditions, if the conductor "A" is energized with step voltage.....	85

Figure 4.19: VSC Transmission System.....	86
Figure 4.20: Cable System: Two coaxial cable system .....	87
Figure 4.21: Dc line current of the converter.....	88
Figure 4.22: Voltage difference between the converter and inverter.....	88
Figure 5.1: Passive Electrical Network.....	90
Figure 5.2: Cable System: Two coaxial cable system .....	94
Figure 5.3: Eigenvalues of $H(s)$ .....	95
Figure 5.4: Magnitude of A(1,1) after Vector Fitting over [1Hz, 1 MHz] .....	96
Figure 5.5: Eigenvalue of $H(s)$ .....	97
Figure 5.6: First eigenvalue of $H(s)$ .....	104
Figure 5.7: Eigenvalues of $H(s)$ with Modified Functional Form method .....	105
Figure 5.8: Short circuit test.....	106
Figure 5.9: Short circuit current at sending-end .....	106
Figure 5.10: Cable System: Three coaxial cable system .....	113
Figure 5.11: Eigenvalues of $H(s)$ for the original formulation .....	114
Figure 5.12: Eigenvalues of $H(s)$ with Modified Functional Form method .....	114
Figure 5.13: Second eigenvalue of $H(s)$ before and after passivity enforcement.....	115
Figure 5.14: Sending-end current under short circuit conditions .....	115
Figure 5.15: Sending-end current under short circuit conditions .....	116
Figure A.1: Voltages and currents at sending-end and receiving-end of a TL .....	124
Figure F.1: $H(s)$ as a function of frequency .....	149
Figure F.2: Plot of time domain function $h(t)$ for $[0,1]$ s.....	150
Figure F.3: Expanded section of figure F.2 .....	151
Figure F.4: Plot of time domain function $h(t)$ with filter .....	152
Figure F.5: Plot of time domain function $h(t)$ with $c = 6.9078$ .....	153
Figure F.6: Plot of time domain function $h(t)$ with $c = 4.6052$ .....	153
Figure F.7: Plot of time domain function $h(t)$ with $c = 9.2103$ .....	154
Figure I.1: An eigenvalue of Hermitian matrix (H) crossing frequency axis .....	167
Figure I.1: Real part of the admittance function $G(j\omega_0)$ .....	171
Figure I.2: Real part of the admittance function $G(j\omega_0)$ .....	172
Figure I.3: Real part of the admittance function $G(j\omega_0)$ .....	173

## List of Tables

Table 3.1: Conversion table .....	47
Table 3.2: Cable data .....	56
Table 3.3: Order comparison (per element) .....	58
Table 4.1: $Z_{\text{internal}}$ and $Z_{\text{aerial\&ground}}$ at very low and very high frequency .....	69
Table 4.2: Impedances at low and high frequencies .....	72
Table 4.3: Cable data .....	75
Table 4.4: Order of rational function approximation .....	76
Table 4.5: Data for the cable .....	87
Table 5.1: Cable data .....	95
Table 5.2: Cable data .....	113
Table 5.3: CPU time comparison and rms error before and after perturbation .....	116



# Chapter 1

## Introduction

The mathematical analysis of the electrical behaviour of transmission lines was originally introduced by James Clark Maxwell, Lord Kelvin and Oliver Heaviside. In 1855 Lord Kelvin formulated a diffusion model of current in a submarine cable. In 1885 Heaviside described the analysis of propagation in cables and the modern form of telegrapher's equations [29].

The term *transmission line* (TL) refers to overhead transmission lines and underground cables in text to follow. In most power system textbooks, the transmission line (TL) parameters are calculated assuming very low frequency conditions i.e. the current is uniform across the cylindrical conductor neglecting skin effect. These constant line parameter models are valid only for analysis at and in the vicinity of fundamental frequency (e.g. Load flow studies) [45]. It is very important to consider the frequency dependent nature of TL (e.g. skin effect and proximity effect) for the accurate analysis of harmonics and electromagnetic transients [48].

In the first stage, TL equations are formulated in frequency domain. There are no direct time domain equations available in theory except for simplified structures. Time domain simulations are of great interest in practice. This is because this is the only general way to handle nonlinear elements such as thyristors in converter stations, nonlinear inrush currents of transformers and sudden changes in the network such as operation of circuit breakers and faults.

The goal of this thesis is to develop an accurate, stable and improved time domain TL model to simulate electromagnetic transients from frequencies ranging from zero Hz to 1 MHz.

The frequency domain TL equations are expressed in terms of two parameters namely characteristic admittance function  $Y_c(s)$  and propagation function  $A(s)$  ( $s = j\omega$ ). These parameters are frequency dependent and in case of multi-conductor TLs, they become square matrices. In general, the frequency domain expressions for the TL parameters are complicated and are not in a form readily simulated in the time domain. In order to have a time-domain implementation, the line's characteristic admittance function  $Y_c(s)$  is first approximated (curve-fitted) by rational transfer functions. The same is done for the propagation function  $A(s)$ , except that the fitting now includes a transportation lag in addition to the transfer function. Once expressed in rational function form, the model becomes implementable in the time domain [29], and can be used to investigate transients on transmission lines with arbitrary (including non-linear) terminations.

For multi-conductor underground cables and unsymmetrical overhead transmission lines, the frequency response of the propagation function  $A(s)$  shows oscillatory behavior, when plotted as a function of frequency. This irregular behaviour causes difficulty in low order rational function approximation and extracting optimum time delay [44], [57].

A new time domain TL model called *Mesh Domain Model* is proposed in this thesis to get over this difficulty. In this model, the original phase domain parameters are converted into mesh domain by a linear constant transformation. In contrast to the phase parameters, the mesh domain parameters exhibit less oscillatory frequency response. As a result, delay extraction and the rational function approximation for the propagation function  $A(s)$  formulated in mesh domain are much easier. This mesh domain model is represented by a current source and real shunt admittance at each end of the TL and hence can be readily implemented in electromagnetic transient (EMT) programs. The examples including underground cable systems are shown to exhibit the validity of the proposed

algorithm. The time domain results are compared with an analytical solution obtained via numerical inverse Laplace transform.

Although TL models accurately represent electromagnetic transients from frequencies ranging from a fraction of a Hz to 1 MHz, it has been difficult to get a good fit in the close neighborhood of 0 Hz (dc). For HVDC lines and cables, it is very important to accurately reproduce the response in the close vicinity of 0 Hz, as that is the nominal frequency on the line. Forcibly attempting to fit the line characteristic at these extremely low frequencies requires a high order for the rational function and sometimes leads to inaccurate fitting.

This thesis introduces two novel procedures for improvements in the accuracy of time domain simulation models for overhead lines and underground cables at very low frequencies. In these two methods, a suitable modification is introduced to the functional form of the rational function approximated in the curve fitting procedure for the phase-domain model, such that the model is accurate at dc frequency. The above proposed methods are also compared against a third less accurate method which simply adds a series dc resistor to correct the dc response. The proposed approaches are validated by comparing the time domain simulations with analytically obtained responses for simple linear terminations. The practical use of the developed procedures is demonstrated using the example of a Voltage Sourced Converter based High Voltage Dc Transmission (HVDC) System that uses underground cables.

This thesis proposes an improved algorithm to enforce passivity on the time-domain simulation model for a multi-conductor cable or overhead line. The physical transmission line, by necessity must always be passive, i.e., regardless of its terminations, the line itself cannot generate active power at any frequency. However one of the major problems of the above modeling method is that the

straightforward implementation of curve fitting cannot guarantee a passive time domain model of a transmission line. Depending on its terminating connections, a non-passive transmission line model may lead to incorrect, unstable simulations.

In this passivity enforcement algorithm, the model first employs one of the two low frequency correction methods used to obtain accurate response at 0 Hz (dc), thereby also reducing the likelihood of passivity violations. The frequency sweep method is then used to identify any remaining passivity violating regions of the model's frequency response. These small passivity violations are then removed using a linear constrained least squares algorithm to perturb the diagonal elements of propagation matrix or characteristic admittance.

The passivity enforcement algorithm is applied to the Universal Line Model (ULM), a widely used robust phase domain formulation implemented in many commercial electromagnetic transient simulation programs. Two examples, of multi-conductor underground cable systems, one for ac and the other for HVDC transmission are presented to demonstrate the proposed approach.

## **1.1 Overview of the report**

Chapter 2 summarizes the transmission line theory and modelling methods found in literature. The first part of the chapter gives an introduction to the basic TL modelling techniques and later, different modeling techniques are discussed in detail (e.g. modal domain, direct phase domain and combined phase & modal domain methods etc.). In addition, some multi-conductor transmission line models such as the Universal Line Model (ULM) are discussed.

The proposed new *Mesh Domain Method* to simulate multi-conductor coaxial cable systems is described in Chapter 3. Simulation results involving underground cable examples are presented to validate the model. The curve-fitted functions obtained from proposed model are compared with that from a direct phase domain model to emphasize its efficiency and accuracy. Time domain simulation results from the proposed model are also compared with the analytical solution obtained via numerical inverse Laplace transform.

Chapter 4 discusses the inaccuracy of time domain simulations at low frequencies, which is a crucial problem in simulating HVDC underground cable systems and overhead lines. Two novel procedures are introduced to guarantee the exact dc response for transmission lines. Time domain simulations involving HVDC underground cable systems are compared with the solution from numerical inverse Laplace transform to verify the accuracy at very low frequencies including zero Hertz and high frequencies (up to 1 MHz).

Chapter 5 begins with a brief introduction to the concept of passivity and then discusses the definition of passivity in context to the multi-conductor transmission lines. The error between the fitted functions and the actual functions are shown and how it related to the passivity problem is discussed using suitable examples. A two-stage robust algorithm to enforce passivity on multi-conductor transmission line models is introduced in this chapter. Time domain simulations involving underground cable examples are compared with the solution obtained from numerical inverse Laplace transform to verify the validity of the algorithm.

## Chapter 2

### Review of Multi-Conductor Transmission Line Modelling

The objective of this chapter is to explain the basic theory for transmission line modelling and different models for multi-conductor transmission lines found in literature. The chapter begins with a discussion on single-conductor transmission line modelling and then extends it to the multi-conductor case. The fundamental concepts on multi-conductor modelling methods such as Modal domain modelling, Phase domain modelling are explained and later in the chapter, various phase domain models found in literature are discussed such as the Universal Line Model. Finally the time domain solution obtained directly via frequency response is explained.

#### 2.1 Single conductor transmission line model

The following section describes how to model single conductor overhead line, which gives good insight into the basics of transmission line and cable modelling, before considering the more complicated multi-conductor case.

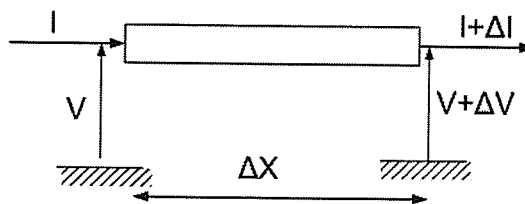


Figure 2.1: Small section of the transmission line

The above schematic shows a differentially small section of length  $\Delta x$  of a homogeneous transmission line (or underground cable) of total length  $l$ . Let  $Z$  be the impedance and  $Y$  be the shunt admittance per unit length of the transmission line respectively. From Kirchoff's current and voltage laws:

$$\Delta V = -(Z\Delta x)I \quad (2.1a)$$

$$\Delta I = -(Y\Delta x)V \quad (2.1b)$$

Here  $\Delta V$  and  $\Delta I$  are the frequency domain phasors of the incremental voltage and current across the section. The alternating current tends to travel near the surface of a conductor as its frequency increases (skin effect). In deriving  $Z$ , the skin effect of the conductor and the soil is considered and hence the series impedance  $Z(\omega)$  is frequency dependent. The shunt admittance  $Y(\omega)$  is also a function of frequency and accounts for the capacitance between the transmission line and its image to the earth. In (2.2a) and (2.2b)  $R(\omega)$ ,  $L(\omega)$ ,  $G$  and  $C$  denote unit length series resistance, series inductance, shunt conductance and shunt capacitance respectively. The expressions for these parameters can be found in [1], [6], [7], [3].

$$Z(\omega) = R(\omega) + j\omega L(\omega) \quad (2.2a)$$

$$Y(\omega) = G + j\omega C \quad (2.2b)$$

### A note on frequency dependency nature of shunt conductance ( $G$ ) and capacitance ( $C$ )

Some models, use frequency dependent values for the shunt conductance and capacitance. For overhead lines, the approximation of assuming capacitance is very accurate [27], and can be calculated from the line geometry. The shunt conductance value also depends on other factors such as ageing, type of insulators, environmental parameters e.g. humidity, temperature and pollution etc. This shunt conductance value is very small, since the electrical conductivity of air is extremely small (typical value,  $3e-11$  S) [68], [55], and is sometimes entirely omitted in many models.

For underground cables, the capacitance value is much higher than the overhead lines, since the distance between conductor and return path is small. The permittivity value of insulators is assumed to be a constant in emtp-type programs such as EMTP and PSCAD/EMTDC, resulting in a constant capacitance (see equation B.10 in Appendix B) [27]. However, in case of pipe-type cables the frequency dependent nature of permittivity may be significant, requiring the consideration of frequency dependent capacitance. Such cables have not been considered in this thesis.

The conductance  $G$  value of the insulators can be derived from the frequency dependent loss angle ( $\tan(\delta)$ ) and the capacitance  $C$  of the insulators ( $G = \tan(\delta) \cdot \omega C$ ) [27]. Since the conductance value is very small ( $G \ll \omega C$ ), the effect of conductance on electromagnetic transient simulations is very small in practical cases. Hence it is reasonable to assume a constant conductance. This is the common practice in many emtp-type programs and has been shown to be sufficiently accurate [27]. The equations used for determining all parameters are presented in Appendix B.

The Maxwell equations are the set of four fundamental equations used to describe the dynamics of the electromagnetic (EM) waves. Transmission line equations (also called telegrapher's equations) can be



derived from Maxwell's equations (and also using basic circuit theory as in 2.1) [29]. The general form of the telegrapher's equations in the frequency domain are given by,

$$-\frac{\partial}{\partial x}V(x, \omega) = Z(\omega)I(x, \omega) \quad (2.3a)$$

$$-\frac{\partial}{\partial x}I(x, \omega) = Y(\omega)V(x, \omega) \quad (2.3b)$$

For simplicity,  $Z(\omega)$ ,  $Y(\omega)$ ,  $I(x, \omega)$  and  $V(x, \omega)$  are represented as  $Z$ ,  $Y$ ,  $I$  and  $V$  in the following text. The equations (2.4a) and (2.4b) show the solution to the above equations (2.3a) and (2.3b) obtained from elementary partial differential equation theory [5],

$$I = \sqrt{\frac{Y}{Z}}e^{-\sqrt{ZY}x}V_f - \sqrt{\frac{Y}{Z}}e^{\sqrt{ZY}x}V_b \quad (2.4a)$$

$$V = e^{-\sqrt{ZY}x}V_f + e^{\sqrt{ZY}x}V_b \quad (2.4b)$$

Where,  $V_f$  and  $V_b$  are arbitrary phasors constants, which can be evaluated by applying boundary conditions at the sending-end and receiving-end of the TL. At the sending-end of the line (i.e. at  $x = 0$ ),

$$V_k = V_f + V_b \quad (2.5a)$$

$$I_k = \sqrt{\frac{Y}{Z}}V_f - \sqrt{\frac{Y}{Z}}V_b \quad (2.5b)$$

Similarly at the receiving-end,  $x = l$  (length of the transmission line)

$$V_m = e^{-\sqrt{ZY}l}V_f + e^{\sqrt{ZY}l}V_b \quad (2.6a)$$

$$I_m = -\sqrt{\frac{Y}{Z}}e^{-\sqrt{ZY}l}V_f + \sqrt{\frac{Y}{Z}}e^{\sqrt{ZY}l}V_b \quad (2.6b)$$

Note that in the above expressions, subscripts “ $k$ ” and “ $m$ ” denote sending-end and receiving-end. The current direction is to the transmission line at both end of the line (see figure 2.9). Frequency domain TL equations are usually expressed in terms of the characteristic admittance function  $Y_c(\omega)$  and propagation function  $A(\omega)$  (2.7a and 2.7b respectively), which are also functions of per unit length parameters  $Z(\omega)$  and  $Y(\omega)$ .

$$Y_c(\omega) = \sqrt{\frac{Y(\omega)}{Z(\omega)}} \quad (2.7a)$$

$$A(\omega) = e^{-\sqrt{Y(\omega)Z(\omega)}l} \quad (2.7b)$$

After eliminating the unknowns ( $V_f$  and  $V_b$ ) from equations (2.5a), (2.5b), (2.6a), (2.6b), the relationship between sending-end and receiving-end variables can be expressed as,

$$I_k = Y_c V_k - A(Y_c V_m + I_m) \quad (2.8a)$$

$$I_m = Y_c V_m - A(Y_c V_k + I_k) \quad (2.8b)$$

Here,  $V_k$  and  $V_m$  are the conductor voltages to ground (ground/earth is considered as reference for the voltage) and  $I_k$  and  $I_m$  are conductor currents. The terms  $A(Y_c V_m + I_m)$  and  $A(Y_c V_k + I_k)$  represent the contribution from the remote-end of the transmission line. Electromagnetic transient (EMT) programs require a time domain form of (2.8a) and (2.8b). In equations (2.8a) and (2.8b), each product of two frequency domain functions becomes convolution between the corresponding time domain functions. For example (2.9) is the time domain form of (2.8a):

$$i_k(t) = y_c(t) * v_k(t) - a(t) * (y_c(t) * v_m(t) + i_m(t)) \quad (2.9)$$

Note that lower case letters represent time domain impulse response function of corresponding uppercase letter frequency domain (FD) function (e.g.  $y_c(t)$  is the inverse Laplace transform of the  $Y_c(s)$  in equation 2.8a). The symbol '\*' denotes convolution. The straightforward numerical integration of the convolution is not computationally efficient. The mathematical technique called *recursive convolution* is a numerically efficient technique to evaluate the convolution. For the recursive convolution, either one of the two functions should be expressed as a sum of exponentials. To explain, consider the following convolution,

$$s_1(t) = y_c(t) * v_k(t) \quad (2.10)$$

The admittance impulse response term  $y_c(t)$  can be approximated as a summation of exponentials in the following way. Since the characteristics admittance function is originally formulated in the frequency domain (FD), numerical inverse Fourier transform methods such as IFFT are used to get

it's corresponding discrete time domain function. The time domain function  $y_c(t)$  is then approximated by a summation of exponentials as shown in (2.11) using a suitable curve fitting technique.

$$y_c(t) = \sum_{i=1}^n c_i e^{a_i t} \quad (2.11)$$

A more convenient approach that avoids the step of obtaining the time domain form of  $y_c(t)$  is to approximate the FD function  $Y_c(\omega)$  using a least square based curve fitting technique in the following form (called pole residue form as shown in equation (2.12) with  $(s = j\omega)$ ) in the frequency domain directly. The direct frequency domain fitting has several advantages over time domain fitting. If the fitted function closely matches the actual function over a range of frequencies, then the corresponding steady state time domain simulation is highly accurate over that particular frequency range. Also the unknown coefficients ( $c_i$ ,  $a_i$  and  $Y_\infty$  in equation (2.12)) can be efficiently evaluated using a robust curve fitting technique based on linear least squares called Vector Fitting [43], [41] (for more details, see Appendix D).

$$Y_c(s) = \sum_{i=1}^n \frac{c_i}{s - a_i} + Y_\infty \quad (2.12)$$

Figure (2.2) shows the typical plot of the fitted function and the actual function for  $Y_c(\omega)$  as a function of frequency.

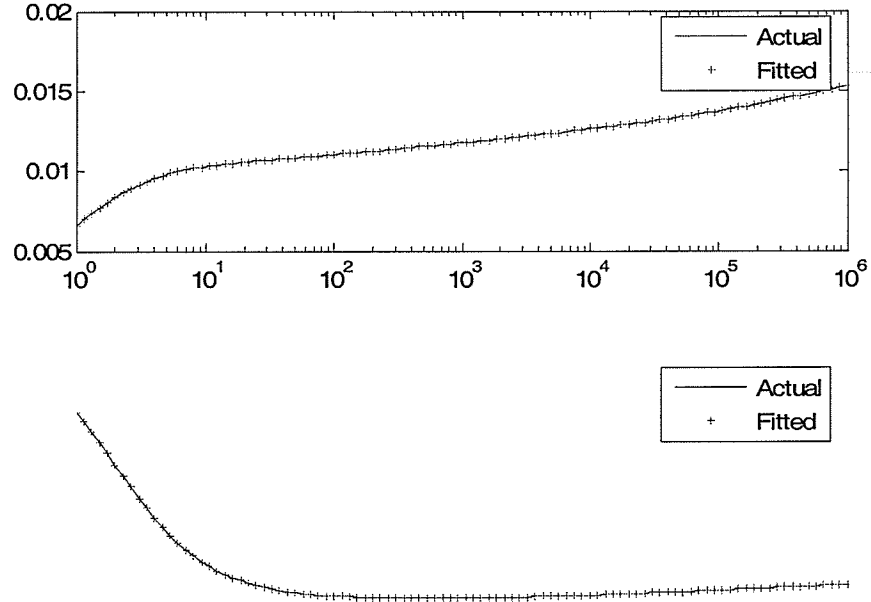


Figure 2.2: Actual and fitted frequency responses of  $Y_c$

The time domain form of (2.12) is,

$$y_c(t) = \sum_{i=1}^n c_i e^{a_i t} + Y_\infty \delta(t) \quad (2.13)$$

With  $y_c(t)$  in above formulation, the convolution (2.10) can be written in discrete recursive form as [27], [20],

$$s_1(t) = \alpha v_k(t) + \beta v_k(t - \Delta t) + \gamma s_1(t - \Delta t) \quad (2.14)$$

Where,  $\Delta t$  is the simulation time step selected. It is interesting to note that value of the convolution is expressed as a combination of the voltage at the current time step, voltage at the previous time step and the previous value of the convolution. For further details, the derivation of constants can be found in appendix E.

Equation (2.15) represents the other convolution term in (2.9).

$$s_2(t) = a(t) * f(t) \quad (2.15)$$

where,

$$f(t) = (y_c(t) * v_m(t) + i_m(t))$$

The same procedure (used to evaluate  $y_c(t) * v_k(t)$  in (2.10)) can be utilized to evaluate the convolution. However the exponential term ( $e^{-\sqrt{Y(\omega)Z(\omega)}t}$  in equation (2.7b)) prohibits direct curve fitting of  $A(\omega)$  using low order rational functions.

Physically  $A(\omega)$  is the factor, which defines the attenuation and the phase shift of forward travelling wave coming from the remote end of the transmission line after some delay. The reason for the delay is due to the relativistic speed limit. The signal cannot travel faster than the speed of light. Therefore the propagation function  $A(\omega)$  contains a true delay (transportation lag). This time delay in time domain means a phase shift in frequency domain. The propagation function  $A(\omega)$  can be represented with the delay explicitly separated as shown in equation (2.16) leaving a simpler function  $A_{uw}(\omega)$ , which is readily fittable by a rational transfer function. This process is referred to as “unwinding”.

$$A(\omega) = A_{uw}(\omega) e^{-j\omega\tau} \quad (2.16)$$

The delay ( $\tau$ ) can be physically depicted as the time required for the travelling waves to travel to the other end of the transmission line. Time delay is frequency dependent. However time domain models require constant delay, which can be calculated in several ways. Further details can be found in Appendix C.

Once the delay is removed, the  $A_{uv}(\omega)$  shows less oscillatory phase behaviour as shown in figure (2.3). It now becomes easy to fit with low order rational functions. The fitted and the actual functions are shown in figure (2.4). It appears that there is a significant phase fitting error after  $10^4$  Hz. However, the magnitude is entirely zero at these large frequencies and so the phase error is inconsequential. The final form of the propagation function is,

$$A(s) = \sum_{i=1}^M \frac{c_i}{s - a_i} e^{-s\tau} \quad (2.17)$$

where,  $s = j\omega$ .

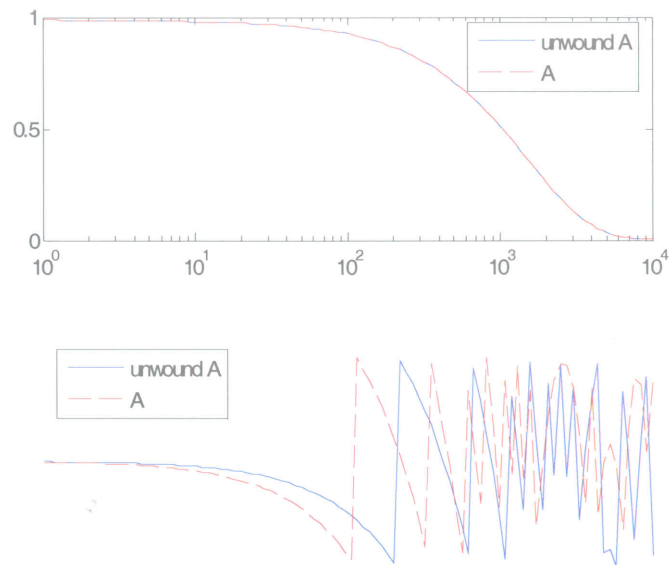


Figure 2.3: Propagation function after and before unwinding

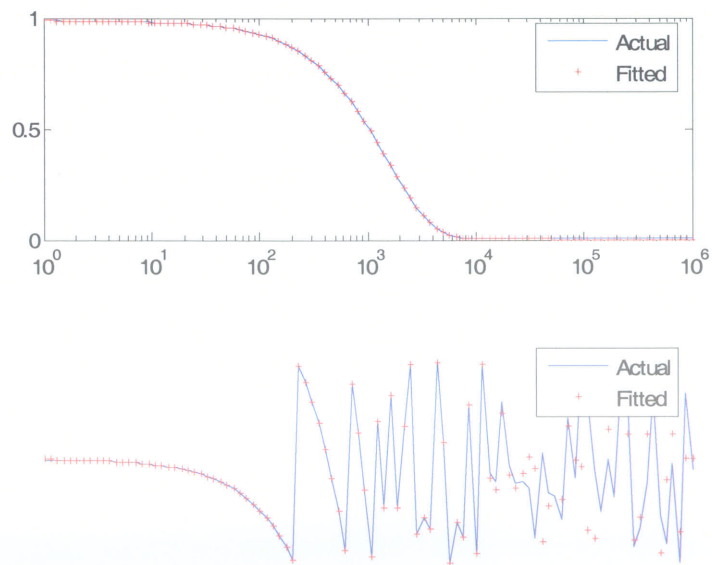


Figure 2.4: Actual and fitted frequency responses of  $A_{uw}$



After applying recursive technique, the convolution in (2.15) becomes,

$$s_2(t) = \alpha' f(t - \tau) + \beta' f(t - \Delta t - \tau) + \gamma' s_2(t - \Delta t) \quad (2.18)$$

It is evident that all the terms in (2.18) are history terms (i.e. only involve values from the past). Finally, the formula for the current (2.9) can be expressed as a summation of present and past values as follows.

$$i_k(t) = y_{eq} y_k(t) + i_{hist\_k}(t) \quad (2.19)$$

where,

$$y_{eq} = \alpha$$

$$i_{hist\_k}(t) = \beta v_k(t - \Delta t) + \gamma s_1(t - \Delta t) - s_2(t)$$

Equation (2.19) represents a real current source and a real admittance for the sending-end in the time domain. Similar representation can be obtained for the receiving-end, so that the model can be represented by the equivalent circuit in figure 2.5.

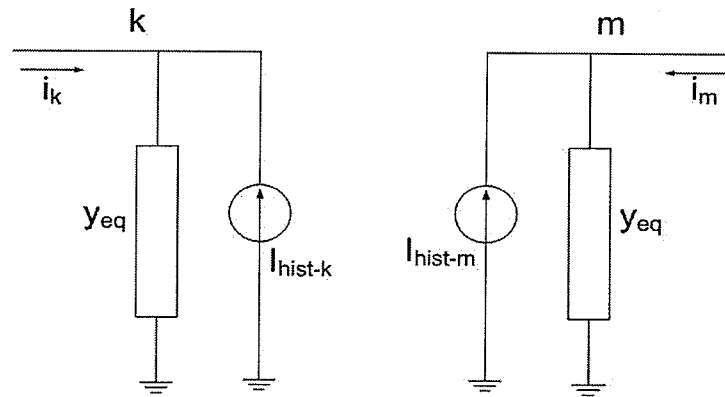


Figure 2.5: Time domain equivalent circuit

This model is in the standard form used in the admittance matrix based network solutions [27] and hence is easily incorporated into the EMT algorithm.

## 2.2 Multi-conductor Transmission lines and Cables

Modelling of multi-conductor transmission lines (MTL) is more complicated than the single conductor case. Various approaches have been developed for the multi-conductor case. The equations (2.8a) and (2.8b) are valid for this case, but  $Y_c(\omega)$  and  $A(\omega)$  are square ( $n \times n$ ) matrices and  $I$  and  $V$  are  $n$ -dimensional vectors for the  $n$ -conductor system.

This electromagnetic coupling phenomenon in MTL causes irregular behaviour in the elements of propagation matrix  $A(\omega)$ , both in magnitude and angle in their frequency response, shown for a typical cable in Fig 2.6.

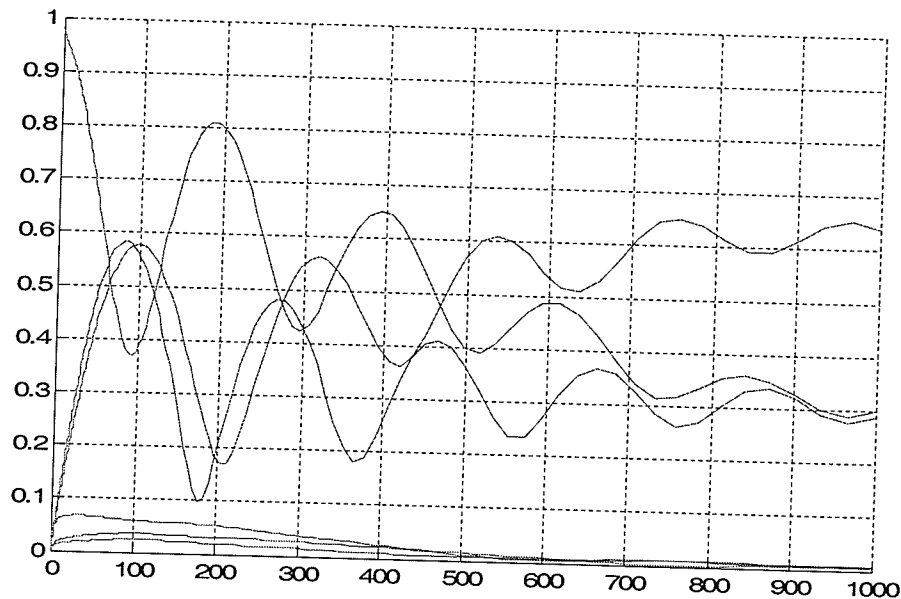


Figure 2.6: Magnitude plots of elements of a column of  $A$  matrix for 6 conductor case

As a consequence, there can be difficulties in time delay extraction and low order rational function approximation, which are essential components in time domain modelling.

## 2.3 Modal Domain Methods

The problems described above, relating to coupled frequency domain equations (2.8a) and (2.8b) can be avoided by decoupling them using modal theory [41], [22], [7], [26]. The coupled frequency domain equations (sometimes called direct phase equations) can be decoupled using transformation matrices. Consider the following system of equation.

$$Y = GX \tag{2.20}$$

where, G is a square matrix and Y and X are output and input vectors respectively. For simplicity, consider a two dimensional case. Equation (2.20) can be written in matrix vector form as shown in equation (2.21),

$$\begin{bmatrix} y_1 \\ y_2 \end{bmatrix} = \begin{bmatrix} g_{1,1} & g_{1,2} \\ g_{2,1} & g_{2,2} \end{bmatrix} \begin{bmatrix} x_1 \\ x_2 \end{bmatrix} \tag{2.21}$$

The above coupled equation can be decoupled by separating eigenvalues and eigenvectors of matrix G as shown in equation (2.22) and (2.23).

$$\begin{bmatrix} y_1^m \\ y_2^m \end{bmatrix} = \begin{bmatrix} g_{1,1}^m & 0 \\ 0 & g_{2,2}^m \end{bmatrix} \begin{bmatrix} x_1^m \\ x_2^m \end{bmatrix} \tag{2.22}$$

$$Y^M = G^M X^M \quad (2.23)$$

where,

$$G^M = EGE^{-1}$$

$$Y^M = E^{-1}Y$$

$$X^M = E^{-1}X$$

$E$  and  $g_{i,j}^m$  are the matrix of the right eigenvectors and  $i^{\text{th}}$  eigenvalue of matrix  $G$  respectively. Equations (2.8a) and (2.8b) can be converted into modal domain as described in Appendix A. Application of modal theory to the transmission lines was first introduced by L.M. Wedephol and later becomes an essential tool in TL modelling [28], [22], [7], [26]. Once the equations are transformed in to the modal domain, the frequency response of each modal element (such as elements of modal  $A$ ) is smooth and well behaved. The extraction of the transportation delay as well as the low order rational function approximation of the modal function is much easier. The modal domain formulae are tabulated in Appendix A.

In general the transformation matrix from direct phase domain to modal domain is frequency dependent and complex. However for most overhead transmission lines (e.g. horizontally symmetrical overhead lines) or simple cable systems this transformation matrix is almost constant and also the imaginary part of the transformation matrix is negligible compared with the real part. For such cases, the transformation matrices can be considered to be real and constant with little error in the time domain solution.

The assumption of the real constant transformation matrices leads to efficient time domain modelling, since only  $4n$  convolution are required in each time step for an  $n$ -conductor transmission line. As transformation matrices typically converge to a real constant value as the frequency tends to infinity, it is customary to obtain the above real-constant transformation by evaluating the true transformation at the highest frequency point to be considered (usually 1 MHz). For certain geometries  $E$  can be determined from physical arguments. For example, for horizontal ideally transposed transmission lines, the Clark transformation can be used.

The paper [21] describes a method to simulate transmission line transients in the time domain using constant transformation matrices.

The constant transformation matrix assumption is not valid for highly asymmetrical overhead line configurations and for most underground cable systems. In such cases, assumption of constant transformation matrix causes significant errors in time domain simulations. The frequency dependency effects of transformation matrices must be accurately taken into account. The paper [37] describes a modal domain transmission line model considering frequency dependent transformation matrices.

Modal domain models with frequency dependent line parameters have several drawbacks. Due to the additional convolutions involved between modal matrices and transformation matrices, the model is numerically inefficient and less accurate compared with direct phase domain methods. It was observed that some elements of transformation matrices can not be satisfactorily approximated using rational functions.

An essential part in modal domain models is the computation of modal elements (eigenvalues). If the eigenvalues are calculated using normal eigenvalue/eigenvector algorithms such as power method or QR method [30], the eigenvalue plots vs. frequency are not smooth as shown in figure (2.7) due to the phenomena called “eigenvalue switching”. The mathematical methods for eigenvalue calculations are well known [30] and not elaborated in this thesis. If such algorithms are used, then the eigenvalues calculated at the current frequency are not always corresponding to the eigenvalues at the previous frequency. The eigenvalue  $\lambda_A$  move along a smooth locus, as frequency is measured up to point 1 and that appears to jump to point 2 and smoothly to point 3 and jump to 4. This sudden jump is also seen in the locus of eigenvalue  $\lambda_B$ .

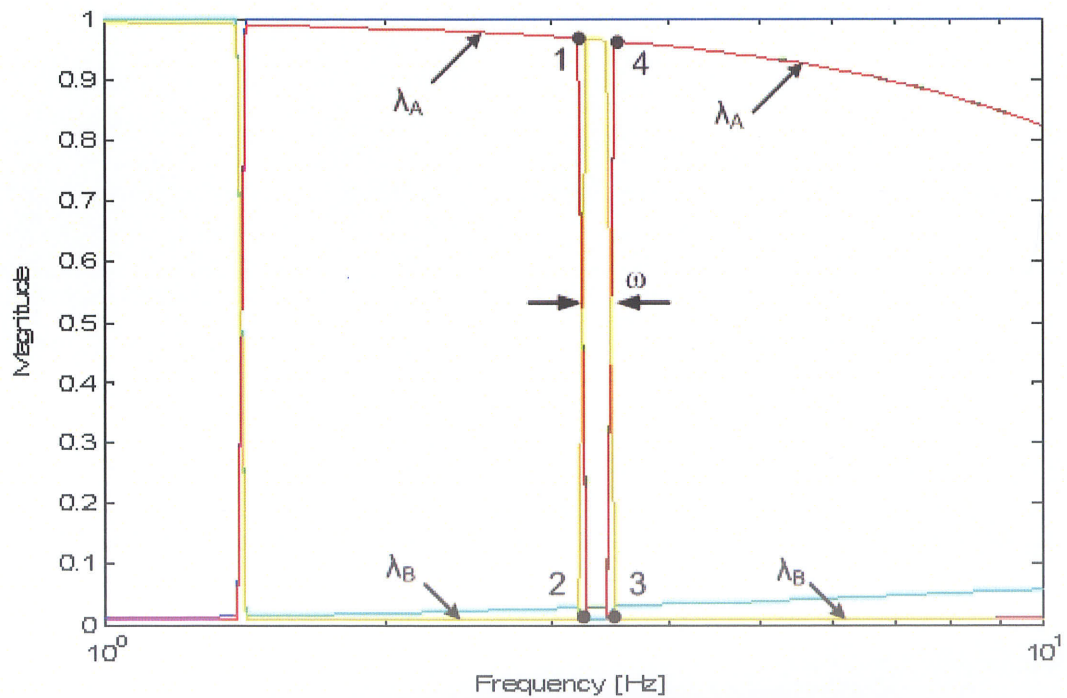


Figure 2.7: Shows the phenomena of eigenvalue switching

Alternatively, one could argue that in the jump region  $\omega$ , eigenvalue  $\lambda_A$  should have continued along the trajectory of  $\lambda_B$  to produce a smooth locus. As the naming of eigenvalues is arbitrary, this makes no differences to the mathematical behaviour in the frequency domain. However the jump makes curve fitting of  $\lambda_A$  and  $\lambda_B$  very difficult. Hence in order to facilitate good curve fitting a method must be produced (such as the Newton Raphson method [33] or a nonlinear optimization method [46]) that allows identification of eigenvalues so that their loci are smooth. Figure (2.8) shows the magnitude of eigenvalues vs. frequency, if Newton Raphson based method [33] is used to calculate eigenvalues and eigenvectors for the six conductor cable configuration.

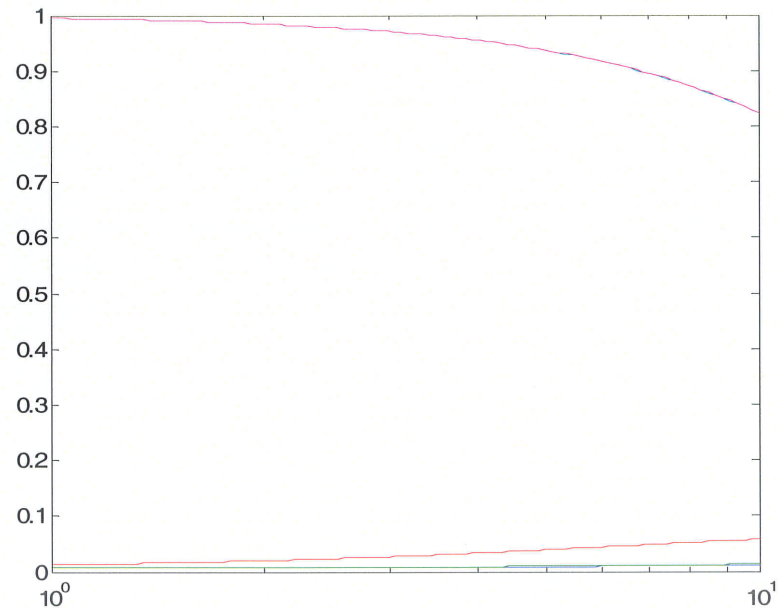


Figure 2.8: Magnitude plots of normalized eigenvalues of YZ matrix, if NR method is used

## 2.4 Direct Phase Domain Models

### 2.4.1 Basic Concept of Phase Domain Models

Direct phase domain models have been developed in order to overcome difficulties associated with frequency dependent transformation matrices. The TL equations remain coupled, but the problem of frequency dependent transformation matrices does not arise. For Direct Phase Domain models, the general derivation is briefly described as follows. For an n-phase transmission line having length  $l$ , the FD expressions are (equations (2.8a) and (2.8b) restated below),

$$I_m = Y_c V_m - A(Y_c V_k + I_k) \quad (2.24)$$

$$I_k = Y_c V_k - A(Y_c V_m + I_m) \quad (2.25)$$

where [36],

$$Y_c = \sqrt{(YZ)^{-1}} Y \quad (2.26)$$

$$A = e^{-\sqrt{YZ}l} \quad (2.27)$$



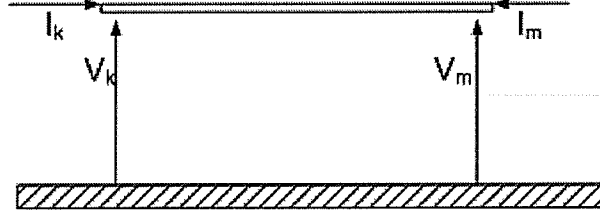


Figure 2.9: Voltages and currents at sending-end and receiving-end of a TL

Suffices “k” and “m” denote sending-end and receiving-end respectively.  $Y_c(\omega)$  is the characteristic admittance matrix.  $A(\omega)$  is the propagation matrix.  $V$  and  $I$  are voltage and current vectors.  $Y(\omega)$  and  $Z(\omega)$  are shunt admittance and series impedance square matrices per unit length respectively. The frequency dependent term  $\omega$  is removed for simplicity in equations (2.24) to (2.31).

The matrices  $Y_c(\omega)$  and  $A(\omega)$  are computed first by finding the eigenvalues and eigenvectors of  $P(\omega) = Y(\omega) \times Z(\omega)$  matrix. Let  $\gamma_i(\omega)$  be the  $i^{\text{th}}$  eigenvalue of matrix  $P(\omega)$ .

$$A = E_I \Gamma E_I^{-1} \quad (2.28)$$

Where,  $E_I(\omega)$  is the matrix whose columns are the eigenvectors of matrix  $P(\omega)$ .  $\Gamma(\omega)$  is a diagonal matrix, whose elements are defined as,

$$\Gamma_{i,i} = e^{-\sqrt{\gamma_i} l} \quad (2.29)$$

Similarly, the matrix  $Y_c(\omega)$  is,

$$Y_c = E_I \Psi E_I^{-1} Y \quad (2.30)$$

where,  $\Psi(\omega)$  is a diagonal matrix whose elements are defined as,

$$\Psi_{i,i} = \sqrt{\frac{1}{\gamma_i}} \quad (2.31)$$

The ultimate objective of modelling is to find an equivalent circuit in time domain as described in section 2.1. The same procedure can be applied, but there are exceptions. The first stage is the rational function approximation of  $A(\omega)$  and  $Y_c(\omega)$  in frequency domain (as discussed in section 2.1). For n-conductor transmission line, these are square matrices and each entry of those matrices is approximated by low order rational functions.

Since  $Y_c(\omega)$  in phase domain is a symmetric ( $n \times n$ ) matrix, only  $(n + n \times (n-1)/2)$  elements are to be fitted. As  $Y_c(\omega)$  is the admittance seen by the sending-end for an infinite line, diagonal elements of  $Y_c(\omega)$  are of minimum phase type. The off-diagonal elements are multiplied by -1 before rational function approximation, so that they too become minimum phase functions, whose angles lie in the first or fourth quadrant. The minimum phase property of  $Y_c(\omega)$  allows entries of  $Y_c(\omega)$  to be approximated only using real poles and zeros with a reasonable accuracy (Any physical admittance (or impedance) can be synthesized to an electrical network consisting of only passive elements such as capacitors, inductors and resistors. The transfer function of such networks contains only real poles and zeros) [36].

The propagation matrix is an un-symmetrical square ( $n \times n$ ) matrix. Using the approach described in section 2.1, all the elements must first be unwound as in (2.16) and the entries of unwound matrix  $A_{uw}(\omega)$  are curve-fitted by low order rational functions.

It is observed that the elements of  $A_{uw}(\omega)$  are close to minimum phase (but in some cases, considerably deviate from minimum phase) and can be approximated using low order rational functions [44]. Complex poles and residues are required in curve-fitting to obtain a reasonable accuracy.

In modal domain methods described in section 2.3, transportation delay can be successfully calculated using Bode's gain-phase formula. Modal domain elements (modal form of  $A(\omega)$ ) are smooth functions of frequency (less oscillatory behavior). There is a unique delay associated with each mode, because each mode has its own modal velocity. But delay extraction is very difficult in the phase domain elements, due to the oscillatory nature in the entries of  $A(\omega)$ , when plotted as a function of frequency. Usually an optimization technique is implemented to calculate the optimum delay, which results in a low order rational function approximation (see Appendix C for further details).

At the end of first stage, the elements of matrices  $A_{uw}(\omega)$  and  $Y_c(\omega)$  are expressed as rational functions in the forms shown in (2.12) and (2.7) respectively. In time domain, these functions are summation of exponentials. Using the same techniques like application of recursive convolution described in section 2.1, the frequency domain equations (2.24) and (2.25) are converted into time domain equations.

$$i_m(t) = y_{eq} v_m(t) + i_{hist\_m}(t - \Delta t, t - \Delta t - \tau, t - \tau) \quad (2.32)$$

$$i_k(t) = y_{eq} v_k(t) + i_{hist\_k}(t - \Delta t, t - \Delta t - \tau, t - \tau) \quad (2.33)$$

where  $y_{eq}$  is a real constant matrix and history current terms ( $i_{hist\_k}$  and  $i_{hist\_m}$ ) are evaluated using past information as discussed in section (2.1). The equations reveal a time domain equivalent circuit having a shunt admittance and history current source as shown in figure (2.5). This formulation can be readily implemented in electromagnetic transient programs.

## 2.4.2 Phase Domain Models in literature

Recently direct phase domain models are of greater interest than modal domain models, because phase models avoid problems with frequency dependent transformation matrices. Various phase domain models have been developed in the past few decades.

### 2.4.2.1 Direct phase domain model

A direct phase domain model for overhead transmission lines can be found in [36]. The term *direct* means this model does not involve curve-fitting of modal elements or transformation matrices, but only phase elements. In this model, the transportation delay in (2.16) is extracted based on speed of light, however this is successful only for simple overhead transmission line configurations. There may be difficulties in low order rational function approximation for more complicated configurations, if the delay is simply calculated based on speed of light. For such cases, the optimum delay (which gives minimum least square error of curve-fitting for a given entry) is significantly different from the delay calculated on speed of light. The curve-fitting method used for the model is the *modified*

*magnitude fitting* in which only magnitude of  $A_{uv}(\omega)$  is considered for fitting. This fitting method is based on the assumption that  $A_{uv}(\omega)$  is a minimum phase function.

#### 2.4.2.2 Autoregressive moving-average (ARMA) model

Some models incorporate transportation delay  $\tau$  directly into fitting process[32]. In phase domain ARMA model [32], the rational function approximation of  $Y_c(\omega)$  and  $A_{uv}(\omega)$  is done in the  $z$  ( $z = e^{s\Delta t}$ ) domain rather than in  $s$  ( $s = j\omega$ ) domain. One important advantage of this method is that there is no need to calculate the delay explicitly, as the delay terms are represented in the  $z$  domain formulation.

The  $e^{-s\tau}$  in  $s$  domain can be approximated by,

$$e^{-s\tau} \approx \frac{1}{1+s\tau} \quad \text{or} \quad \approx \frac{1 - \frac{s\tau}{2}}{1 + \frac{s\tau}{2}}$$

This approximation is not sufficiently accurate to represent the exponential term in TL applications. But the delay  $\tau$  can be accurately represented in  $z$  domain as shown below.

$$e^{-s\tau} \approx z^{-n}$$

Where,

$$n = \frac{\tau}{\Delta t} \quad \text{and} \quad z = e^{s\Delta t}$$

$\Delta t$  and  $\tau$  are the time step selected and the transportation delay respectively. The  $n^{\text{th}}$  order rational function in  $z$  domain is used to curve-fit  $A_{uv}(\omega)$  or  $Y_c(\omega)$  as shown below.

$$G(z) = \frac{a_0 + a_1 z^{-1} + \dots a_n z^{-n}}{1 + b_1 z^{-1} + \dots b_n z^{-n}} \quad (2.34)$$

$$Y(z) = G(z) X(z)$$

The unknown coefficients ( $a_i$ 's and  $b_i$ 's in (2.34)) are evaluated by a least squares fitting method. The corresponding time domain form of (2.34) is shown below.

$$y(k) = a_0 x(k) + a_1 x(k-1) + \dots a_n x(k-n) - b_1 y(k-1) + \dots + b_n y(k-n) \quad (2.35)$$

This model can be implemented into electromagnetic transient (EMT) programs. Note that as the coefficients  $a_i$  and  $b_i$  are identified from the discrete model ( $Z$  domain), their values are time step dependent and must be reevaluated if the simulation is run with a different time step  $\Delta t$ .

So far, the each entry of the propagation matrix  $A(\omega)$  is attributed to a single delay. Alternative approach is to treat each entry of  $A(\omega)$  with multiple delays (modal delays) instead of single delay. It is meaningful, because each entry can be expressed as a linear combination of modal elements of  $A(\omega)$  at any frequency [7]. Hence entries of  $A(\omega)$  compose of delays in each mode (modal delays). The accuracy of curve-fitting with multiple delay approach is greater than single delay method and multiple delay technique shows clear advantage, when dealing with cable configurations having widely different modal delays.

### 2.4.2.3 Universal Line Model (ULM)

An example for the phase domain model, which uses multiple-delay approach, is the Universal Line Model (ULM) [44]. In this model, modal delays are first calculated and then modes of  $A_{uw}(\omega)$  are curve-fitted using a robust least square technique called Vector Fitting [43]. The functional form of  $k^{\text{th}}$  mode is,

$$A_k^{\text{mode}}(s) = \sum_{m=1}^{N_k} \frac{c_{mk}}{s - a_{mk}} e^{-s\tau_k} \quad (2.36)$$

where  $N_k$ ,  $a_{mk}$ ,  $c_{mk}$ ,  $\tau_k$  are the order of approximation,  $m^{\text{th}}$  pole and  $m^{\text{th}}$  residue and the delay corresponding to  $k^{\text{th}}$  mode respectively. It is assumed that each  $A_{i,j}(\omega)$  can be approximated by a rational function in the form shown in (2.37) with modal delays and poles, used to curve-fit modes.

$$A_{i,j}(s) = \sum_{k=1}^n \left( \sum_{m=1}^{N_k} \frac{\bar{c}_{mk}}{s - a_{mk}} e^{-s\tau_k} \right) \quad (2.37)$$

where  $n$  is the number of modes. Idempotent theory gives a good insight into the mathematical background of this model [5]. According to idempotent theory, matrix  $A(\omega)$  can be stated as a linear combination of its eigenvalues or modal elements at any frequency as in (2.38).

$$A = \sum_{k=1}^n T_k A_k^{\text{mode}} \quad (2.38)$$

where  $T_k(\omega)$  is a frequency dependent matrix derived from corresponding eigenvectors. By substituting  $A_k^{mode}$  from (2.36),

$$A = \sum_{k=1}^n T_k \left( \sum_{m=1}^{N_k} \frac{c_{mk}}{s - a_{mk}} e^{-s\tau_k} \right) \quad (2.39)$$

It is observed that the entries of the matrix  $T_k(\omega)$  show smooth behavior for practical TL configurations, when plotted as a function of frequency. This justifies the assumption that the frequency dependency behavior of  $T_k(\omega)$  can be flexibly accounted by choosing suitable residues (selecting new set of residues instead of  $c_{mk}$ 's in (2.39)) and  $A(\omega)$  now becomes a form similar to (2.37).

According to the formulation (2.37), there is no unique time delay for each element of  $A(\omega)$  matrix but a superposition of modal delays in time domain. This significantly improves the accuracy of the fitted propagation functions particularly for TL configuration with widely different modal time delays. Another plus point is that since all elements have same set of poles, there is a computational saving in calculating the convolution terms (2.15), leading to a numerically efficient model.

The ULM is accurate, robust and numerically efficient model. This model requires a robust eigenvalue tracking algorithm like NR method to eliminate eigenvalue switching.

There are several problems common to many time domain models. One issue is that although these models simulate the frequency range from a few Hertz to about several kilohertz, it has been difficult



to get a good fit around zero Hz (dc); a significant error in modelling HVDC underground cables and overhead TLs. Two novel procedures are introduced to improve the accuracy of time domain simulation at very low frequencies (see Chapter 4). Another shortcoming is that these time domain models cannot be guaranteed to be always passive, which may result in unstable Time Domain simulation. An algorithm is proposed to enforce passivity on the time-domain simulation model (see Chapter 5).

## **2.5 Method for validity determination of time domain implementation**

In this thesis, many approaches to time domain simulations are discussed and new ones are introduced. It is important to check the validity of these approaches. However, unless for simplified approaches, the direct theoretical solution is not available. Instead, a numerical method to obtain the time domain solution from frequency domain solution is used to validate the transient simulation.

For linear networks, the relationship between an applied voltage or current excitation (input) and the desired output can be represented by a frequency domain transfer function. The applied input can be transformed with a Laplace Transform into its frequency components. The Laplace Transform of the response is then obtained directly in the frequency domain by multiplying the above transfer function by the (frequency domain) input. The time domain solution can now be obtained by inverse Laplace transform of this frequency domain solution. Although such an approach is only applicable for linear networks and thus has little use in general-purpose simulation that usually includes non-linearities; it is nevertheless an independent means to validate the time domain solutions of transmission lines obtained by numerical integration of differential equations.

Consider a case where, the TL is connected to a load admittance ( $Y_m$ ) at the receiving-end and sending-end is connected to a current source ( $I_s$ ) parallel with an admittance ( $Y_k$ ). The frequency domain equations at both ends can be written as shown in equation (2.40) and (2.41).

$$I_s = I_k + Y_k V_k \quad (2.40)$$

$$I_m = -Y_m V_m \quad (2.41)$$

The frequency domain solution of the sending-end current can be calculated by combining equations (2.40) and (2.41) with (2.8a) and (2.8b).

$$I_k = I_s - Y_k (H_1 + H_2 Y_k - H_2 Y_c)^{-1} (I + H_2) I_s \quad (2.42)$$

where,  $I$  is the identity matrix.

$$H_1 = Y_c + Y_k$$

$$H_2 = A(Y_c - Y_m)(Y_c + Y_m)^{-1} A$$

The time domain solution for the sending-end current is obtained using numerical inverse Laplace transform of equation (2.42). A detailed discussion on Inverse Laplace Transform can be found in Appendix F.

## **2.6 Chapter Summary**

This chapter described the basic theory of transmission line modelling and summarized the modelling methods found in literature. At the beginning, the derivation of frequency domain transmission line equations using telegrapher's equations was briefly presented. The concepts of TL modelling for the single-conductor case were then described in detail. This gives a good understanding in to the basics of transmission line modelling, before explaining the more complicated multi-conductor case in section (2.2). Multi-conductor models fall into two major categories namely modal domain methods and phase domain methods. Finally the use of frequency domain methods to obtain time domain responses was briefly described. This method is useful to validate the transmission line models.

## **Chapter 3**

### **Modelling of Co-axial Cables in the Mesh Domain**

#### **3.1 Introduction**

A new method is developed in this thesis to simulate time-domain transients in underground cables accurately considering frequency dependent effects. The idea of mesh domain modelling arose from a relaxed chat over coffee with Prof. L.M. Wedephol to which the author is greatly indebted.

Rather than convert the equations using eigenvector matrices to true modal form, the proposed mesh method uses mesh voltages and currents. The advantage of the approach is that the resulting transformation matrix between phase and mesh domains is frequency independent. The conventional phase domain formulation, which uses conductor and sheath voltages and currents, can be numerically challenging due to the superposition of independent traveling waves arising from the coupling of modes. This results in oscillatory behaviour in the frequency response of elements of  $A$ , which makes delay extraction and low order rational function approximation difficult and numerically inefficient. As will be shown, in the proposed mesh domain formulation, the mesh currents and voltages in co-axial cables are naturally decoupled at high frequencies due to the shielding effects of the conductors, suggesting the possibility that the above oscillatory behaviour may be avoidable.

#### **3.2 Development of the Mesh Domain Model**

The mesh –domain equations are developed for the co-axial cable geometry shown in Fig 3.1.

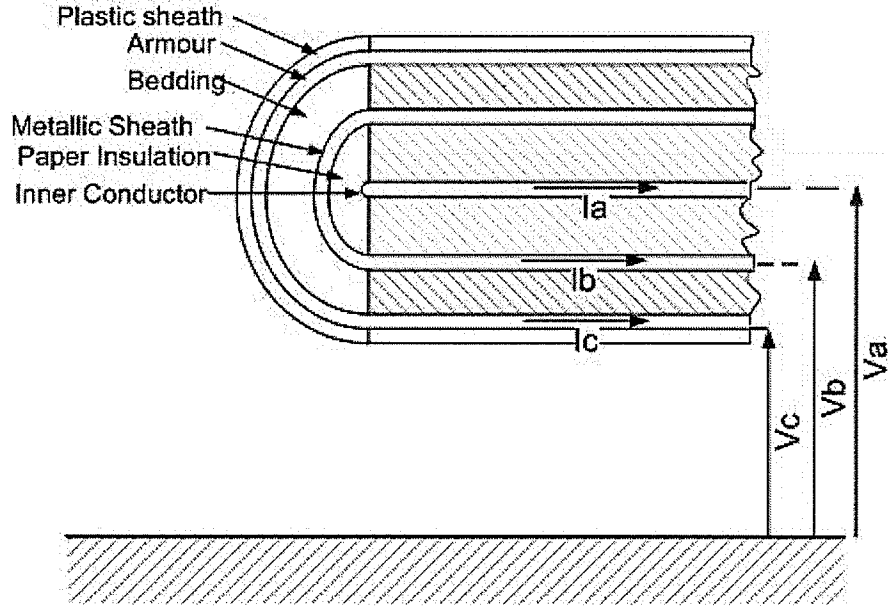


Figure 3.1: Phase voltages and currents in a coaxial cable system

### 3.2.1 Basic Mesh-Domain Equations

Series impedance ( $Z$ ) and shunt admittance ( $Y$ ) matrices are the basic building blocks of any TL model. The approach of section 2.1 is also valid for underground cables, and the resulting relationships between phase voltage and current phasors for a cable are as given below in (3.1a) and (3.1b),

$$\frac{dV_p}{dx} = -ZI_p \quad (3.1a)$$

$$\frac{dI_p}{dx} = -YV_p \quad (3.1b)$$

where,  $V_p$  is the vector of phase voltage (conductor to ground) phasors,  $I_p$  is the vector of phase current (current through each phase or conductor) phasors through each conductor and  $x$  is the

distance along the line. The dimension of the current (or voltage) vector is  $n \times 1$  for an  $n$ -conductor system.  $Z$  and  $Y$  are square  $n \times n$  matrices.

In this new approach, the currents and voltages of a cable are defined in mesh domain as shown in figure 3.2. Instead of selecting inner conductor to ground, sheath to ground, armour to ground voltages, the new set of voltages are chosen as voltage between inner conductor and sheath, sheath and armour, and armour and ground. Similarly the currents are selected from conductor to conductor, instead of conductor to ground.

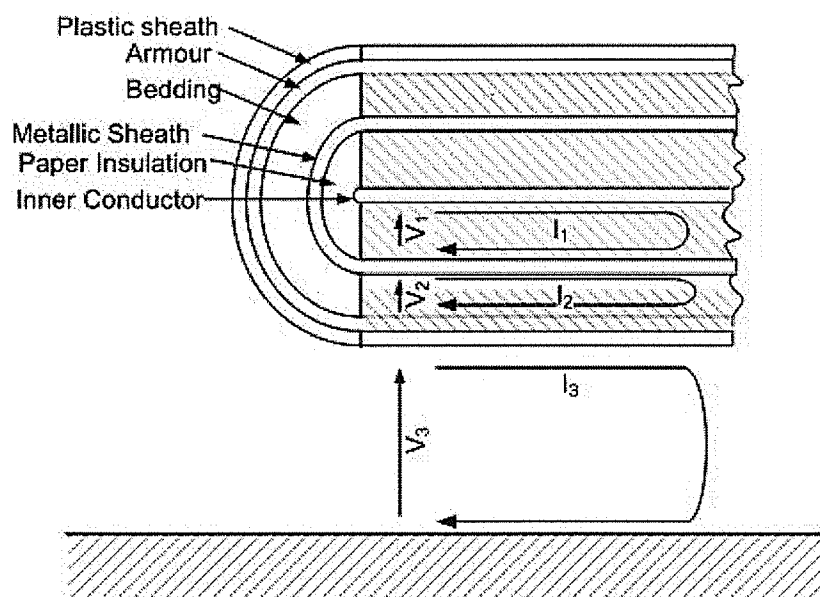


Figure 3.2: Mesh voltages and currents in a cable

The series impedance and shunt admittance matrices are formulated in the mesh domain, which causes separation of modes as the frequency increases. This results in smooth frequency responses of entries of matrix  $A$ . The transformation matrix from phase to mesh domain is real and constant as it is based directly on Kirchhoff's current law.

$$\frac{dV_{mesh}}{dx} = -Z_{mesh}I_{mesh} \quad (3.2a)$$

$$\frac{dI_{mesh}}{dx} = -Y_{mesh}V_{mesh} \quad (3.2b)$$

### 3.2.2 Shunt admittance and series impedance matrices in mesh domain

The self and mutual impedances and admittances between the cable conductors can be represented using the per unit length equivalent circuit shown in Fig. 3.3. Here,  $Z_{jj}$  is the self impedance of  $j^{th}$  loop. And  $Z_{ij}$  is the mutual impedance between  $i^{th}$  and  $j^{th}$  loops.

$$Z_{11} = \text{impedances of internal conductor } (Z_{conductor}) + \text{insulator between first sheath and conductor } (Z_{insulator}) + \text{inner first sheath } (Z_{inner\_sheath}). \quad (3.3)$$

$$Z_{mi} = \text{mutual impedance of } i^{th} \text{ sheath } (Z_{sheath\_mutual}) \quad (3.4)$$

$$Z_{ii} = \text{sum of impedances of outer } (i-1)^{th} \text{ sheath } (Z_{outer\_sheath}) + (i-1)^{th} \text{ insulator } (Z_{insulator}) + \text{inner } i^{th} \text{ sheath } (Z_{inner\_sheath}). \quad (3.5)$$

$$Z_{nn} = \text{sum of impedances of outer } (n-1)^{th} \text{ sheath } (Z_{outer\_sheath}) + \text{the } (n-1)^{th} \text{ insulator } (Z_{insulator}) + \text{self earth return}. \quad (3.6)$$

$Y_{ii}$  = shunt admittance between two adjacent conductor layers.

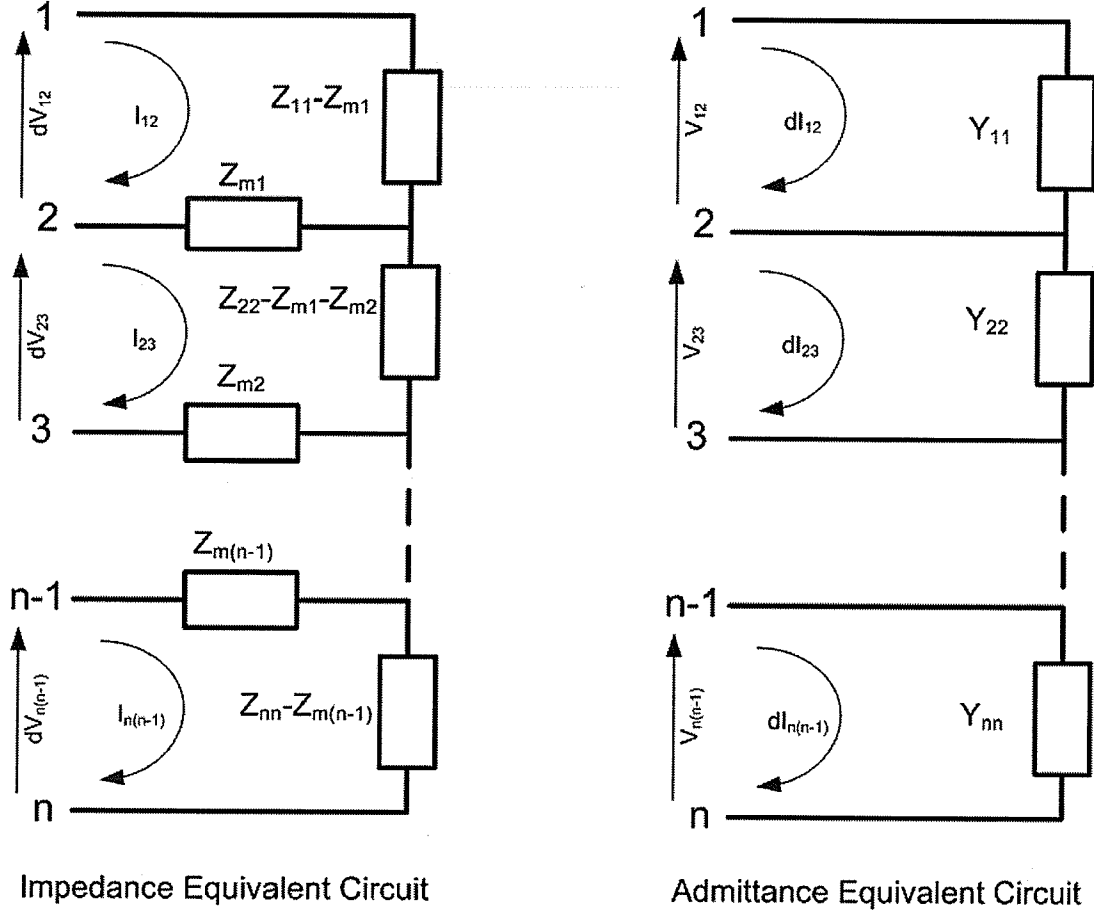


Figure 3.3: Equivalent circuits for unit length admittance and impedance

The traditional phase domain series impedance and shunt admittance matrices per unit length can be written in terms of the above mesh-domain impedances and admittances. With the meshes selected from phase to ground, the impedance and admittance matrices can be constructed as follows.

- (1) The series impedance matrix per unit length ( $\tilde{Z}$ ) can be defined as,



$$\text{k}^{\text{th}} \text{diagonal element, } \tilde{Z}(k,k) \quad (3.7)$$

$$= \sum_{i=k}^n Z_{ii} - 2 \sum_{i=k}^{n-1} Z_{mi}$$

$$\text{Off diagonal term, } \tilde{Z}(p,q) \quad (3.8)$$

$$= \sum_{i=p}^n Z_{ii} - Z_{mp}$$

$$= Z_{q,p}$$

$$\tilde{Z} = \begin{bmatrix} Z_{11} + ..Z_{nn} - 2(Z_{m1} + ..Z_{m(n-1)}) & Z_{22} + ..Z_{nn} - Z_{m1} - 2(Z_{m2} + Z_{m3}) & \cdot & Z_{nn} - Z_{m(n-1)} \\ Z_{22} + ..Z_{nn} - Z_{m1} - 2(Z_{m2} + Z_{m3}) & Z_{22} + ..Z_{nn} - 2(Z_{m2} + ..Z_{m(n-1)}) & \cdot & Z_{nn} - Z_{m(n-1)} \\ \cdot & \cdot & \cdot & Z_{nn} - Z_{m(n-1)} \\ Z_{nn} - Z_{m(n-1)} & Z_{nn} - Z_{m(n-1)} & Z_{nn} - Z_{m(n-1)} & Z_{nn} \end{bmatrix}$$


---

(3.9)

(2) Shunt admittance matrix  $(\tilde{Y})$  per unit length

$$\tilde{Y} = \begin{bmatrix} Y_{11} & -Y_{11} & \cdot & 0 \\ -Y_{11} & Y_{11} + Y_{22} & \cdot & 0 \\ \cdot & \cdot & \cdot & -Y_{(n-1)(n-1)} \\ 0 & 0 & -Y_{(n-1)(n-1)} & Y_{nn} + Y_{(n-1)(n-1)} \end{bmatrix} \quad (3.10)$$

These matrices are formulated in the phase domain choosing the conductor currents 1-g, 2-g, 3-g...n-g as the variables. Phase currents and phase voltages (conductor to ground) have significantly mutual coupling within the frequency range from 0 Hz to 1 MHz. This results in oscillatory behavior in propagation and characteristic admittance functions, when plotted as a function of frequency. Due to this undesirable oscillatory behavior, the delay extraction is very difficult for the elements of propagation matrix. Furthermore a higher order fit is usually required for the rational function approximation due to the oscillatory nature of elements of propagation matrix both in magnitude and phase. This leads to an inefficient model.

This difficulty can be significantly reduced by choosing different formulation for  $\tilde{Y}$  and  $\tilde{Z}$  matrices. The new current meshes or meshes are selected as 1-2, 2-3, 3-4..., and (n-1)-n. The  $\tilde{Y}$  and  $\tilde{Z}$  matrices formulated in this new mesh domain are,

$$\tilde{Z} = \begin{bmatrix} Z_{11} & -Z_{m1} & . & 0 \\ -Z_{m1} & Z_{22} & . & 0 \\ . & . & . & -Z_{m(m-1)} \\ 0 & 0 & -Z_{m(m-1)} & Z_{mm} \end{bmatrix} \quad (3.11)$$

$$\tilde{Y} = \begin{bmatrix} Y_{11} & 0 & . & 0 \\ 0 & Y_{22} & . & 0 \\ . & . & . & 0 \\ 0 & 0 & 0 & Y_{nn} \end{bmatrix} \quad (3.12)$$

The mutual impedances tend to zero as frequency increases. This can be easily proved from the formula for mutual impedance (B.6) in appendix B. Thus the  $\tilde{Z}$  matrix formulated in the new mesh domain becomes increasingly diagonal at high frequencies. Since  $\tilde{Y}$  is already a diagonal matrix, the

currents (as well as voltages) defined in the new mesh domain become decoupled at high frequencies. In other words the system supports almost independent traveling waves. This is a good approximation to a pure modal domain system at very high frequencies.

Both magnitude and phase of elements of propagation matrix ( $A$ ) are relatively smooth functions of frequency compared with that of direct phase domain formulation (phase to ground). This is a significant advantage for rational function approximation of the propagation function. A low order fit can be found and this leads to an efficient model. This is particularly true for the elements of characteristic admittance matrix as well.

Since the frequency responses of the diagonal elements of  $A$  matrix are relatively smooth, it is easy to extract the time delay. The delay is usually evaluated using Bode's gain phase formula (Appendix C) as described in section (2.1) at the highest frequency point of interest (corresponding to the fastest traveling wave). This delay extraction is relatively easy in new mesh domain rather than in phase domain due to smooth behaviour of propagation function at high frequencies. There are still some difficulties in delay extraction for off-diagonal elements for some cable systems (e.g. cable systems with widely different modal time delays, some complicated cable systems). An alternative optimization method was developed to calculate time delay (see Appendix C for details).

### 3.2.3 Transformation Matrices

In order to use the potentially powerful features of the mesh domain method demonstrated earlier, it is necessary to transform voltages and currents in phase domain to new mesh domain and vice versa. The voltage transformation matrix can be derived as follows.

$$\begin{aligned}
 V_{1g} &= V_{12} + V_{23} + V_{34} + \dots V_{(n-1)n} \\
 V_{2g} &= V_{23} + V_{34} + \dots V_{(n-1)n} \\
 &\dots\dots\dots \\
 V_{ng} &= V_{(n-1)n}
 \end{aligned} \tag{3.13}$$

Note that suffix 'g', 'phase', 'mesh' denote ground, traditional phase domain and the new proposed mesh domain respectively.

$$V_{phase} = K_V V_{mesh} \tag{3.14}$$

The voltage transformation matrix  $K_V$  is defined as,

$$K_V = \begin{bmatrix} 1 & 1 & 1 & \dots & 1 \\ 0 & 1 & 1 & \dots & 1 \\ 0 & 0 & 1 & \dots & 1 \\ \dots & \dots & \dots & \dots & \dots \\ 0 & 0 & 0 & 0 & 1 \end{bmatrix} \tag{3.15}$$

Similarly the current transformation matrix can be derived by considering phase to mesh transformation for currents.

$$I_{1g} = I_{12} \quad (3.16)$$

$$I_{2g} = -I_{12} + I_{23}$$

.....

$$I_{(n-1)g} = -I_{(n-2)(n-1)} + I_{(n-1)n}$$

$$I_{phase} = K_I I_{mesh} \quad (3.17)$$

The current transformation matrix  $K_I$  is defined as,

$$K_I = \begin{bmatrix} 1 & 0 & 0 & . & 0 \\ -1 & 1 & 0 & . & 0 \\ 0 & -1 & 1 & . & 0 \\ . & . & . & . & 0 \\ 0 & 0 & 0 & -1 & 1 \end{bmatrix} \quad (3.18)$$

Another advantage of mesh method is that current and voltage transformation matrices are real and constant avoiding the difficulties with frequency dependent transformation matrices.

It can be easily shown that,

$$K_V = (K_I^T)^{-1} \quad (3.19)$$

The relationship between characteristic admittance matrix in mesh  $Y_{c, mesh}$  and in phase domain  $Y_{c, phase}$  is derived as follows,

$$I_{mesh} = Y_{c, mesh} V_{mesh} \quad (3.20)$$

By substituting (3.14) and (3.17) in (3.20), we get

$$Y_{c, phase} = K_I Y_{c, mesh} K_I^T \quad (3.21)$$

In a similar manner, the transformation for the propagation matrix from mesh to phase can be derived as in (3.23),

$$I_{mesh}(x) = A_{mesh} I_{mesh}(x=0) \quad (3.22)$$

By substituting (3.17) in (3.22), we get

$$A_{phase} = K_I A_{mesh} K_V^T \quad (3.23)$$

Table 3.1 shows a summary of conversions from mesh to phase and vice versa.

Phase domain to mesh	Mesh domain to phase
$V_{mesh} = K_I^T V_{phase}$	$V_{phase} = K_V V_{mesh}$
$I_{mesh} = K_V^T I_{phase}$	$I_{phase} = K_I I_{mesh}$
$Z_{mesh} = K_I^T Z_{phase} K_I$	$Z_{phase} = K_V Z_{mesh} K_V^T$
$Y_{mesh} = K_V^T Y_{phase} K_V$	$Y_{phase} = K_I Y_{mesh} K_I^T$
$A_{mesh} = K_V^T A_{phase} K_I$	$A_{phase} = K_I A_{mesh} K_V^T$
$Y_{c,mesh} = K_V^T Y_{c,phase} K_V$	$Y_{c,phase} = K_I Y_{c,mesh} K_I^T$

Table 3.1: Conversion table

### 3.3 Equivalent Circuit in Time Domain

The frequency domain transmission line equations written in terms of new mesh domain variables are,

$$I_{m,mesh} = Y_{c,mesh} V_{m,mesh} - A_{mesh} (Y_{c,mesh} V_{k,mesh} + I_{k,mesh}) \quad (3.24a)$$

$$I_{k,mesh} = Y_{c,mesh} V_{k,mesh} - A_{mesh} (Y_{c,mesh} V_{m,mesh} + I_{m,mesh}) \quad (3.24b)$$

As discussed in section 2.1, the above frequency domain expressions are then to be converted in to time domain equivalent circuit in order to implement in electromagnetic transient programs such as PSCAD/EMTDC. However, the time domain circuit must be ultimately expressed in phase domain,

since phase currents and phase voltages are easily dealt with terminal conditions. If equation (3.24a) is multiplied by current transformation matrix  $K_I$  ,

$$K_I I_{m,mesh} = K_I Y_{c,mesh} K_V^{-1} K_V V_{m,mesh} - K_I A_{mesh} (Y_{c,mesh} V_{k,mesh} + I_{k,mesh}) \quad (3.25)$$

Then by substituting (3.17), equation (3.25) becomes,

$$I_{m,phase} = K_I Y_{c,mesh} V_{m,mesh} - K_I A_{mesh} (Y_{c,mesh} V_{k,mesh} + I_{k,mesh}) \quad (3.26)$$

Define  $F_k$  as,

$$F_k = A_{mesh} (Y_{c,mesh} V_{k,mesh} + I_{k,mesh}) \quad (3.27)$$

Then equation (3.26) becomes,

$$I_{m,phase} = K_I Y_{c,mesh} V_{m,mesh} - K_I F_k \quad (3.28)$$

The time domain form of (3.28) is,

$$i_{m,phase}(t) = K_I y_{c,mesh}(t) * v_{m,mesh}(t) - K_I f_k(t) \quad (3.29)$$

Where, the term "\*" denotes convolution and,



$$f(t) = a_{mesh}(t) * (y_{c,mesh}(t) * v_{k,mesh}(t) + i_{k,mesh}(t)) \quad (3.30)$$

The lower case variables are the corresponding time domain form of the upper case variables. The above convolutions can be efficiently evaluated by recursive convolution method described in section (2.1) and the equation (3.29) now becomes,

$$i_{m,phase}(t) = \tilde{y}_{eq\_m} v_{m,mesh}(t) + i_{hist\_m}(t) \quad (3.31)$$

With mesh to phase conversion as in (3.14), equation (3.31) can be written as,

$$i_{m,phase}(t) = y_{eq} v_{m,phase}(t) + i_{hist\_m}(t) \quad (3.32)$$

Where,  $y_{eq\_m} = \tilde{y}_{eq\_m} K_I^T$ . Similarly for the other end of the transmission line,

$$i_{k,phase}(t) = y_{eq} v_{k,phase}(t) + i_{hist\_k}(t) \quad (3.33)$$

Equations (3.32) and (3.33) suggest a time domain equivalent circuit, which can be realized in popular electromagnetic transient programs,

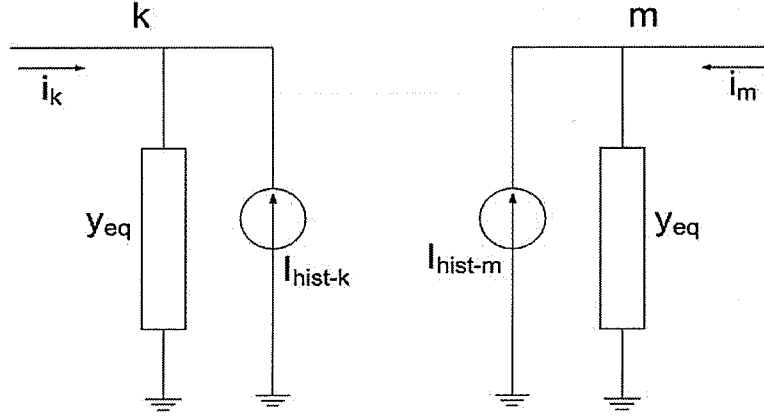


Figure 3.4: Time domain equivalent circuit

### 3.4 Mesh Domain Modelling for Multi-cable Systems

The procedure for modelling multi-cable configurations in mesh domain is same as that described in the preceding section 3.3 for single cable system. However the transformation matrices derived for single-cable case are different from that for multi-cable case. This section briefly describes the derivation of transformation matrices taking a simple example involving a cable configuration similar to a cable system shown in Figure 3.6.

For simplicity, it is assumed that each cable of the two-conductor system has an inner conductor and a sheath. Figure 3.5 shows the per unit length impedance equivalent circuit.  $Z_{me}$  is the earth mutual impedance (frequency dependent) between two cables. By considering mesh voltages and phase voltages, the following relationships can be built.

$$V_{1g} = V_{12} + V_{2n} \quad (3.34)$$

$$V_{2g} = V_{2n}$$

$$V_{3g} = V_{34} + V_{4n}$$

$$V_{4g} = V_{4n}$$

The voltage transformation matrix  $K_V$  becomes,

$$K_V = \begin{bmatrix} 1 & 1 & 0 & 0 \\ 0 & 1 & 0 & 0 \\ 0 & 0 & 1 & 1 \\ 0 & 0 & 0 & 1 \end{bmatrix} \quad (3.35)$$

Similar relationship can be built for the currents in mesh and phase domain,

$$I_1 = I_{12} \quad (3.36)$$

$$I_2 = I_{2n} - I_{12}$$

$$I_3 = I_{34}$$

$$I_4 = I_{4n} - I_{34}$$

The current transformation matrix becomes,

$$K_I = \begin{bmatrix} 1 & 0 & 0 & 0 \\ -1 & 1 & 0 & 0 \\ 0 & 0 & 1 & 0 \\ 0 & 0 & -1 & 1 \end{bmatrix} \quad (3.37)$$

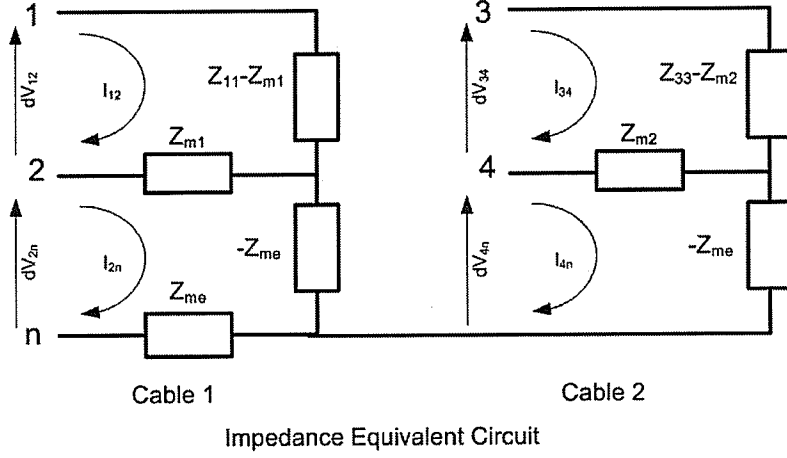


Figure 3.5: Equivalent circuit for unit length impedance

The impedance matrix in mesh domain can be written in terms of self-impedance of each cable and earth mutual impedance as follows.

$$\tilde{Z} = \begin{bmatrix} Z_{1,1}^1 & Z_{1,2}^1 & 0 & 0 \\ Z_{2,1}^1 & Z_{2,2}^1 & 0 & Z_{me} \\ 0 & 0 & Z_{1,1}^2 & Z_{1,2}^2 \\ 0 & Z_{me} & Z_{2,1}^2 & Z_{2,2}^2 \end{bmatrix} \quad (3.38)$$

where,  $Z_{i,j}^k$  is the  $(i,j)^{th}$  element of the impedance matrix for the  $k^{th}$  cable ( $k = 1,2$ ) derived as described in section 3.2.2.  $Z_{me}$  is the earth mutual impedance between two cables. Since only the outermost conductor of each cable is coupled to the other,  $\tilde{Z}(2,4) = \tilde{Z}(4,2) = Z_{me}$  and all other mutual entries are zero ( $\tilde{Z}(1,3) = \tilde{Z}(1,4) = \tilde{Z}(2,3) = 0$  etc.).

Since there is no coupling in the admittance equivalent circuit, the admittance matrix in mesh domain becomes,

$$\tilde{Y} = \begin{bmatrix} Y_{1,1}^1 & 0 & 0 & 0 \\ 0 & Y_{2,2}^1 & 0 & 0 \\ 0 & 0 & Y_{1,1}^2 & 0 \\ 0 & 0 & 0 & Y_{2,2}^2 \end{bmatrix} \quad (3.39)$$

where,  $Y_{i,j}^k$  is the  $(i,j)^{th}$  element of the admittance matrix for the  $k^{th}$  cable ( $k = 1,2$ ) derived as described in section 3.2.2. This section briefly described the derivation of mesh domain impedance and admittance matrices for two-cable configuration. The derivation can be generalized for higher number of cable systems.

### 3.4.1 Rational Function Approximation of $Y_c$ and $A$

Once mesh domain  $\tilde{Z}$  and  $\tilde{Y}$  matrices are computed (as discussed in section 3.4), mesh  $A$  and mesh  $Y_c$  are then calculated using equations (2.26) and (2.27). The next step is the rational function approximation (curve-fitting) of entries of the characteristic admittance ( $Y_c$ ) and propagation ( $A$ ) matrices.

#### Time delay estimation and curve-fitting of $A$

The model developed in the thesis assumes multiple-delay form for the propagation function (similar to the ULM) as shown in (3.40), (see section 2.4.2.3 for further details). The modal delays ( $\tau_i$ ) in equation (3.40) are estimated using Bode's gain-phase formula from modes of mesh  $A$  matrix (see appendix C for delay estimation using Bode's formula). The modes are the eigenvalues of  $A$  matrix calculated as described in section 2.3.

$$A_{i,j}(s) \approx e^{-sr_1} \sum_{n_1=1}^{N_1} \frac{c'_{n_1}}{s - a_{n_1}} + e^{-sr_2} \sum_{n_2=1}^{N_2} \frac{c'_{n_2}}{s - a_{n_2}} + \dots \quad (3.40)$$

Identification of poles  $(a_{n_i})$  and residues  $(c'_{n_i})$  in (3.40)

The developed model exploits a feature in the Vector Fitting algorithm, in which two or more functions can be simultaneously curve-fitted using a common set of poles [40], [43], [41]. Each column of the mesh propagation matrix is approximated with a common set of poles using the modified Vector fitting algorithm [67] (i.e. the unknown residues and poles in (3.40) are calculated by curve-fitting each column of the propagation matrix and the entries in a column share same set of poles); hence the numerical efficiency of the model is improved.

This model can be also used in situations where the phase domain Universal Line Model (ULM) [44] does not always give satisfactory results. Earlier researchers observed that there were difficulties in curve-fitting the modes in ULM for some cable systems [67]. Since this model does not involve curve-fitting of modes of propagation matrix and the mesh domain formulation is based on actual mesh currents and voltages, entries of mesh propagation matrix can be satisfactorily approximated using rational functions.

### 3.5 Application Example

In order to explain the advantages of the proposed mesh domain method, an example underground cable system is considered. Figure 3.6 shows a three-cable system (each has an inner conductor and sheath) with data shown in Table 3.2. The typical plots of entries of the propagation matrix

formulated in traditional phase domain are shown in Figure 3.7, clearly indicating the oscillatory behavior of phase domain elements, when plotted as a function of frequency.

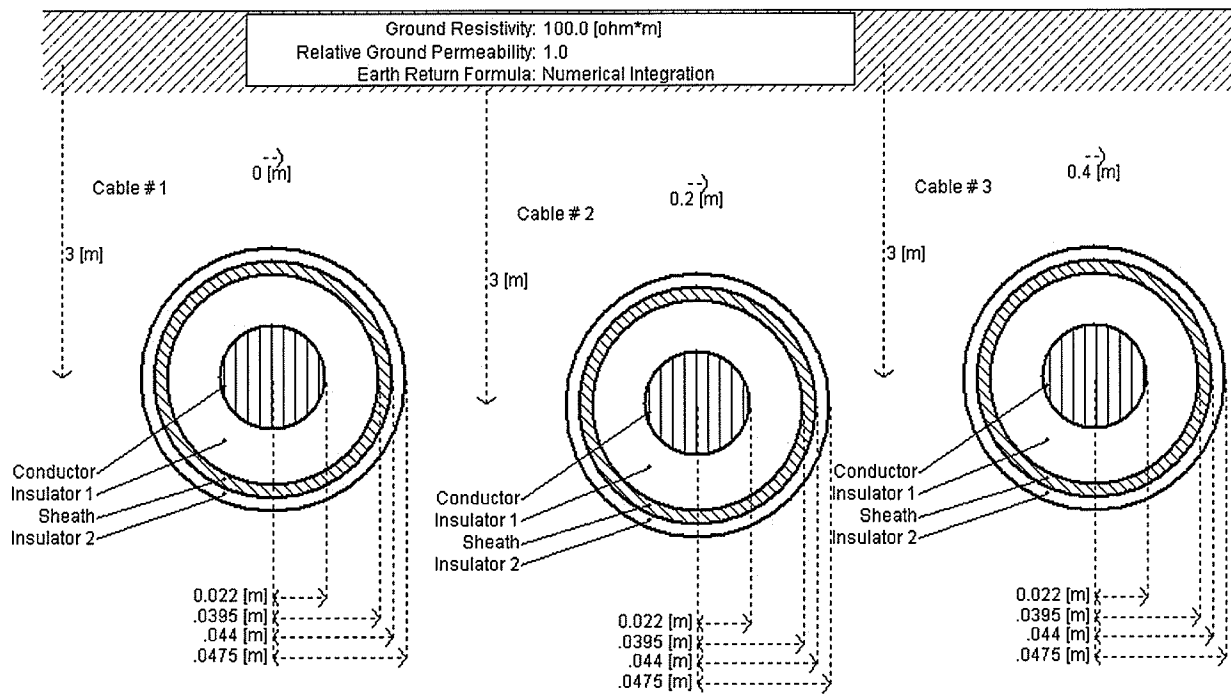


Figure 3.6: Three cable system

Resistivity of the inner conductor $\square (\Omega m)$	1.68e-8
Resistivity of the outer conductor $(\Omega m)$	2.2e-7
Relative permittivity of inner and outer insulators	4.1/3.2
Earth resistivity $(\Omega m)$	100
Length of the cable system (km)	30

Table 3.2: Cable data

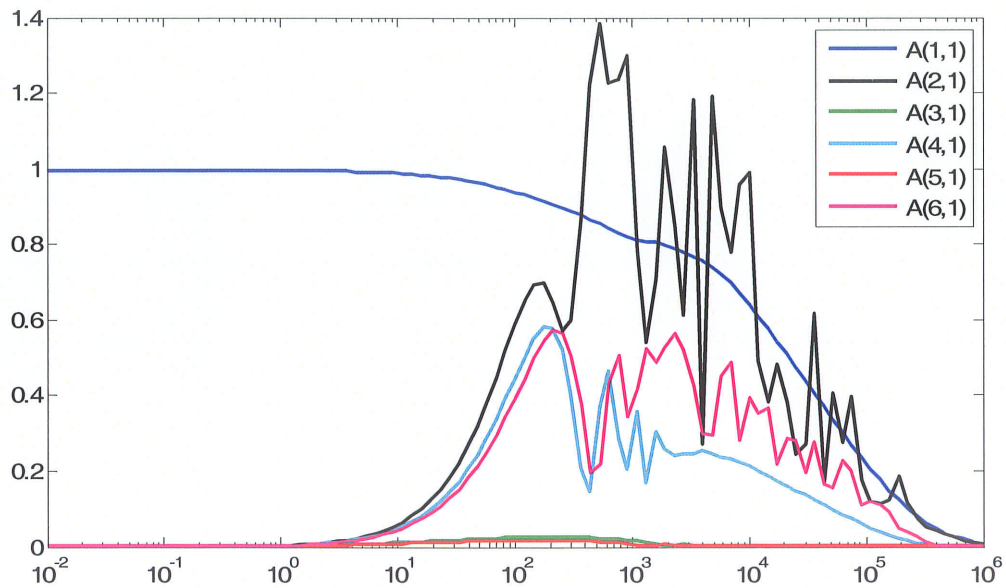


Figure 3.7: First column of the phase propagation matrix

If the propagation matrix is formulated in the mesh domain, the frequency domain responses of elements of mesh propagation matrix (see Figure 3.8) show smooth behaviour in contrast to that of the phase domain functions. The fitted first column of mesh domain propagation matrix is shown in



Figure 3.9 as a function of frequency. Also shown in the graphs are the theoretical (actual) curves (the solid lines in the same figure) indicating that the fitting is accurate. In comparison with phase domain elements, mesh domain elements are smooth and hence easy to curve-fit using low order rational functions. Table 3.3 compares the order of rational function for mesh domain with phase domain formulation. For the propagation function, order of the transfer function is reduced noticeably by 30%, if mesh formulation is used and hence leads to a numerically efficient model.

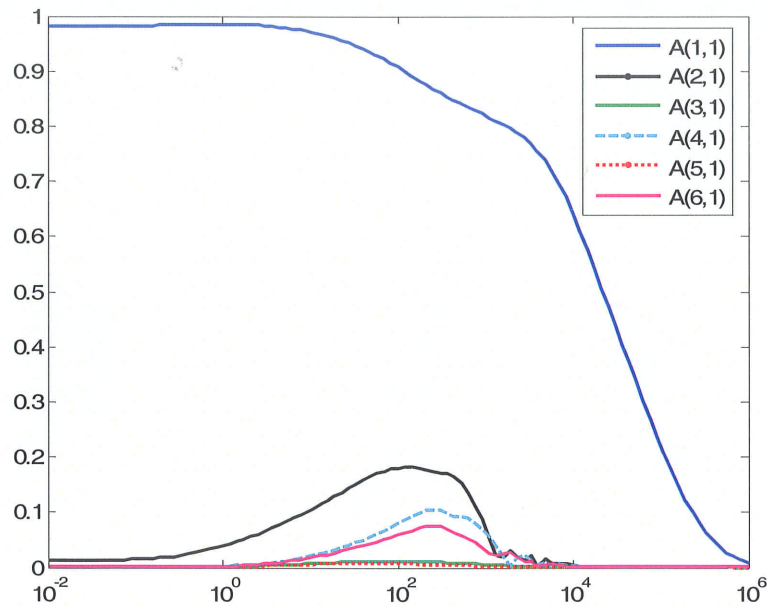


Figure 3.8: First column of the mesh propagation matrix

Order of phase Yc	10
Order of mesh Yc	10
Order of phase A	43
Order of mesh A	33

Table 3.3: Order comparison (per element)

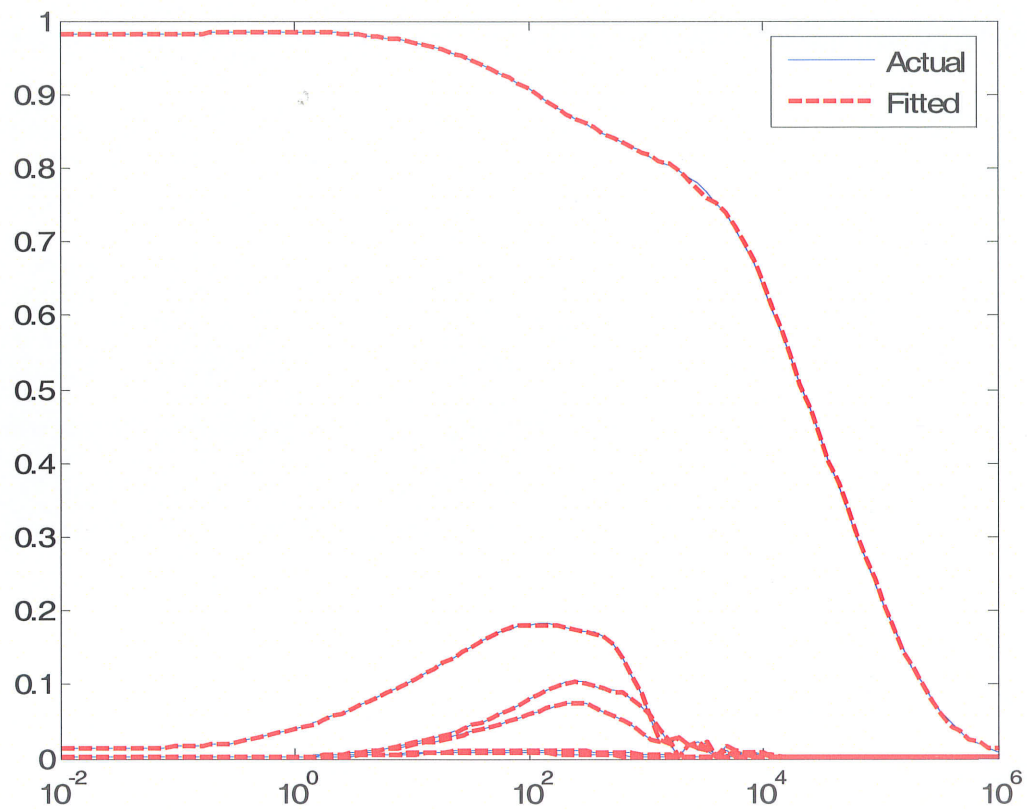


Figure 3.9: Actual and fitted mesh propagation functions (first column)

Time domain simulations are conducted to validate the proposed mesh domain model. A short circuit test is conducted for the same cable system. The inner conductor of cable 1 is energized with 1V step, while all other conductors are connected to the ground. Figure 3.10 shows the sending-end current waveform (solid conductor) through inner conductor of cable 1 and the theoretical solution (dotted line) obtained via numerical inverse Laplace transform method. The current waveform from mesh domain model is in a close agreement with theoretical solution, indicating that simulation results from mesh domain model are accurate.

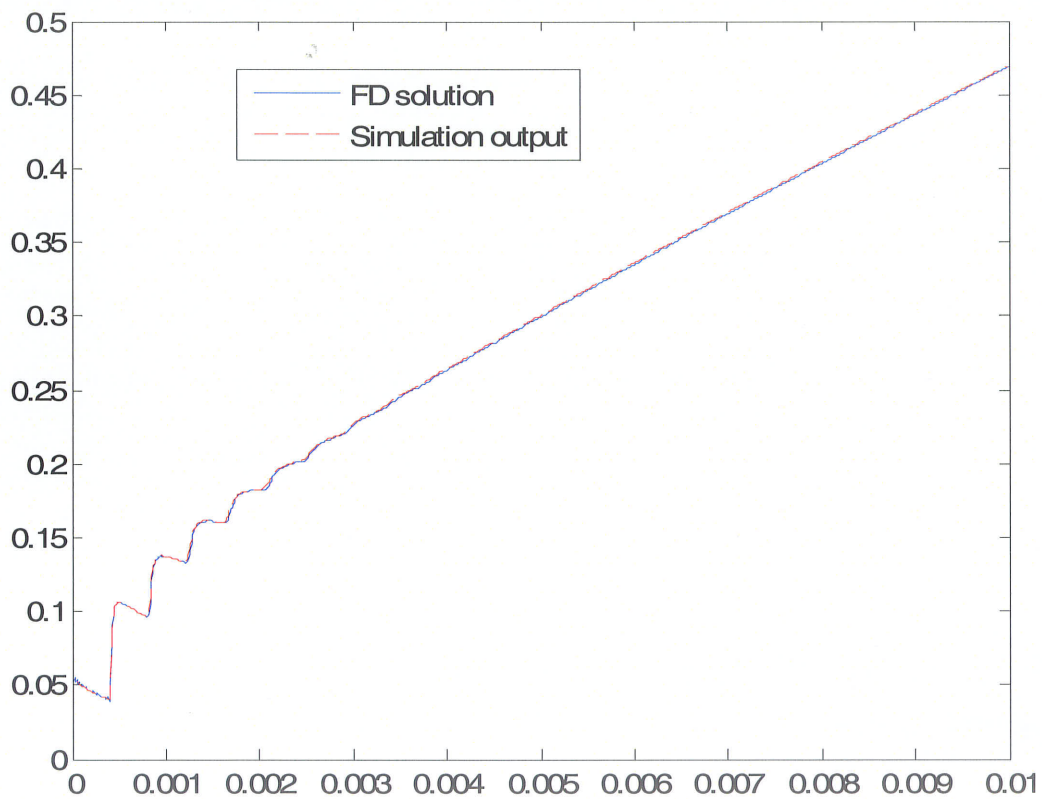


Figure 3.10: Sending-end current

Another simulation is conducted for the same cable system. A 1V step is applied to the inner conductor of cable 1 and all other terminations are kept open. Figure 3.11 shows the induced voltage (solid line) at the sending-end of the inner conductor of cable 2. Also shown in the graph (dotted line) is the theoretical solution. This confirms that the induced voltage is in a close agreement with theoretical results.

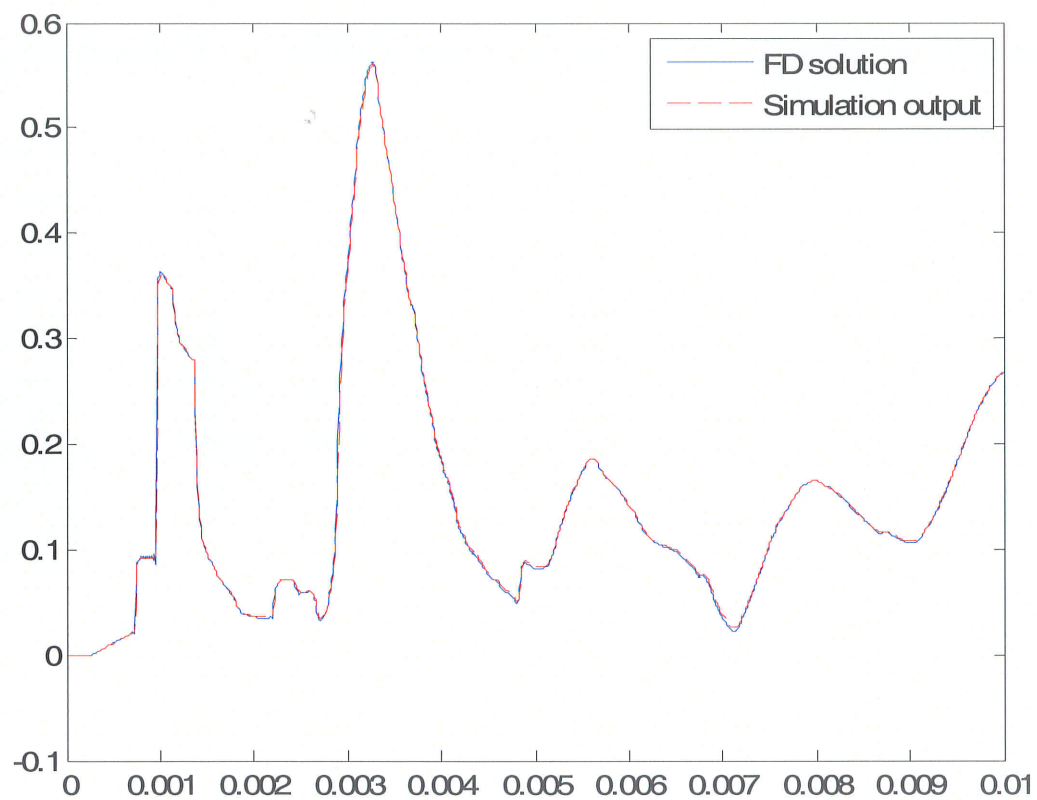


Figure 3.11: Induced voltage in the inner conductor of the cable 2

### 3.6 Chapter Summary

This chapter proposed a new mesh-domain method to simulate time-domain transients in underground cables accurately considering frequency dependent effects. One advantage of this approach is that the resulting transformation matrix between phase and mesh domains is frequency independent. The mesh currents and voltages in co-axial cables are naturally decoupled at high frequencies hence the propagation function shows relatively smooth behaviour. The rational function approximation in mesh domain is relatively easier than in basic phase domain methods. This model can be used in situations, where Universal Line Model does not give satisfactory results [67].



## Chapter 4

### Improving the asymptotic fitting of TL and cable models

#### 4.1 Introduction

This chapter introduces improvements to the low frequency fitting of the propagation and characteristic admittance functions [66]. These developments are driven by the need for accurate dc fitting for simulating High voltage direct current (HVDC) transients. HVDC transmission of power over long distances is seeing increasing application with HVDC lines and cables being installed all over the world. Simulation models for such systems are required to be accurate over a very wide frequency range from zero Hertz, which is the nominal frequency on the line to several tens of kilohertz for thyristor switching and other transients.

As discussed in Chapter 2, the use of modern phase domain modelling techniques coupled with transfer function estimation using Vector Fitting has greatly improved the accuracy of time-domain models for overhead transmission lines and cables [43]. However, although these time-domain models simulate the frequency range from a few Hertz to about several kilohertz, it has been difficult to get a good fit in the close neighborhood of 0 Hz (dc). For HVDC lines and cables, it is very important to accurately reproduce the response in the close vicinity of 0 Hz, as that is the nominal frequency on the line. Later in this chapter, it is shown that forcibly attempting to fit the line characteristic at these extremely low frequencies requires a high order for the rational function and sometimes leads to inaccurate fitting.

An efficient new approach is proposed in this thesis based on linearization and constrained least squares that achieves a highly accurate fitting over the full frequency range, with zero error at dc frequency. A modification is introduced to the functional form of the rational function approximated in the curve fitting procedure, such that the entries of the characteristic admittance and propagation matrices can be fitted with more accuracy without having to substantially increase the number of poles. Two possible variants of the functional form were attempted. In the first approach, the admittance and propagation transfer functions are reformulated so that the dc response is factored out as an additive constant which can be directly selected.

In the second approach, the transfer function is first fitted over the entire frequency range, which typically results in some fitting error at zero Hz. A low frequency first order pole is then added to the resultant fitted function in order to realize the exact response at dc, without significantly affecting the remainder of the frequency response. One of the issues with earlier models was that although the Vector Fitting procedure always had negative real parts in its poles, it sometimes violated conditions for passivity [62]; and hence the simulations could go unstable with certain types of line terminations. Later in the discussion, it is shown that the proposed approaches are less likely to result in passivity violations.

The above proposed methods are also compared with a simplified alternative approach which merely adds a corrective series resistance into each conductor to get the correct dc line resistance. However, this approach is shown to have poorer accuracy compared with the above approaches. Time domain simulations of various transients on HVDC underground cables are presented to verify the validity of the proposed methods. Finally the practical application of the developed modeling technique to a large non-linear network is demonstrated through the example of a Voltage Sourced Converter (VSC) based HVDC transmission system using underground cables.

## 4.2 Asymptotic behavior of transmission line parameters

This section presents the asymptotic behavior of transmission lines. As discussed in Chapter 2, the general TL equations, so called Telegrapher's equations are expressed in terms of series impedance and shunt admittance matrices (see equations (2.3a) and (2.3b) in Chapter 2). The series impedance of the overhead transmission lines consists of sum of basic impedances such as internal impedance of the conductor, ground return impedance etc [43], [15], [1]. In the case of underground cables, the components of the series impedance are internal impedance of inner conductor, sheath mutual, inner and outer sheath impedances etc. (see Appendix B for further details). The basic impedances of cables and transmission lines are functions of frequency, several other parameters and also depend on the geometry of the transmission line.

### 4.2.1 Overhead Transmission Lines

To demonstrate the asymptotic behavior of characteristics for overhead transmission lines, consider a single conductor transmission line. For overhead lines, the approximation formulae for conductor internal impedance, aerial and ground return impedance are given by [43], [15], [1],

$$Z_{internal}(\omega) = \frac{\rho_c}{2\pi r d_c} \coth\left(\frac{0.777r}{d_c}\right) + \frac{0.3585\rho_c}{\pi r^2} \quad (4.1)$$

$$Z_{aerial\&ground}(\omega) = \frac{j\omega\mu}{2\pi} \ln\left(\frac{D'}{r}\right) \quad (4.2)$$



where,

$\rho_c$  = resistivity of the conductor ( $\Omega\text{m}$ )

$d_c$  = complex depth of penetration for the conductor

$$= \sqrt{\frac{\rho_c}{j\omega\mu}}$$

$\mu$  = permeability of air (H/m)

$r$  = radius of the conductor (m)

$$D' = 2(y + d_g)$$

$d_g$  = complex depth of penetration for the ground

$$= \sqrt{\frac{\rho_g}{j\omega\mu}}$$

$\rho_g$  = resistivity of ground ( $\Omega\text{m}$ )

$y$  = height of the conductor from ground (m)

The complex depth of penetration of the conductor  $d_c$  can be regarded as the (complex) thickness of an annular tube of the same outer radius as the conductor, to which the current in the conductor is effectively confined. The complex depth of penetration for the ground can be visualized as an effective increase in the height of the conductor by the complex quantity  $d_g$  as shown in figure 4.1 [20], [24].

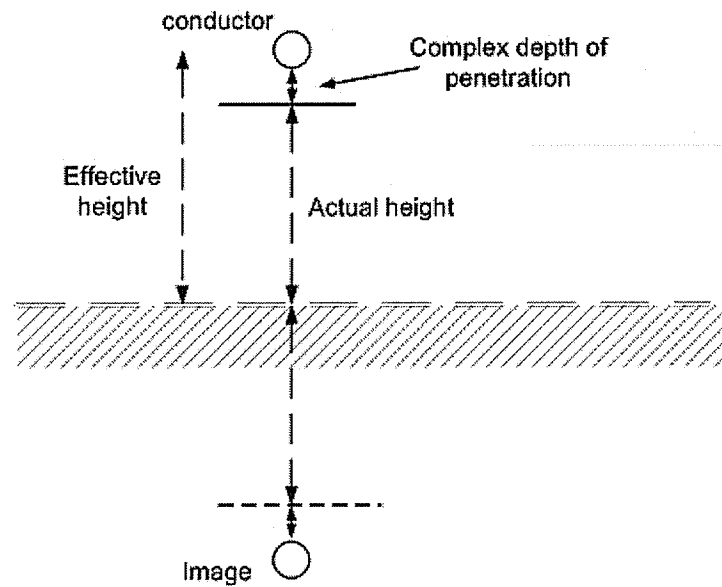


Figure 4.1: Actual height and the effective height of a conductor in the transmission line.

As the frequency tends to zero, the complex depth of penetration of the conductor,  $d_c$  becomes large. Thus the current density is equal throughout the cross section of the conductor, resulting in its internal impedance attaining a value equal to its dc resistance. The aerial and ground return impedance tends to zero. At very high frequencies, the internal impedance equals to skin effect impedance, which is equivalent to the impedance of an annulus with radius and thickness equal to  $r$  and  $d_c$  respectively [20], [24]. The typical plots of conductor internal impedance and aerial & ground return impedances are shown in figures (4.2) and (4.3) respectively for single conductor case.

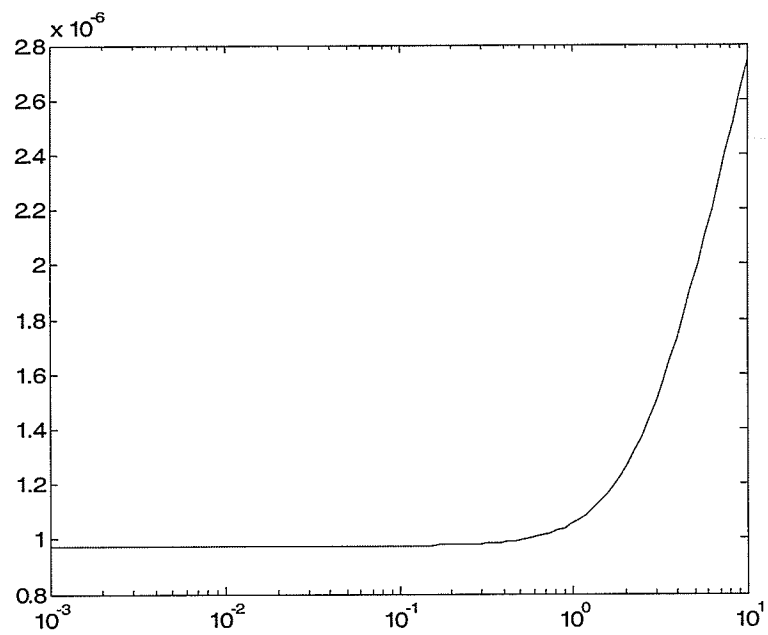


Figure 4.2 : Conductor internal impedance

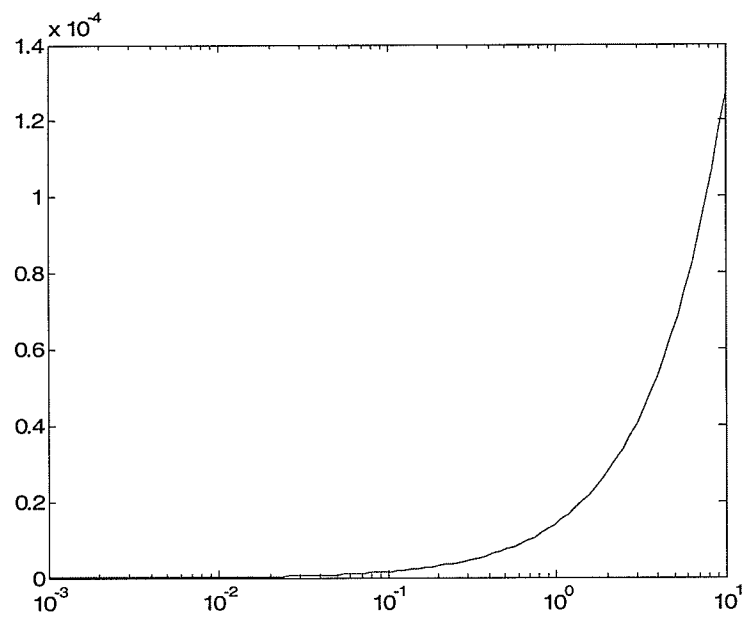


Figure 4.3 : Aerial & ground return impedance

For simplicity, a single conductor case is explained. The series impedance of the conductor is,

$$Z(\omega) = Z_{\text{internal}}(\omega) + Z_{\text{aerial \& ground}}(\omega) \quad (4.3)$$

The typical plot of the series impedance as a function of frequency is shown in figure 4.3.

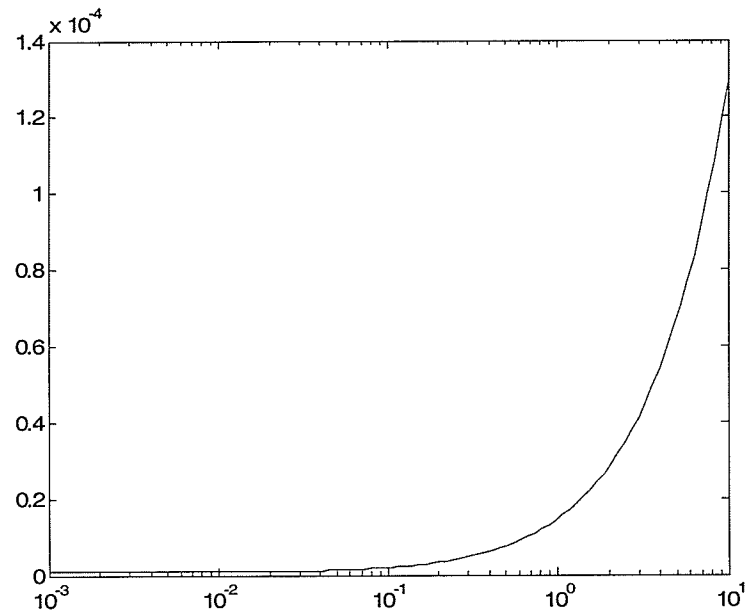


Figure 4.4 : Series impedance function

The shunt admittance  $Y(\omega)$  per unit length in Telegrapher's Equation (2.3b) can be written as,

$$Y(\omega) = g + j \frac{2\pi\epsilon_0\omega}{\ln\left(\frac{D}{r}\right)} \quad (4.4)$$

where,

$$D = 2y$$

$g$  = conductance per unit length (conductance of air)

	$Z_{\text{internal}}$	$Z_{\text{aerial\&ground}}$
Low frequencies	$\frac{\rho_c}{\pi r^2}$	0
High frequencies	$\frac{\rho_c}{2\pi r d_c}$	$\frac{j\omega\mu}{2\pi} \ln\left(\frac{D}{r}\right)$

Table 4.1:  $Z_{\text{internal}}$  and  $Z_{\text{aerial\&ground}}$  at very low and very high frequency

At zero frequency, the ground return impedance tends to zero and the  $Z(\omega = 0)$  and  $Y(\omega = 0)$  functions have the following form,

$$Z(\omega = 0) = R_{dc} \quad Y(\omega = 0) = g \quad (4.5)$$

where,  $g$  is the conductance per unit length and  $R_{dc}$  is the resistance per unit length. The propagation  $A(\omega)$  and characteristic admittance  $Y_c(\omega)$  functions are accordingly calculated as described in Chapter 2. At very high frequencies,  $Z(\omega)$  and  $Y(\omega)$  have the approximate forms  $j\omega L$  and  $j\omega C$ , where  $L$  and  $C$  are constants. Hence  $Y_c(\omega)$  approaches a constant and  $A(\omega)$  matrix tends to zero. The typical plots of  $Y_c(\omega)$  and  $Y_c(\omega)$  functions are shown in figure (4.5) and (4.6) respectively.

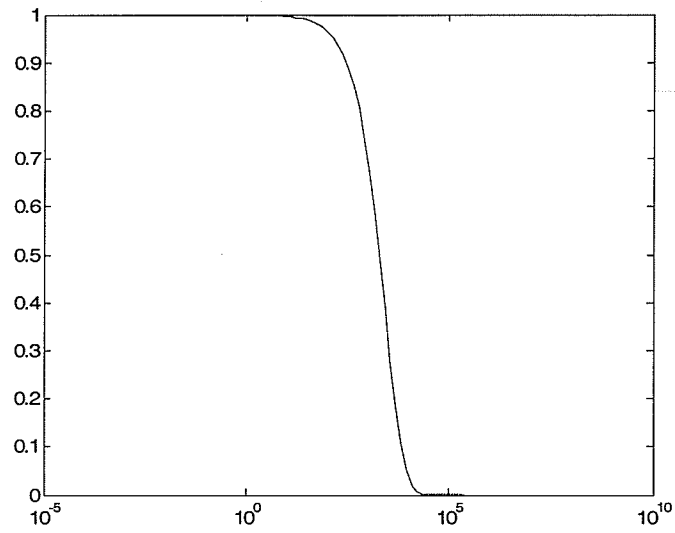


Figure 4.5: Typical plot of propagation function,  $A$

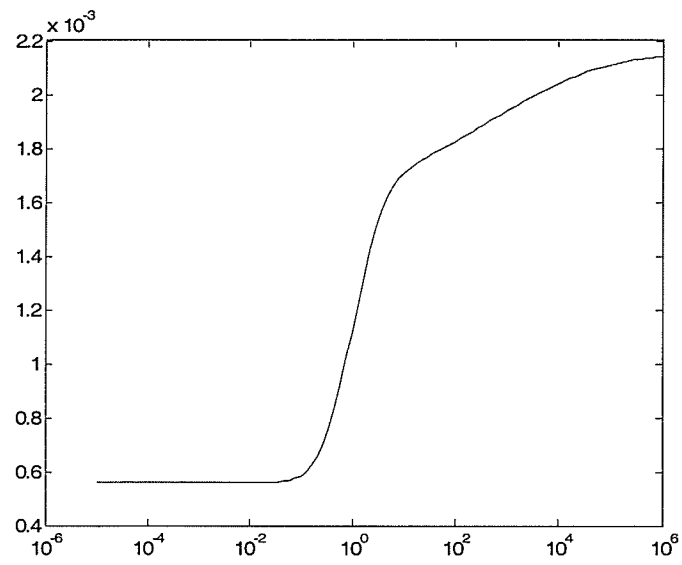


Figure 4.6: Typical plot of characteristic admittance function,  $Y_c$

### 4.2.2 Underground Cables

At very low frequencies, the conductor internal impedance approaches the dc resistance of the conductor (as calculated considering conductor cross sectional area, length and electrical resistance) . The sheath outer, mutual and inner impedances also approach to the sheath dc resistance and earth return impedance tends to zero. At very high frequencies, the internal, sheath inner, sheath outer and earth return impedances equal to the skin effect impedances. However the mutual impedance tends to zero. These impedances are shown in figures (4.7) and (4.8). As for the case of overhead transmission lines,  $Y_C(\omega)$  approaches a constant and  $A(\omega)$  matrix tends to zero at very high frequencies. The asymptotic behaviors of  $Y_C(\omega)$  and  $A(\omega)$  are similar to the case of overhead lines.

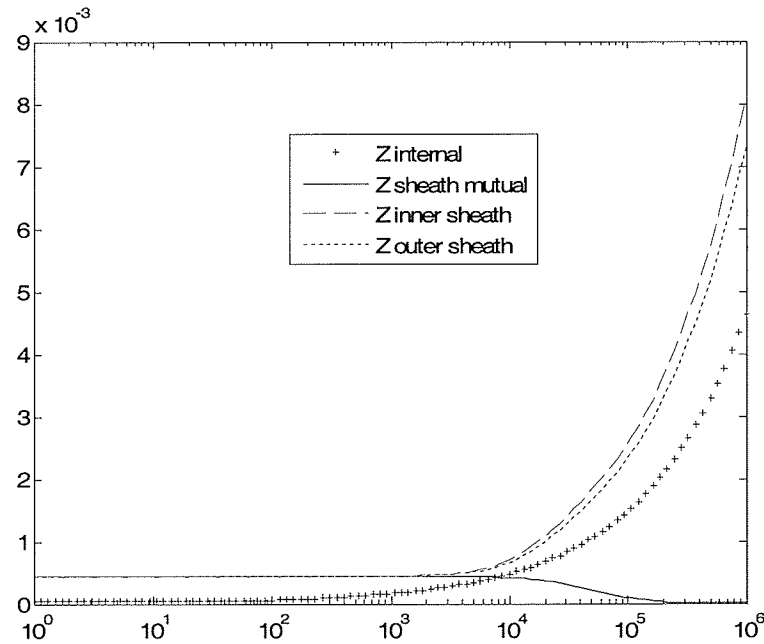


Figure 4.7: Typical plots of sheath and conductor impedances

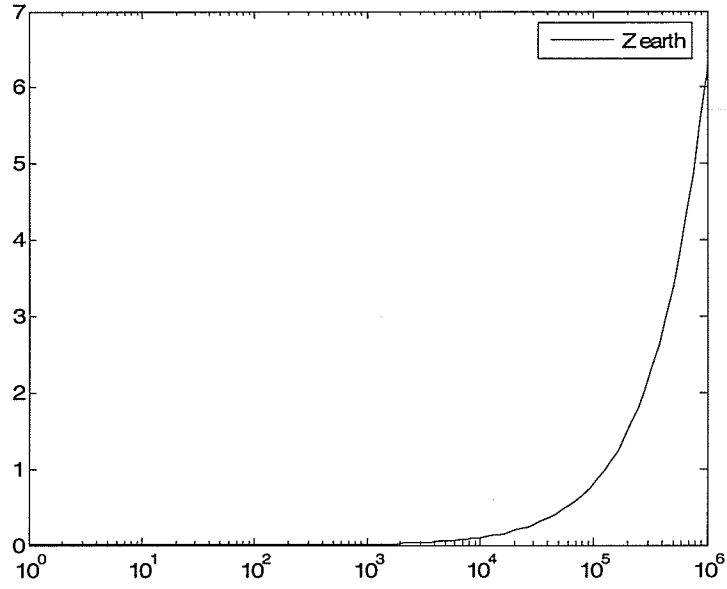


Figure 4.8: Typical plot of earth return impedance

	$Z_{\text{internal}}$	$Z_{\text{inner\_sheath}}$	$Z_{\text{sheath\_mutual}}$	$Z_{\text{outer\_sheath}}$
At Zero Hz	$\frac{\rho_c}{\pi r^2}$	$\frac{\rho_s}{\pi(r_{i+1}^2 - r_i^2)}$	$\frac{\rho_s}{\pi(r_{i+1}^2 - r_i^2)}$	$\frac{\rho_s}{\pi(r_{i+1}^2 - r_i^2)}$
High frequencies	$\frac{\rho_c m_c}{2\pi r}$	$\frac{\rho_s m_s}{2\pi r_i}$	0	$\frac{\rho_s m_s}{2\pi r_{i+1}}$

Table 4.2: Impedances at low and high frequencies

where,

$\rho_c$  = resistivity of the inner conductor ( $\Omega\text{m}$ )

$m_c$  = reciprocal of complex depth of penetration for inner conductor

$$= \sqrt{\frac{j\omega\mu_c}{\rho_c}}$$

$\mu_c$  = permeability of the conductor (H/m)

$r$  = radius of the conductor (m)



$\rho_s$  = resistivity of the sheath ( $\Omega\text{m}$ )

$m_c$  = reciprocal of complex depth of penetration for sheath

$$= \sqrt{\frac{j\omega\mu_s}{\rho_s}}$$

$\mu_s$  = permeability of the sheath (H/m)

$r_i$  = inner radius of sheath (m)

$r_{i+1}$  = outer radius of sheath (m)

The full expressions for cable impedances are stated in appendix B.

### 4.3 Issues with fitting of the transfer matrices at low frequency

It can be shown that at very low frequencies (derived from (2.7a) and (2.7b) in chapter 2),

$$Y_c(s \rightarrow 0) \approx \sqrt{\frac{sC}{R_{dc}}} \quad (4.6)$$

$$A(s \rightarrow 0) \approx 1 - \sqrt{sCR_{dc}}l \quad (4.7)$$

where,

$C$  = capacitance per unit length (F/m)

$R_{dc}$  = dc resistance of the line per unit length ( $\Omega/\text{m}$ )

$l$  = length of the line

$s$  =  $j\omega$

The square root term in equations (4.6) and (4.7) is difficult to approximate by a low order rational function. Consider the simple three single-core coaxial cable configuration shown in figure 4.9, with data as in table 4.3. The frequency response of a typical entry  $A(1,1)$  of its propagation matrix  $A$  is shown in figure 4.10., which also shows a plot of a rational function approximation obtained by fitting over the frequency range [1 Hz, 1 MHz]. Note that the fitting at frequencies lower than the lower bound  $f_{\min} = 1$  Hz is poor. Table 4.4 shows the order of the fitted transfer function (maintaining the same fitting error), with different lower bounds  $f_{\min}$ . For the propagation function, decrease in the lower bound from 1 Hz to  $1e-3$  Hz results an increase in the order by 6 for each element of the propagation matrix (i.e. 54 additional poles in the  $3 \times 3$  sized matrix). This clearly indicates that the required order of the fitted function rises rapidly as the lower fitting frequency is reduced.

In order to observe the impact of using a lower fitting bound, simulations are carried out on the cable system in figure 4.9 with the sending-end of the first conductor energized by a step voltage and with all other terminations being grounded. Figure 4.11 shows time domain simulation response curves for the sending-end current obtained with different lower bounds for curve fitting. The template for comparison, also included in the figure, is an analytical solution obtained by a direct frequency domain (FD) solution attained by numerically inverting the Laplace Transform of the accurate transfer function (see Chapter 2 for details).

If the lower bound used in the fitting is not sufficiently small, as time progresses, the time domain simulation diverges from the analytical solution and results in an incorrect dc response, as seen from the plots of in figure 4.11 after a period of about 0.5 s. The response with a lower bound of 1 Hz, which is often selected by simulation tool users when studying dc systems, has 33 % steady state error. Reducing the lower bound to 0.001 Hz, reduces the error to 3.3%, but achieves this with a

significant increase in the fitting order (see table 4.4) as discussed earlier. Note that poor fitting at very low frequencies is a major source of error when modelling dc lines.

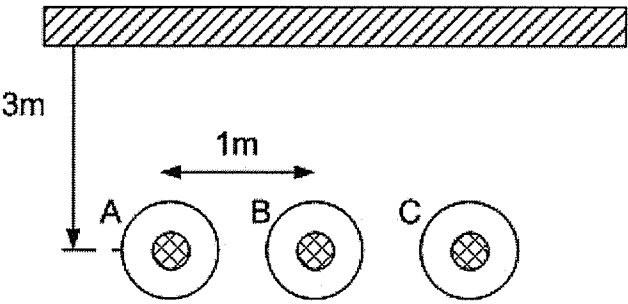


Figure 4.9: Simple Cable System: 3 single-core coaxial cables.

Radius of solid conductor (m)	0.00127
Outer radius of insulation (m)	0.00228
Dc resistance ( $\Omega$ / km)	0.034
Relative permittivity of the insulation	2.85
Earth resistivity ( $\Omega$ -m)	100
Length (km)	50

Table 4.3: Cable data

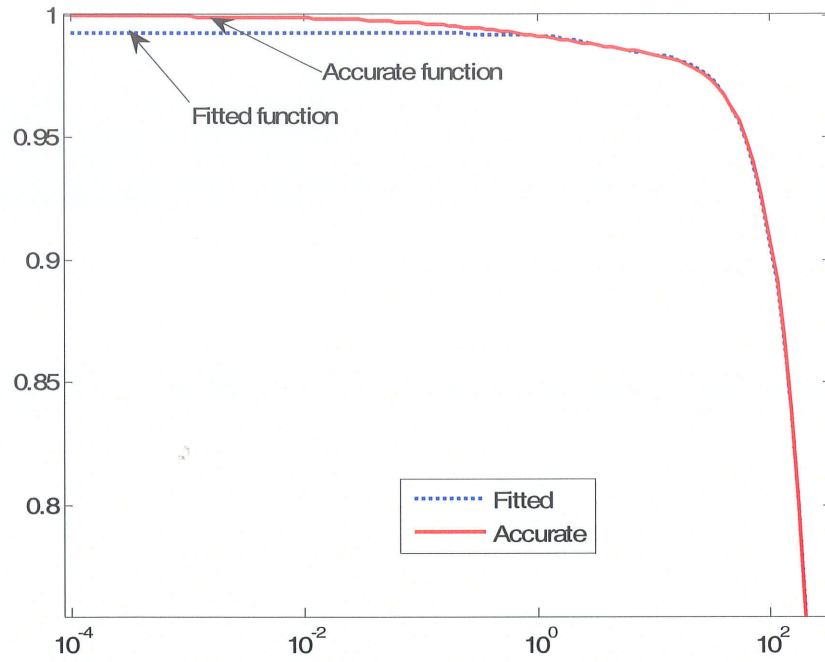


Figure 4.10: Magnitude of  $A(1,1)$  after Vector Fitting over [1Hz, 1 MHz]

$f_{\min}$ (Hz)	$f_{\max}$ for A (Hz)	Order for A(1,1)	Order for Yc(1,1)
1e-3	1e6	22	20
1e-1	1e6	20	18
<b>1</b>	<b>1e6</b>	<b>16</b>	<b>16</b>
10	1e6	16	16

Table 4.4: Order of rational function approximation

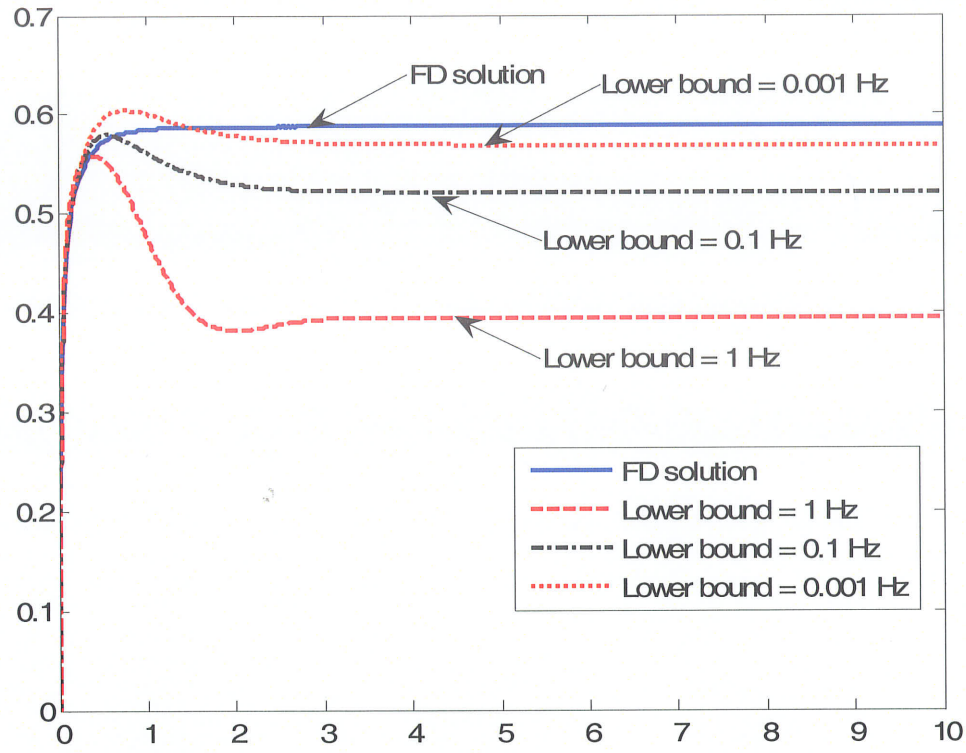


Figure 4.11: Sending-end current of the first conductor under short circuit conditions with different lower bounds considered for fitting

#### 4.4 Methods for dc correction for the Universal Line Model

This section first presents a simplified approach sometimes used in the modelling of HVDC lines that uses compensating series dc resistances to correct for the dc error. It then introduces two novel improved approaches for enhancing the dc and low frequency, without significantly increasing the order of fitting. The proposed methods are described with Universal Line Model (ULM) (a popular phase domain model currently implemented in PSCAD/EMTDC and details can be found in chapter 2). However these methods are general and can be applied to any phase domain model.

#### 4.4.1 Dc correction by adding series resistance in each phase

The simplest method for correcting the error at dc frequency is to add a suitable series resistance in each conductor. The value of this series resistance is equal to the correct dc resistance minus the value obtained from the fitted function. Note that it is possible that this correction may at times give a negative value for the added resistance. For example, consider the cable system as shown in Figure 4.9 in which compensating negative series dc resistances (-0.45 ohms and -0.47 ohms) must be added to outer conductors ("A" and "C" in figure 4.9) and inner conductor ("B") respectively. Figure 4.12 shows the current for conductor "A", with the sending-end phase "A" energized using a 1V step voltage. All other terminations are grounded. Three traces are shown, the first showing the current that would result with no correction to the model, the second showing the current after modifying the model with the compensating resistances and the third showing the theoretical response obtained by Frequency Domain analysis using numerical inverse Laplace transformation. With the resistance added, the sending-end current attains the theoretical steady state value roughly after 3 seconds. Although this method of correction does compensate for the dc response, it can introduce errors at other frequencies. This can be seen from the traces in figure 4.13, which is a close-up view of the first 50 ms of figure 4.12. On this time-scale, the compensated solution deviates significantly from the theoretical solution, whereas the uncompensated one does not.

A more serious problem with this method is that the addition of the (sometimes) negative resistance could in many instances result in a non-passive formulation and lead to unstable simulations. Hence, this method is not recommended.

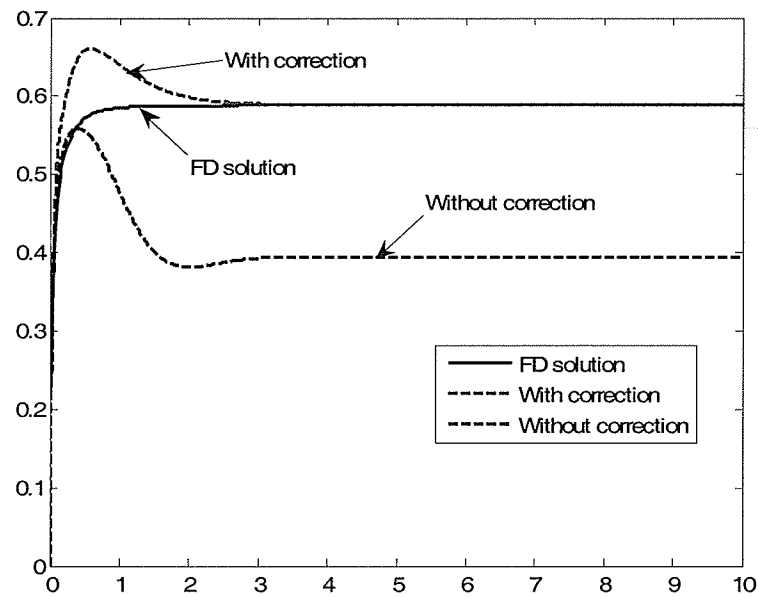


Figure 4.12: Sending-end current for conductor "A" with Series Resistance Compensation

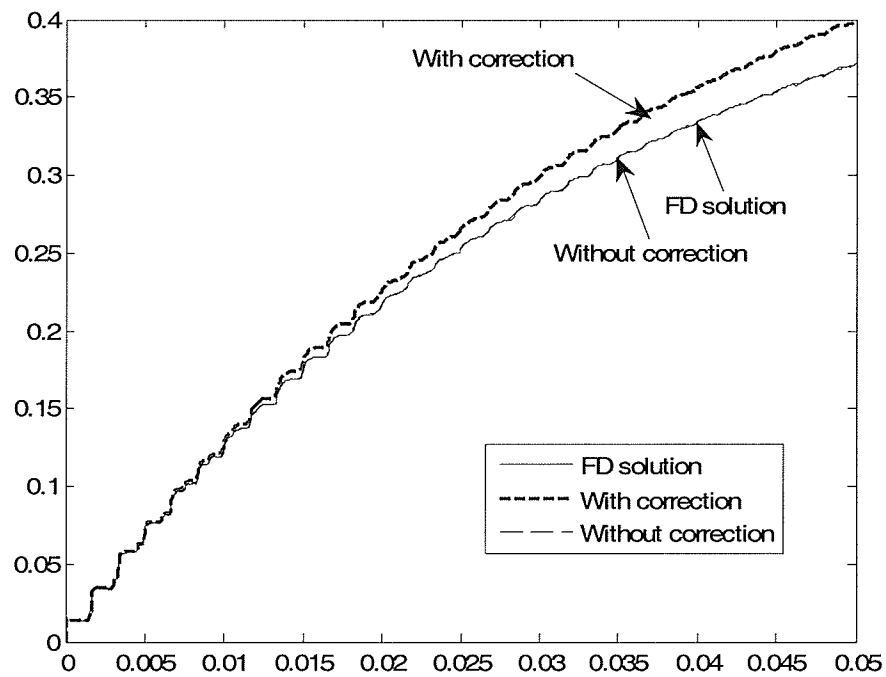


Figure 4.13: Sending-end current for conductor "A" with Series Resistance Compensation

#### 4.4.2 Dc Correction by Adding a Pole and Residue

This section discusses a new approach introduced in the thesis. The known characteristic (an element of admittance or propagation matrix) is first fitted with a rational polynomial  $f^{fitted}(s)$  as in the conventional phase domain method. A real pole  $a_0 \in (0, 2\pi f_{\min} k)$ ,  $k < 1$  with a suitable residue  $c_0$  is added to it, so that the modified function gives the exact dc value at zero frequency. This modification increases the order of the rational function by only one and does not affect the high frequency asymptote. Also, as the cutoff frequency of the additional term is smaller than the lower fitting bound, this correction is achieved with a very small error to the fitted part.

$$f^{mod}(s) = \frac{c_0}{s + a_0} + f^{fitted}(s) \quad (4.8)$$

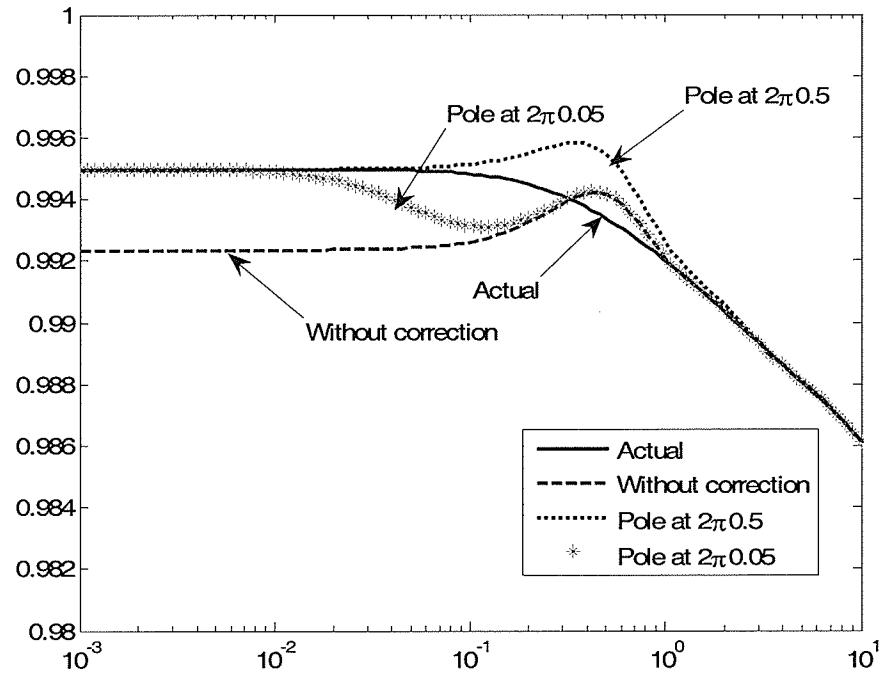


Figure 4.14: Magnitude of A(1,1) after and before addition of pole and residue



This method is different from just adding a dc resistance to the phase as it introduces a correction in each element of Yc and A matrices. The choice of  $a_0$  (or  $k$  in above paragraph) is selected by another optimization process that minimizes the error between the actual frequency response and that of  $f^{\text{mod}}(s)$ . As seen in the frequency response of one of the propagation matrix elements A(1,1) in figure 4.14, the selection of the pole at either of the frequencies  $2\pi \times 0.05$  r/s or  $2\pi \times 0.5$  r/s, gives the accurate response at frequencies approaching dc, but the pole at  $2\pi \times 0.5$  r/s gives the closest fit over the entire low frequency range. Note that without any correction, the frequency response curves of figure 4.14 indicate the presence of a steady state error. Figure 4.15 shows the corresponding time domain simulations for the line current with 1V applied to sending end conductor "A", and all other terminations short circuited. The steady state error is clearly visible.

When no correction is applied, this error is unacceptably large  $\sim 0.2$  A (33.2 %), whereas when the correction is applied, there is no error in the steady state response. The pole frequency must be carefully selected. If it is too small, then the time required to reach steady state becomes large as seen in figure 4.15 for  $2\pi \times 0.05$  r/s. This is also seen from figure 4.14, where the frequency curves for  $2\pi \times 0.05$  r/s begins to deviate from the analytical result at  $10^{-2}$  Hz. If the pole frequency is too large, it begins to interfere with the original fitted result  $f^{\text{fitted}}(s)$  as indicated by (4.8). In the above case, the original function was fitted with a lower frequency bound of 1 Hz so the pole must be at a frequency less than 1 Hz. Selecting a frequency of 0.5 Hz ( $2\pi \times 0.5$  r/s) gives a more accurate response that more closely matches the analytical result as seen in figure 4.15. There is some error in the initial 2 s, with the maximum error of 0.13 A occurring at about 1 s.

The proposed method of adding a pole is carried out after the Vector Fitting approach described in chapter 2. The Vector Fitting is used to fit the frequency response characteristic with a relatively large value of  $f_{\text{min}}$  of say, 1 Hz. As seen in table 4.4, this can be achieved with a much reduced number of poles (6 less for A(1,1), 4 less for Yc(1,1)) than a fit to a lower frequency of say  $10^{-3}$  Hz. Hence the order of the modified fitted function  $f^{\text{mod}}(s)$  is just increased by one (due to the added pole). Hence the corresponding time domain model has a much reduced number of poles and is thus numerically more efficient. In addition, it guarantees the exact value for the dc component and is less likely to

show passivity violations in comparison with the method described in subsection 4.4.1 above where negative (non-passive) resistances may be required.

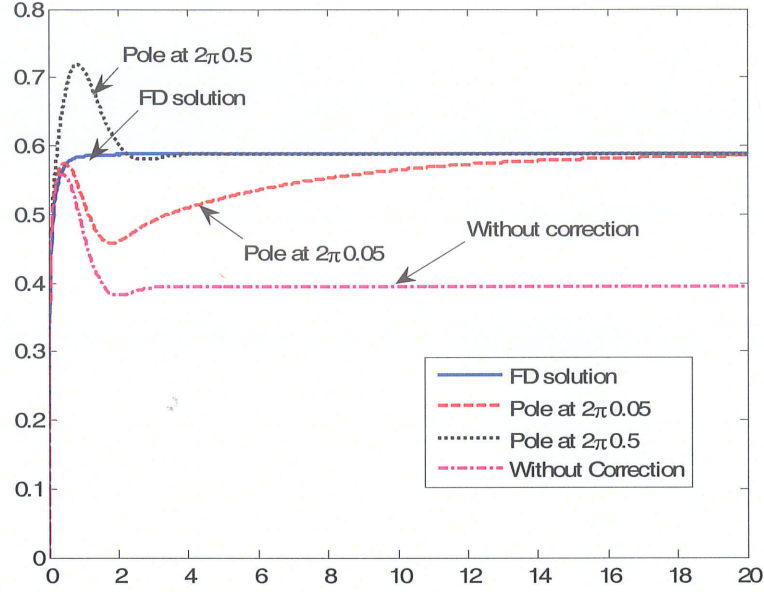


Figure 4.15: Sending-end current of first conductor with different poles selected (pole-residue method)

#### 4.4.3 Dc correction by Modified Functional Form method

This section describes a new approach to attain an accurate dc response of any phase domain multi-conductor TL model. The functional form of the fitted functions  $A(s)$  and  $Y_C(s)$  for the ULM can be found in equations (2.37) and (2.12) in chapter 2. These functions are written in an equivalent mathematical form (4.9) and (4.10), it is readily seen that putting  $s = 0$  results in a single term which is the response at dc (i.e. the term  $d_{dc,theoretical}$ ). By selecting this term to be precisely the known (exact) dc value, a perfect fit at dc is guaranteed. (The detailed discussion on the actual implementation of this method for ULM is described in Appendix H).

$$A_{i,j}^{mod}(s) \approx \sum_{n_1=1}^{N_1} \frac{c_{n_1} s e^{-s\tau_1}}{s - a_{n_1}} + \sum_{n_2=1}^{N_2} \frac{c_{n_2} s e^{-s\tau_2}}{s - a_{n_2}} + \dots + d_{dc,theoretical} e^{-s\tau_1} \quad (4.9)$$

$$Yc_{i,j}^{\text{mod}}(s) = \sum_{m=1}^M \frac{c_m s}{s - a_m} + d_{dc, \text{theoretical}} \quad (4.10)$$

A minor drawback is that although the dc error is eliminated, the resultant propagation function at very large frequency deviates marginally from zero, which is contrary to that fact that propagation function approaches to zero as frequency tends to infinity (equation (2.7b) tends to zero as  $s \rightarrow j\infty$ ). To correct this small error, the terms  $c_{n_i}$ 's in equation (4.9) are slightly perturbed using another least squares fitting to taper the high frequency response to zero without altering the correct dc value. The procedure is briefly described in Appendix G.

As seen from the frequency response plots of (typically) the three elements of the first column of propagation matrix  $A(s)$  in figure (4.16), this approach results in a very good fit over the entire frequency range, without any increase in the order of the fitted function. The corresponding sending-end current waveform with phase “A” energized to 1 V and all other terminations short circuited is shown in figure (4.17). The simulation covers a period of 10 s and, in contrast with the uncorrected formulation, the result from this method closely conforms to the theoretical response obtained by frequency domain calculations.

Figure (4.18) shows the time domain responses (simulated and theoretical) for a different set of cable terminations, in which the receiving-ends of all conductors are open-circuited while phases “B” and “C” are grounded at the sending-end. A 1 V step is applied to the sending end of phase “A”. The figure shows phase “B” receiving end voltage over a shorter duration (50 ms). The close agreement with the theoretical response attests to the fact that accurate reproduction of higher frequency phenomena has not been compromised by the dc correction.

For the cable system shown in figure 4.9, the proposed change in functional form results in a perfect dc fit of the actual frequency response characteristic. The orders of the fitted transfer functions for typical parameters, say  $A(1,1)$  and  $Yc(1,1)$  are both 16. This is the same number as that required for a fitting with a lower frequency of 1 Hz (see table 4.4), which has been shown to give a poor dc

response. This is a significant advantage of the functional form approach. As reported in section 4.3, trying to achieve a good dc response by reducing the lower fitting frequency to say  $10^{-3}$  Hz adds several additional poles to the matrices (e.g. 6 to  $A(1,1)$  and 4 to  $Yc(1,1)$ ) and yet, unlike this approach, did not give the correct response at exactly 0 Hz.

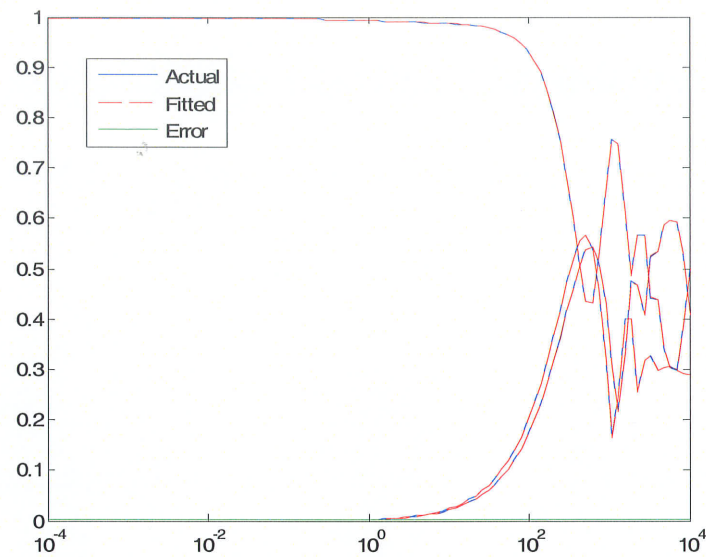


Figure 4.16: Actual and fitted magnitudes of  $A(1,1)$ ,  $A(2,1)$  and  $A(3,1)$  with Functional Form method

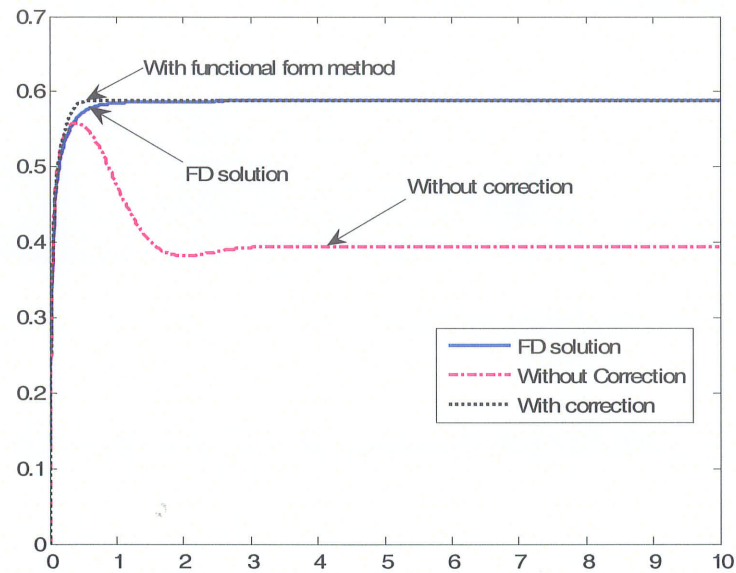


Figure 4.17: Sending-end current of first conductor with and without correction

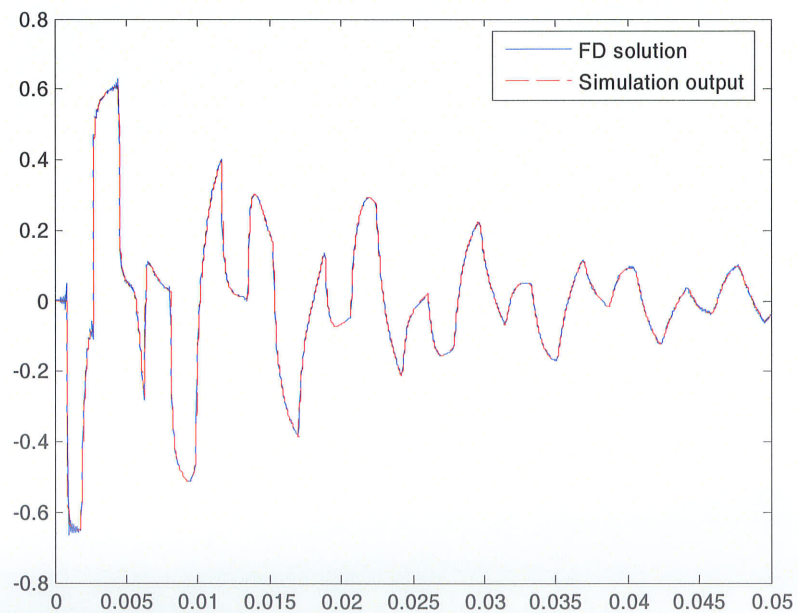


Figure 4.18: Induced voltage on middle conductor "B" under open circuit conditions, if the conductor "A" is energized with step voltage

One of the difficulties in a conventional Vector-Fitting approach is that it is difficult to guarantee that the curve-fitted model is always passive. A non-passive formulation for the transmission line or cable can sometimes lead to an unstable simulation. An unanticipated advantage of this method is that the Modified Functional Form method minimizes the likelihood of passivity violations. The effect of Modified Functional Form method on passivity is discussed in detail in chapter 5 and hence is not repeated here.

#### 4.5 Application Example- Voltage Sourced HVDC with Underground Cables

As an example for the use of the method in a typical application, voltage sourced converter (VSC) based medium voltage DC transmission system example shown in figure 4.19 [71] is considered. The converter consists of six pulse VSC rated at 110 kV, 75 MW transmitting power to the receiving-end through the 100 km underground cable system shown in figure 4.20. This case also demonstrates the need for good time domain models - here the cable connects into a highly non-linear system (the HVDC converter and the ac network reflected through it) and so frequency domain solutions are not possible.

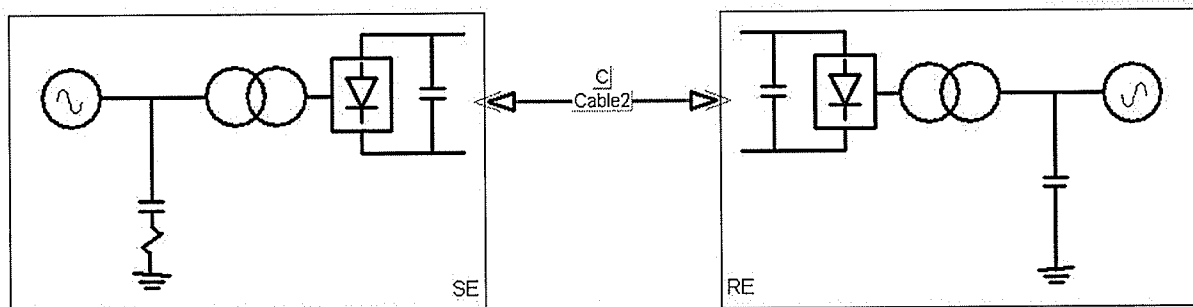


Figure 4.19: VSC Transmission System

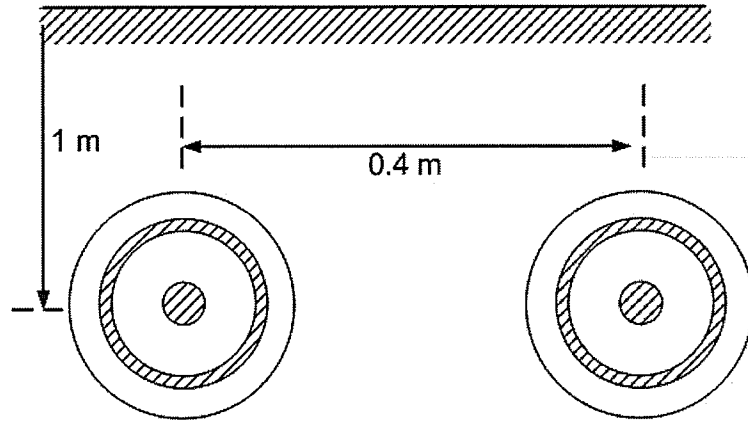


Figure 4.20: Cable System: Two coaxial cable system

Radius of inner solid conductor (m)	0.0104
Dc resistance ( $\Omega/\text{km}$ )	0.0830
Outer radius of first insulation (m)	0.016
Relative permittivity of first insulation	4.1
Outer radius of sheath (m)	0.0205
Relative permittivity of second insulation	2.3
Outer radius of second insulator (m)	0.0215

Table 4.5: Data for the cable

Figure 4.21 compares the dc line current through the underground cable with and without correction between 0 to 0.5 seconds indicating that the functional form method does not alter the high frequency response of the original curve fitted model. Figure 4.22 shows the voltage difference between the two ends of the cable system for a much longer duration (50 s). With the functional form method, the steady-state voltage drop and the dc current observed are 4.1 kV and 0.495 kA respectively. This is in exact agreement with the theoretical dc resistance of  $8.3 \Omega$  (note:  $4.1 \text{ kV}/0.494 \text{ kA} = 8.3 \Omega$ ).



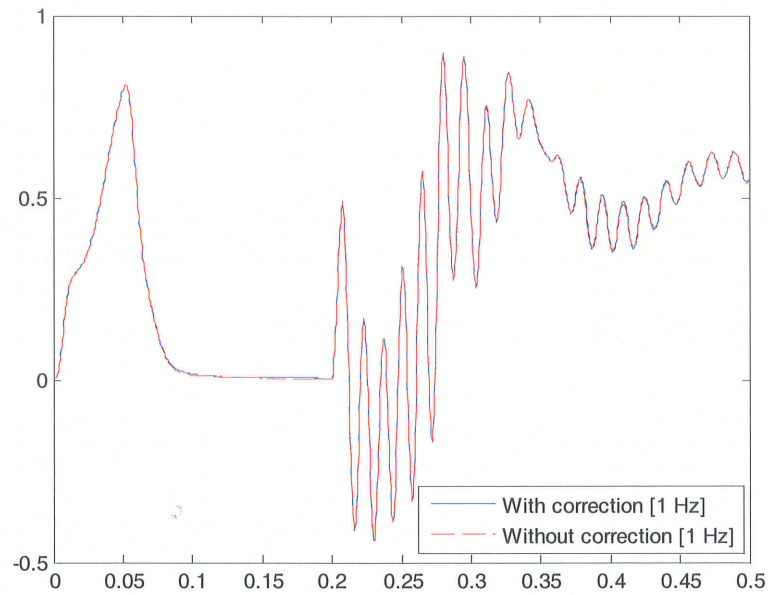


Figure 4.21: Dc line current of the converter

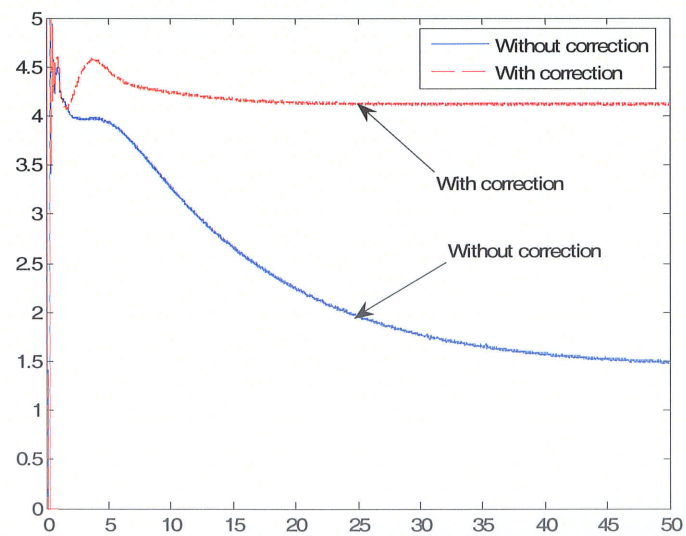


Figure 4.22: Voltage difference between the converter and inverter



Without any correction, the voltage difference is 1.45 kV for the line current of 0.52 kA, which implies an incorrect dc resistance of 2.84  $\Omega$ . The above simulations demonstrate that the proposed dc correction method yields a model that is applicable over the full frequency range of interest and is thus useful for studying the steady-state and low frequency dynamics as well as the high frequency transient and harmonic behavior of the dc link.

## 4.6 Chapter Summary

The traditional approach to modelling cables and transmission lines in the time domain using fitted admittance and propagation characteristics can result in significant errors at frequencies approaching dc. Although some improvements can be made by reducing the lower bound of the fitting frequency to make the dc fitting more accurate, this usually results in an increase in the order of the fitted transfer functions. Alternative approaches which modify the form of the implemented transfer function, either by adding a low frequency pole or by reformulation in a form that permits direct specification of the dc values, were shown to result in accurate simulations over the entire frequency range from dc to higher frequencies. These two methods were shown to be more accurate and potentially more stable in comparison with a simplified treatment of adding a corrective series resistance in each phase. In particular, the second of these two methods is especially easy to implement and is recommended for the modelling of HVDC transmission systems in which faithful reproduction of the very low frequency behavior is just as important as high frequency behavior.

## Chapter 5

# Robust Passivity Enforcement Scheme for Multi-Conductor Transmission Lines and Cables

### 5.1 Introduction

Passivity of an electrical system is an important aspect in determining its stability. The physical meaning of passivity with regard to electrical circuits is that passive networks always absorb real power and thus the total energy delivered to the network is positive [13], [4]. Figure 5.1 shows a single-port passive electrical network and  $v(t)$  and  $i(t)$  are the input voltage and current to the network respectively..

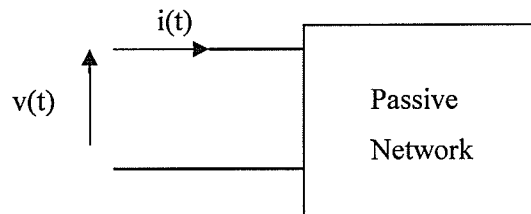


Figure 5.1: Passive Electrical Network

The total energy delivered to the network is,

$$\xi = \int_0^T v(t) i(t) dt \quad (5.1)$$

For any given voltage  $v(t)$ , passive circuit requires that the total energy delivered must be non-negative. i.e.

$$\xi > 0, \forall T > 0 \quad (5.2)$$

Using Parseval's theorem [4], the equation (5.1) can be expressed in frequency domain as in (5.3)

$$\begin{aligned} \xi &= \frac{1}{2\pi} \int_0^{\infty} V(\omega) \overline{I(\omega)} d\omega \\ &= \frac{1}{2\pi} \int_{-\infty}^{\infty} V(\omega) \overline{Y(\omega)} V(\omega) d\omega \\ &= \frac{1}{\pi} \int_0^{\infty} \text{Re}(\overline{Y(\omega)}) |V(\omega)|^2 d\omega \end{aligned} \quad (5.3)$$

where,  $Y(\omega)$  is the admittance of the electrical network and the condition for passivity is that  $\text{real}(Y(\omega))$  is positive real for all  $\omega$  [4]. For multi-conductor systems with symmetric admittance matrix, the corresponding condition becomes  $\forall \lambda : \lambda \text{ is an eigenvalue of } \Re(Y(\omega)), \lambda > 0$ . An equivalent condition [50] used later in this section 5.2, that also applies to non-symmetric matrices is that  $\forall \lambda : \lambda \text{ is an eigenvalue of } H(\omega) = Y(\omega) + Y(\omega)^*, \lambda > 0$  for all  $\omega$ .

The passivity related to transmission line (TL) models based on method of characteristics is an ongoing research topic. The physical transmission line, by necessity must always be passive, i.e., regardless of its terminations, the line itself cannot generate active power at any frequency. However one of the major problems of the TL models based on method of characteristics is that the curve-fitted resultant model of the (passive) transmission line cannot be guaranteed to be always passive. Depending on its terminating connections, a non-passive transmission line model may lead to incorrect, unstable simulations.

To compensate for this error, it is necessary to modify the parameters of the curve-fitted transmission line model with a passivity correction algorithm. In general, passivity correction algorithms based on nonlinear optimization can be computationally expensive [56]. Alternatively, algorithms can be formulated as a linear constrained least square problem [47], [62], [54], [63], [52]. However the above methods can only be successfully applied, if the passivity violations are very small.

The development of a passivity enforcement method for delay based multi-conductor transmission line models is an ongoing research topic and recent advancements can be found in [60], [63], [65]. The above methods assume that the passivity violations are small and are applicable to modal-domain transmission line formulations (i.e. those that use constant transformation matrices for converting between the phase and modal domains). These models are often adequate for vertically symmetrical overhead transmission lines, where the assumption of constancy of the transformation matrix is fairly accurate, but they are not so effective for asymmetrical overhead transmission line configurations and arbitrary cable arrangements, where these matrices show a high amount of frequency dependence.

Although time-domain models simulate the frequency range from a few Hertz to about several hundreds of kilohertz, the curve fitting algorithms are usually unable to obtain a good asymptotic fit at very low frequency. An observed problem with this poor fitting at low frequencies is the presence of large passivity violations. The measure of the degree of passivity violation is discussed in detail later in section 5.2 and is the degree of negative excursions in the frequency response plot of the eigenvalues of a certain Hermitian matrix which is derived from the admittance and propagation matrices of the cable system.

As discussed in Chapter 4, an alternate formulation of the curve-fitting problem, referred to as the Modified Functional Form method, guarantees an asymptotic fit of the frequency domain characteristic of the transmission line as the frequency approaches zero, while maintaining a good fit over the entire frequency spectrum. As will be shown later in this chapter, an additional benefit of this approach, is that the accurate fitting at low frequency reduces the constraints on the curve-fitting problem and results in formulations which are passive or have only small passivity violations. This favorable property is exploited in designing a robust algorithm for passivity enforcement. As the above reformulation reduces the severity of the passivity violations, the reformulated problem becomes amenable to solution using perturbation methods.

Based on the above observation, a new algorithm is proposed to ensure passivity in the transmission line model. Unlike earlier approaches [60], [63], [65] the proposed method is not restricted to constant transformation matrix based models, but can be applied to any phase domain model. This method first reformulates the form of the transmission line's admittances and propagation functions to be fitted using the Modified Functional Form. With this approach, passivity violations are less likely and when present, they are minor. Next, any (small) remaining passivity violations are removed using a least-squares fitting to introduce corrective perturbations to the elements of the characteristic admittance and propagation matrices.

This approach is demonstrated with examples of underground dc and ac cable systems, and validated by comparison with frequency domain solutions.

## 5.2 Passivity criteria for multi-conductor transmission lines

Treating the finite length transmission line as a multi-port electrical network, passivity is guaranteed, if and only if its transfer admittance  $\tilde{Y}(s)$  is positive real for every value of frequency  $\omega$  (with  $s = j\omega$ ) [59]. The transfer admittance  $\tilde{Y}(s)$ , relating sending and receiving-end voltages to the currents, is shown below in (5.4a) for the TL representation in figure (2.9). Using (5.4a), (2.8a) and (2.8b),  $\tilde{Y}(s)$  is readily obtained as a function of  $A$  and  $Y_c$  as shown in (5.4b).

$$\begin{bmatrix} I_k \\ I_m \end{bmatrix} = \tilde{Y} \begin{bmatrix} V_k \\ V_m \end{bmatrix} \quad (5.4a)$$

$$\tilde{Y} = \begin{bmatrix} (I - A^2)^{-1}(I + A^2)Y_c & (I - A^2)^{-1}(-2A)Y_c \\ (I - A^2)^{-1}(-2A)Y_c & (I - A^2)^{-1}(I + A^2)Y_c \end{bmatrix} \quad (5.4b)$$

Note that  $\tilde{Y}$ ,  $A$  and  $Y_c$  are functions of frequency,  $s = j\omega$  and for simplicity, “ $s$ ” term is removed in (5.4a) and (5.4b). The necessary and sufficient conditions for the transfer admittance matrix  $\tilde{Y}(s)$  to be positive real (and hence, for the transmission line model to be passive) are [60],

$$\begin{aligned} (a) \quad & \tilde{Y}(s) \text{ is analytic } \forall s : \text{Re}(s) > 0 \\ (b) \quad & \tilde{Y}(s) = \tilde{Y}(s)^* \\ (c) \quad & H(s) = \tilde{Y}(s) + (\tilde{Y}(s)^*)^T \quad (\text{Hermitian Matrix}) \\ & \text{is positive definite} \end{aligned} \tag{5.5}$$

As complex, poles and residues always appear in conjugate pairs, the first two conditions stated above are automatically fulfilled [59]. The satisfaction of the third condition requires all eigenvalues of the matrix  $H(s)$  with  $s = j\omega$ , to be positive at every frequency  $\omega$ .

As an example, consider the 100 km twin HVDC cable depicted in figure 5.2 with data as shown in Table 5.1. The system has four conductors (core and sheath for each cable), and hence has 4x4 dimensioned shunt admittance  $Y(s)$  and series impedance  $Z(s)$  matrices.

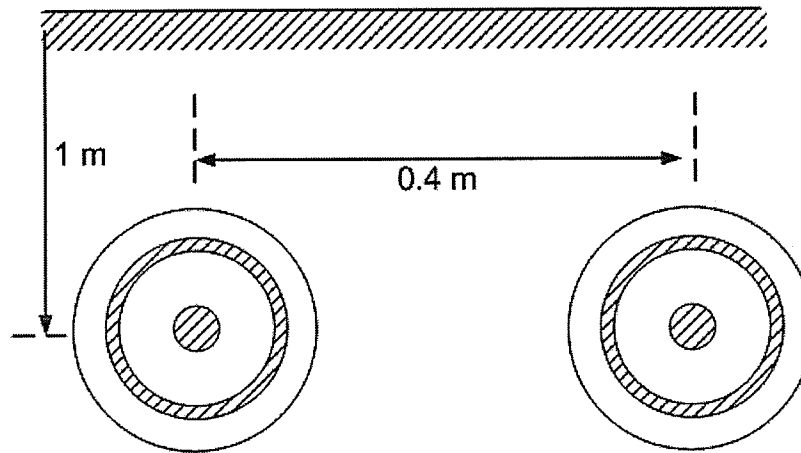


Figure 5.2: Cable System: Two coaxial cable system

Radius of inner solid conductor (m)	0.0104
Dc resistance ( $\Omega/\text{km}$ )	0.0830
Outer radius of first insulation (m)	0.016
Relative permittivity of first insulation	4.1
Outer radius of sheath (m)	0.0205
Relative permittivity of second insulation	2.3
Outer radius of second insulation (m)	0.0215

Table 5.1: Cable data

The matrices  $Y_c(s)$ ,  $A(s)$  and the  $8 \times 8$  dimensioned  $\tilde{Y}(s)$  &  $H(s)$  are accordingly calculated using equations (2.26), (2.27), (5.4) and (5.5c) respectively. Figure 5.3 shows the plot of the 8 eigenvalues of  $H(s)$  as functions of frequency. As all eigenvalues are positive at every frequency, the passivity condition is satisfied. This confirms that the frequency domain formulation is passive for the actual cable system in Figure (5.2). It should be from the physical reasoning (i.e. the cable should not be able to produce energy).

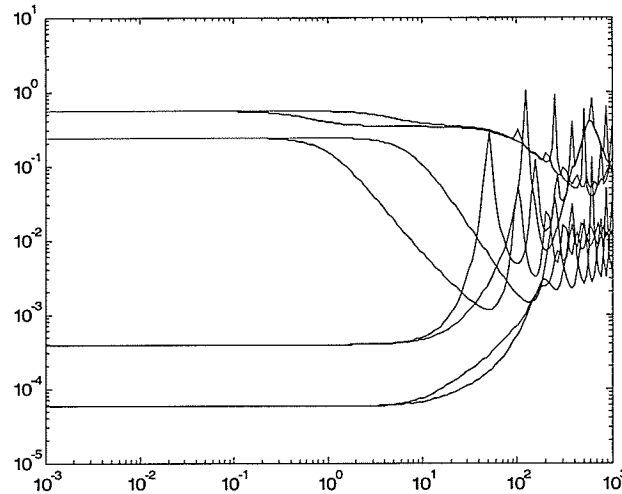


Figure 5.3: Eigenvalues of  $H(s)$

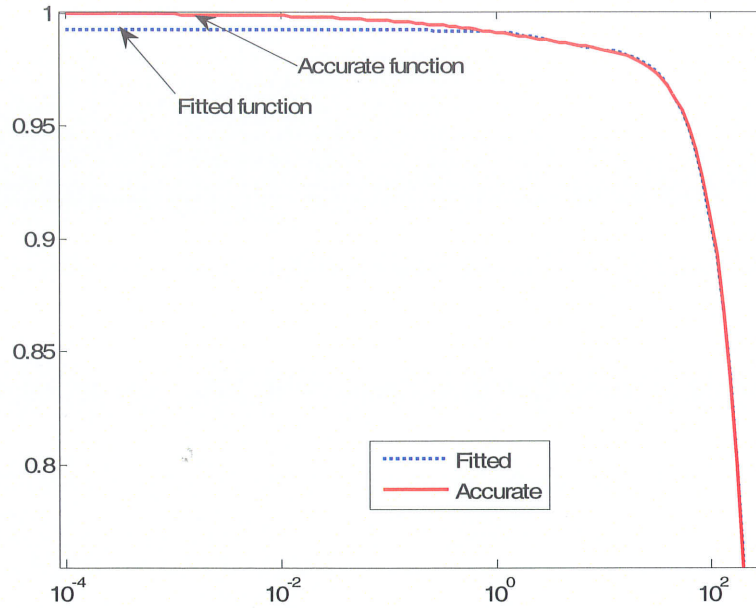


Figure 5.4: Magnitude of  $A(1,1)$  after Vector Fitting over [1Hz, 1 MHz]

As discussed in Chapter 2, the time domain modelling requires a rational function approximation (curve fitting) of matrices  $Yc(s)$  and  $A(s)$ . The frequency response of a typical entry  $A(1,1)$  of its propagation matrix  $A$  is shown in figure 5.4, which also shows a plot of a rational function approximation of the form (2.37) obtained by fitting over the frequency range [1 Hz, 1 MHz]. Note that the fitting at frequencies lower than the lower bound  $f_{\min} = 10^0$  Hz is poor. In most power system transient studies, applied frequencies are in the range of 50-60 Hz. Switching transients typically excite frequencies up to a few kHz. Hence fitting accurately in a region say 1 Hz to 100 kHz would seem adequate. However poor fitting lower than 1 Hz may be a problem for HVDC system transients as the base frequency values are incorrect. More importantly it would lead to passivity violations and this is a problem even for ac system transients.

Figure (5.5) presents the plots of two typical eigenvalues of the Hermitian matrix  $H(s)$ , computed based on fitted matrices (i.e. fitted  $Yc(s)$  and fitted  $A(s)$ ). Also shown in the graphs are the actual



(theoretical) eigenvalues for comparison. The eigenvalues based on fitted matrices deviate significantly from theoretical values, due to the poor fitting below the minimum bound of 1 Hz. Although the first eigenvalue as calculated from fitted matrices (Figure 5.5a) still remains positive over the full frequency range shown; the plot of the second eigenvalue from the fitted matrices (Figure 5.5b) is significantly negative with a value of about -1 at approximately  $3 \times 10^{-2}$  Hz. This negative eigenvalue indicates that there is a large passivity violation in the fitted model as a result of the error caused by the rational function approximations (curve fitting) of the entries of  $A(s)$  and  $Y_c(s)$ .

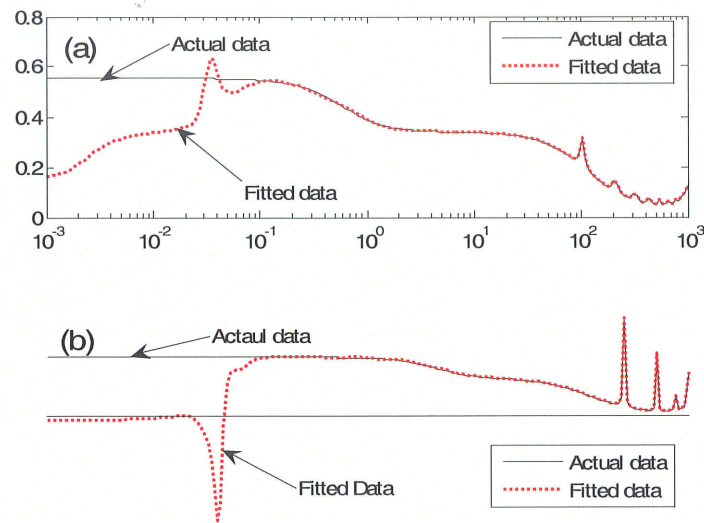


Figure 5.5: Eigenvalue of  $H(s)$

By consideration of several example cases of different underground cable arrangements, it is observed that the poor curve fitting at lower frequencies (1 Hz or smaller) often results in large passivity violations (negative eigenvalues of large magnitude). Negative eigenvalues at higher frequencies are usually rare and if present, are of relatively small magnitude. Passivity correction can be introduced for these small passivity violations more easily by using perturbation methods as described in section 5.6.

### 5.3 Identification of passivity violated regions

The accurate identification of the passivity violated regions is a crucial requirement for any passivity enforcement scheme. Some earlier work [54], [51] has reported analytical approaches based on state variable formulation and Hamiltonian matrices to determine the passivity violating regions. However these approaches are strictly restricted to linear systems without transportation lag and thus are not directly applicable to transmission lines or cables. More recent work [59], [60] has extended such analysis to transmission lines (detailed discussion can be found in Appendix I). However these techniques require significant computational effort and frequency sampling as for the frequency sweep method discussed in section 5.3.2.

Alternatively, the frequency sweep method is used to identify passivity violations, in which passivity is verified by carefully evaluating all eigenvalues of  $H(s)$  by stepping through the entire frequency range.

#### 5.3.1 State variable approach

This section is prepared based on passivity identification method for a single conductor line found in the reference [31]. In state variable technique, first the fitted rational functions of transmission lines parameters ( $A(s)$  and  $Yc(s)$ ) are expressed in state variable form. As an example, matrix  $Yc(s)$  in (2.12) can be expressed in the state variable form as in (5.6).

$$\begin{aligned}\dot{x}(t) &= Ax(t) + Bu(t) \\ y(t) &= Cx(t) + Du(t)\end{aligned}\tag{5.6}$$

The diagonal square matrix  $A$  (dimension  $N$ ) contains poles of the transfer function as diagonal elements and the row vector  $C$  (dimension  $N$ ) contains residues.  $B$  is a column vector of ones

(dimension  $N$ ) and the scalar  $D$  is the constant term ( $Y_\infty$  in (2.12)).  $N$  is the order of the function. Hence the transmission line equations ((2.8a) and (2.8b)) can be expressed in the state variable form as in (5.7).

$$\begin{aligned} K\dot{x}(t) &= \tilde{A}x(t) + Px(t-2\tau) + \tilde{B}v(t) \\ i(t) &= \tilde{C}x(t) + \tilde{Q}x(t-\tau) + Qx(t-2\tau) \end{aligned} \quad (5.7)$$

In the above expression, unknown matrices  $K, \tilde{A}, P, \tilde{B}, \tilde{C}, \tilde{Q}$  and  $Q$  are derived in terms of matrices in state variable formulation for  $Y_c(s)$  and  $A(s)$ .  $x, \tau, v, i$  are a vector containing state variables, time delay, vectors of voltages and currents at both terminals of TL respectively. Equation (5.7) is an Abstract Delay Differential Equation (ADDE). The passivity criteria for the ADDE can be derived based on the fulfillment of the third condition for passivity in (5.5) and the following Theorem states,

Theorem 1

The dynamic system stated in (5.7) is passive if and only if there do not exist any purely imaginary values for “ $s$ ” that satisfy the following problem.

$$s\tilde{K}\xi(s) = H(s)\xi(s) \quad (5.8)$$

The unknown matrices  $(\tilde{K}, H(s))$  in (5.8) are derived from the matrices in state variable equation (5.7). A straightforward solution to (5.8) is not available in literature. However it can be solved indirectly by first discretizing in frequency domain and using the reformulated form shown in (5.9), where  $s_k = j2\pi f_k, k = 1:N$ .  $N$  is the number of frequency samples.

$$\sigma(s_k)\tilde{K}\xi(s_k) = H(s_k)\xi(s_k) \quad (5.9)$$

Equation (5.9) has the form same as generalized eigenvalue formula and can be solved using standard techniques.  $\sigma(s_k), \xi(s_k)$  are the generalized eigenvalues (generally complex number) and eigenvector of matrix  $H(s_k)$ . The equation (5.9) is solved for N frequency samples.

In each frequency sample, the generalized eigenvalues of  $H(s_k)$  are computed using a standard technique and possible existence of pure imaginary eigenvalues are checked. It can be readily seen that pure imaginary eigenvalues (if they exist), satisfy the equation (5.8) at  $s_k (= j2\pi f_k)$ . It can be also shown that  $H(s)$  is a function of  $e^{j\omega\tau}$  and  $e^{j\omega 2\tau}$ . The matrix  $H(s)$  and hence the eigenvalues of  $H(s)$  are periodic with period  $s_0 \left( = \frac{2\pi}{\tau} \right)$  (i.e. The eigenvalue solution at frequency  $s_k$  is identical to the solution at  $s_k + s_0$ ). The pure imaginary eigenvalues of the equation (5.9) are inspected (if exist, satisfy (5.8)), taking N number of frequency samples for the range  $s \in (0, s_0)$ ,  $s_0 = j2\pi f_N$ .

In practice, it may not be able to identify exact location of the eigenvalues with zero real part, since finite number of frequency points are considered for computation. The strategy used in [59] is that the eigenvalues with diminishing real values are checked for each frequency between zero and  $\frac{2\pi}{\tau}$ . If

such eigenvalue at frequency  $f_0 = \frac{2\pi}{\tau n}$  is found then, equation (2.14) is linearized over  $f_0$  and using an iterative technique, a close approximation for the frequency  $f_0$  at which eigenvalue becomes purely imaginary is found.

In conclusion, the state variable approach to find passivity violations for transmission line models is to solve the equation stated in (5.8). Since the equation (5.8) can not be solved directly, an indirect method is employed, where frequency sampling is required and solution is obtained by solving via generalized eigenvalue problem.

Compared with the frequency sweep method (discussed in the next section), the above method has an advantage that the frequency region (where passivity is checked) is limited to a finite frequency

$f_{\max} = \frac{2\pi}{\tau}$ . For 30-km single-conductor overhead line the maximum frequency is

$$f_{\max} = \frac{2\pi}{30e^3/3e^8} = 6.28e^4 \text{ Hz}.$$

The above method can only be applied in situations where the transmission line can be modeled in the modal domain with constant transformation matrices for converting between mode and phase quantities. However, such methods are not easily applicable to more detailed transmission line and cable models which consider frequency dependency of transformation matrices or directly model the transmission line in the phase domain as in the case for the Universal Line Model (ULM).

One purported advantage of this method is that it gives a formula for the frequency boundaries at which passivity violations occur. This is considered superior to other approach (discussed in next section) that uses frequency sampling and checks for passivity violations. However in reality, the above formula also requires a numerical solution as the straightforward analytical solution is not available. Usually this numerical method requires searching through the frequency range to see whether there are pure imaginary values for “s” that satisfy the equation (5.8). Hence it is theoretically possible for this method also to miss the passivity violations on account of having large frequency step. So one might as well use the frequency scan method described below, which also have the same drawback.

### 5.3.2 Frequency sweep method

This section describes the traditional method (Frequency sweep method) [47] used to identify passivity violations. In this method, the passivity is verified by carefully evaluating all eigenvalues of  $H(s)$  by stepping through the entire frequency range (0 Hz to a very large frequency, say, 10 MHz) in small steps. One possible drawback of this method is that a negative eigenvalue may be missed due to the coarseness of the frequency step used or may lie beyond the maximum searched frequency. However, noting that eigenvalues are smooth functions of frequency, this drawback has been addressed by conducting a careful inspection of the eigenvalue plot up to a frequency well in excess of the simulation bandwidth. Any suspicious frequency range (where an eigenvalue approaches very

low values) is flagged for a more refined search and subsequently scanned by conducting a localized frequency sweep with a much smaller frequency step.

## 5.4 Proposed Passivity Enforcement Scheme

If the fitted formulation shows passivity violation, its parameters can be perturbed so as to ensure positive eigenvalues for  $H(s)$ . A nonlinear optimization algorithm can be used, which penalizes negative eigenvalue excursions, however such an algorithm can be numerically inefficient and susceptible to non-convergence. Alternatively a computationally efficient linear constrained least squares algorithm can be used to perturb the fitted parameters to achieve passivity. However, such perturbation methods are only meaningful when the passivity violation is small. For large violations, the perturbed parameters only provide a compromise solution in which the accuracy of the frequency response fitting has to be sacrificed in order to achieve passivity.

The relatively large magnitude negative eigenvalues in figure 5.5 prohibit the use of such perturbation methods. This problem can be overcome by using the Modified Functional Form method described in Chapter 4 to obtain accurate low frequency response. The new form can guarantee asymptotically exact fitting at very low frequency, a region which is often seen to be problematic for passivity enforcement when modeling many cable configurations. The improvement in fitting at very low frequencies has an additional bonus- it is seen to result in significantly smaller violations (i.e. it gives negative eigenvalues of small magnitudes); and in many instances, no passivity violations at all.

In light of the discussion in the previous paragraph, a two-step passivity enforcement procedure is proposed. In the first step, the system matrix elements are fitted using the more accurate modified form of the fitting function, removing any large passivity violations. The second step tweaks the fitted parameters using perturbation methods to remove any remaining small passivity violations.

## 5.5 Eliminating large passivity violations using the Modified Functional Form method

As discussed in Chapter 4, a modification is introduced to the to the curve fitting procedure in which the admittance and propagation transfer functions (equations (2.26) and (2.27) in Chapter 2) are reformulated so that the dc response is factored out as an additive constant that can be directly selected. The modified equations are restated in (5.10) and (5.11), it is readily seen that the Modified Functional Form method gives exact value ( $d_{dc,theoretical}$ ) at zero hertz, hence guaranteeing correct dc response in time domain. The details of the Modified Functional Form method were explained in Chapter 4.

$$A_{i,j}^{mod}(s) \approx \sum_{n_1=1}^{N_1} \frac{c_{n_1} s e^{-s\tau_1}}{s - a_{n_1}} + \sum_{n_2=1}^{N_2} \frac{c_{n_2} s e^{-s\tau_2}}{s - a_{n_2}} + \dots + d_{dc,theoretical} e^{-s\tau_1} \quad (5.10)$$

$$Y_{c,i,j}^{mod}(s) = \sum_{m=1}^M \frac{c_m s}{s - a_m} + d_{dc,theoretical} \quad (5.11)$$

Also, as mentioned in the preceding section, another benefit of this modified functional form is that, it eliminates the large passivity violations typically present at low frequencies. As an example, consider the same cable configuration shown in figure 5.2. Figure 5.6 shows frequency response plots of the first (typical) eigenvalue of the Hermitian matrix for the two different fitting approaches (the original uncompensated formulation, and with the Modified Functional Form method); superimposed on the theoretical frequency response (obtained from the original matrices without fitting). The eigenvalue plot corresponding to the uncompensated method is in poor agreement with the theoretical value, particularly at frequencies below  $10^{-1}$  Hz, and is in fact the attainment of negative values indicate passivity violation. Conversely, the eigenvalue is uniformly positive with the use of the proposed modified functional form. Figure 5.7 shows the full set of eigenvalues of  $H(s)$  when the modified functional form method is applied. Every eigenvalue is always positive, thereby establishing passivity. Note that compared with figure 5.3, some very small eigenvalues in figure 5.7 show slight deviation in the frequency range [1-100 Hz] due to small error introduced by curve-fitting. However

this does not affect the accuracy of the time domain simulation (the accuracy of fitted functions is verified within the frequency range  $[f_{\min}, 1 \text{ MHz}]$  nor the passivity of the model (since all eigenvalues are positive)

In this case, no further passivity enforcement procedure is necessary as using the modified functional form of (5.10) and (5.11) eliminated the passivity violation. However for other cases, a small amount of passivity violations at higher frequencies may still be present and if so, it is removed using the procedure described in the following subsection.

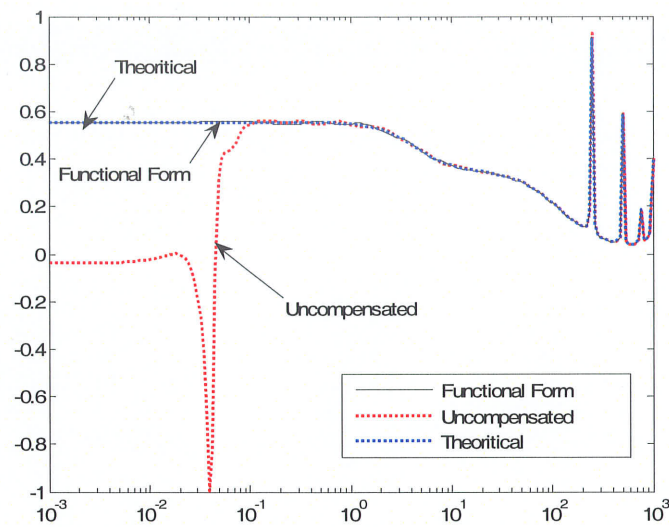


Figure 5.6: First eigenvalue of  $H(s)$



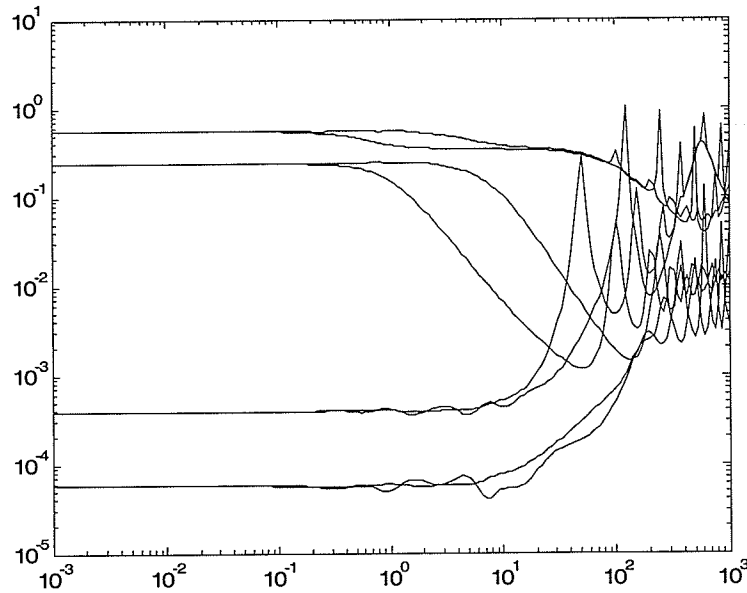


Figure 5.7: Eigenvalues of  $H(s)$  with Modified Functional Form method

Note that rational fitting was implemented in order to construct a time-domain model for the cable system. To validate the time-domain model, a simulation study is conducted by energizing the cable configuration in figure 5.8 with a unit step to one conductor. Simulations are conducted on models obtained by using the conventional fitting approach, as well as the proposed modified fitting approach. For comparison, a theoretical plot calculated using a numerical inverse Laplace transform of the frequency domain formulation is also included. The plot of sending-end current shown in figure 5.9 indicates that the formulation without correction is non-passive and in this case causes the simulation to be unstable. On the other hand the time-domain simulation using the proposed method accurately tracks the theoretical solution.



Figure 5.8: Short circuit test

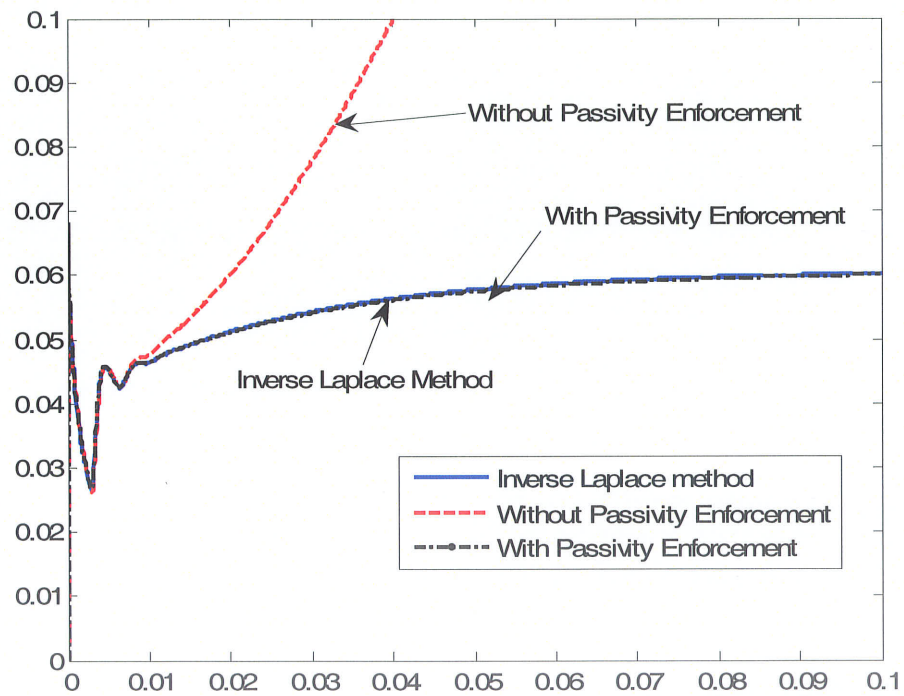


Figure 5.9: Short circuit current at sending-end

### 5.5.1 Selection of shunt conductance value

In many transmission line models, the shunt conductance per unit length is unknown and often assumed to be zero. The conductance value selected can sometimes affect the performance of the passivity algorithm adversely. The appropriate value of the shunt conductance can be selected by experimentally until a satisfactory match between theoretical and fitted values (in the manner of figure 5.5) is attained to reduce likelihood of passivity violations. However for a large number of cable systems, it is experienced that a shunt conductance of  $3 \times 10^{-9}$  S/m (still an extremely small value, which distorts the response at higher frequency only insignificantly), is adequate to obtain a non-passive formulation.

Although the above discussion shows that proposed modified functional form method is likely to result in a passive fitting, it does not guarantee passivity. However, as the fitting at very low frequencies is improved due to the guarantee of an exact fit at 0 Hz, passivity violations with this method are rare and if present, usually small. In such cases, the following section describes the procedure used to eliminate these small passivity violations.

### 5.6 Elimination of small passivity violations using perturbation method

The small negative eigenvalues at high frequencies are forced to be positive by slightly perturbing the residues corresponding to the elements of either characteristic admittance matrix ( $Y_c$ ) or the propagation matrix  $A(s)$  without significantly compromising the accuracy of the fitted function. Perturbing only the diagonal elements of such matrices is sufficient for moving the small negative eigenvalues into the positive range.

In principle, all the elements of the matrix should be perturbed. However, as any remaining passivity violations are small, perturbing only the diagonal elements of such matrices is sufficient for moving the small negative eigenvalues into the positive range. This greatly reduces the computational burden of the Constrained Least Square Fitting Procedure. As an example, for a three-conductor system, the number of variables required for diagonal perturbation is  $3N$  (as opposed to  $9N$ , with all element perturbation), where  $N$  is the order of the function. The dimensions of coefficient matrices in

equations (5.12)-(5.17), (5.20), (5.21) are significantly reduced. The perturbation of diagonal elements leads to fast evolution of CLS method.

### 5.6.1 Implementation using perturbation of propagation matrix, $A(s)$

The following paragraphs describe the passivity enforcement method based on perturbation of the diagonal entries of the propagation function  $A(s)$ .

The first step is to linearize equation (5.10) to construct a relationship between increments in the diagonal elements of  $A(s)$ , for any given frequency  $f_k$  ( $s = j2\pi f_k$ ) and increments of residues,  $c_n$ 's.

$$\Delta A(f_k) = K_1(f_k) \Delta C \quad (5.12)$$

In (5.12),  $\Delta C$  is a vector (dimension  $(N \cdot M)$ ) containing residue increments corresponding to the diagonal elements of the matrix  $A(f_k)$  and  $\Delta A(f_k)$  is a vector (dimension  $M$ ) containing increments of diagonal entries of  $A(f_k)$ . The integer  $N = \sum_{i=1}^{\text{modes}} N_i$  is the order of each of the elements of  $A(f_k)$ , that is, the highest order of the Laplace variable  $s$  in the denominator, as seen in equation (5.10); and  $M$  is the total number of conductors in the line. The complex matrix  $K_1(f_0)$  of dimension  $(M \times (N \cdot M))$  is the matrix of linearized coefficients, with its entries as derived in Appendix J. For simplicity, the term  $f_k$  is dropped in equations to follow. Using equations (5.4b) and (5.5c), a linearized relationship relating increments of  $\tilde{Y}(f_k)$  and  $H(f_k)$  to  $\Delta A(f_k)$  can also be obtained as:

$$\Delta \tilde{Y} = K_2 \Delta A \quad (5.13)$$

$$\Delta H = K_3 K_2 \Delta A = K_3 \Delta \tilde{Y} \quad (5.14)$$

where,  $K_2$  and  $K_3$  are matrices with dimensions  $(4M^2 \times M)$  and  $(4M^2 \times 4M^2)$  respectively. The vectors  $\Delta \tilde{Y}$  and  $\Delta H$  are generated by stacking the columns of the incremental matrices  $\tilde{Y}(f_k)$  and  $H(f_k)$  respectively. A linearized relationship can also be derived between the eigenvalue increments  $\Delta \lambda$  of the matrix  $H(f_k)$ , and the matrix  $H(f_k)$  itself as shown in 5.15, (further details can be found in Appendix J)

$$\Delta \lambda = K_4 \Delta H \quad (5.15)$$

Finally by combining equations (5.12), (5.13), (5.14) and (5.15), we get,

$$\Delta \lambda = M_2 \Delta C \quad (5.16)$$

Where,  $\Delta \lambda$  is a vector of dimension  $2M$  and  $M_2$  is a matrix of dimension  $(2M \times N \cdot M)$ . Equation 5.16 depicts the relationship between increments in eigenvalues of Hermitian matrix  $H(f_k)$  to residues of the propagation function for a single frequency  $f_k$ .

Equation (5.16) is now rewritten for  $N$  sample frequency points  $(f_k, k=1 \dots N)$  used in the rational function approximation of  $A(f_k)$ , and stacked into a single equation of the form (5.17).

$$\Delta \Gamma = \tilde{M} \Delta C \quad (5.17)$$

Here,  $\Delta\Gamma$  is a  $(2M \cdot N_s)$  dimensioned vector containing eigenvalue increments  $(\Delta\lambda)$  corresponding to  $N_s$  frequency samples and  $\tilde{M}$  is a  $(2M \cdot N_s \times N \cdot M)$  matrix derived by stacking  $N_s$  values of  $M_2$ .  $N_s$  is the number of frequency samples.

In selecting the  $N_s$  sample frequency points, the density of sampling is chosen to be higher in the neighborhood of the passivity violated regions. Also some frequency samples outside the fitting range are added to make sure that this procedure does not produce new passivity violations in those regions.

For passivity guaranteed formulation, all the eigenvalues of Hermitian matrix  $H(f_0)$  must be positive at all frequencies.

$$\Delta\Gamma + \Gamma > 0 \quad (5.18)$$

Also this perturbation should alter the accuracy of the original fitted function, only minimally over the entire frequency range. For a small maximum tolerance  $\varepsilon$ ,

$$\min \|A(j\omega)^{fitted} - A(j\omega)^{actual}\| < \varepsilon, \omega > 0 \quad (5.19)$$

Equations (5.18) and (5.19) represent a linear constrained least square problem and can be solved using standard techniques [47]. Since the relationship between the eigenvalues of  $H(f_0)$  and the residues  $(c_{n_i} 's)$  of the propagation matrix is non-linear, some iteration may be required.

### 5.6.2 Implementation using perturbation of admittance matrix, $Y_c(s)$

An alternative approach to perturbing the propagation matrix, discussed earlier, is to perturb elements of the admittance matrix  $Y_c(s)$ . This results in equations (5.20) and (5.21) below, which are obtained by following a similar procedure used to obtain (5.12) and (5.13) earlier on,

$$\Delta Y_c = \tilde{K}_1 \Delta C \quad (5.20)$$

$$\Delta \tilde{Y} = \tilde{K}_2 \Delta Y_c \quad (5.21)$$

$\tilde{K}_1$  and  $\tilde{K}_2$  are obtained analogously to  $K_1$  and  $K_2$  in the previous sub-section. Analogous to (5.19) the minimizing function now becomes

$$\min \left\| Y_c(j\omega)^{fitted} - Y_c(j\omega)^{actual} \right\| < \varepsilon, \omega > 0 \quad (5.22)$$

### 5.6.3 Comment on the usage of Method 1 (perturbation of $A(s)$ ) and Method 2 (perturbation of $Y_c(s)$ )

Both methods have been successfully tested for several cable examples and found to produce almost identical waveforms as confirmed by the example in the following section. As seen from equation (5.4b),  $\tilde{Y}(s)$  from which  $H(s)$  is derived, is a linear function of  $Y_c(s)$ , but is a complicated non-linear function of  $A(s)$ . Hence the derivation of the coefficient matrix in equation (5.21) in method 2 is significantly easier, compared with (5.13) in method 1. Both methods result in a passive model for a finite length transmission line, as they both ensure that  $H(s)$  has real positive eigenvalues. However, in some emtp-type programs (such as PSCAD/EMTDC), there is a provision to set the line-length as infinite. In this situation, the program uses the same model parameters as the finite length line, but sets receiving-end quantities  $V_m$  and  $I_m$  to zero as there are no reflections from the receiving end. Hence equation (2.8a) reduces  $I_k = Y_c V_k$  and hence requires a passive  $Y_c(s)$ . Method 2 uses perturbation of  $Y_c(s)$  to achieve passivity in the finite length model.

However, there is a small risk that this could potentially make  $Y_C(s)$  non-passive. Hence, when the program allows the possibility for setting the line length to infinity, method 1 is advisable, even though it requires more computational effort.

## 5.7 Simulation example

The time domain simulations involving a multi-conductor cable system (example from reference [17]) shown in figure 5.10 are carried out to verify the validity of the proposed passivity enforcement method. Figure 5.11 shows the eigenvalues of  $H(s)$  for the original formulation. The original formulation is characterized by relatively large negative eigenvalues at low frequencies prohibiting the use of passivity enforcement scheme based on linearization approach. With the Modified Functional Form method and assuming a conductance of  $3 \times 10^{-9}$  siemens/m, the large negative eigenvalues are completely removed (see figure 5.12). However as seen in the solid curve in figure 5.13, which is an enlarged view of the circled region of figure 5.12, one eigenvalue is still slightly negative (with a minimum value  $2 \times 10^{-5}$  at 9 Hz) in the frequency range [7, 11] Hz. Such small negative eigenvalues can be forced into the positive range by the perturbation method. This corrected eigenvalue is plotted as the dotted curve in figure 5.13, clearly showing that the negative eigenvalue plot (solid line) is now moved into the positive region. Note that because the change made is very small, the response at other frequencies is largely unaffected, as demonstrated next, by comparing the resultant time domain waveform with a theoretical response.

A short circuit test is carried out for the same cable system to validate the passivity enforcement scheme. The inner solid conductor of Cable A is energized with a 1V voltage step. All other conductors are connected to ground. With passivity enforcement, the sending-end current is in a close agreement with the inverse Laplace solution as depicted in figure 5.14. However the original formulation results in an unstable simulation (see figure 5.15). Table 5.3 shows CPU time comparison and rms error before and after perturbation for methods 1 and 2.



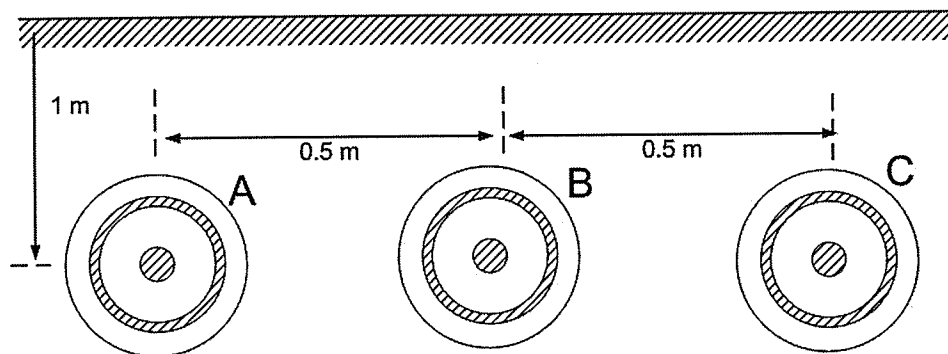


Figure 5.10: Cable System: Three coaxial cable system

Radius of inner solid conductor (m)	0.0127
Dc resistance ( $\Omega/\text{km}$ )	0.034
Outer radius of first insulation (m)	0.0228
Relative permittivity of first insulation	2.85
Outer radius of sheath (m)	0.0254
Relative permittivity of second insulation	0.436
Outer radius of second insulation (m)	0.02795

Table 5.2: Cable data

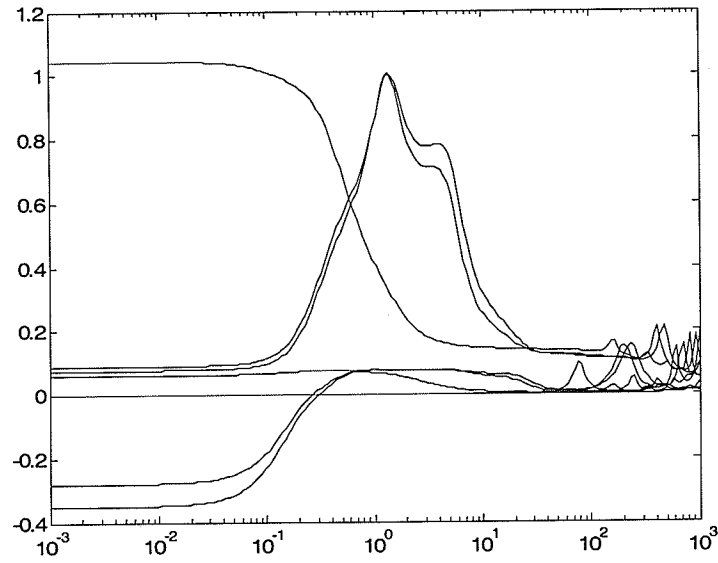


Figure 5.11: Eigenvalues of  $H(s)$  for the original formulation

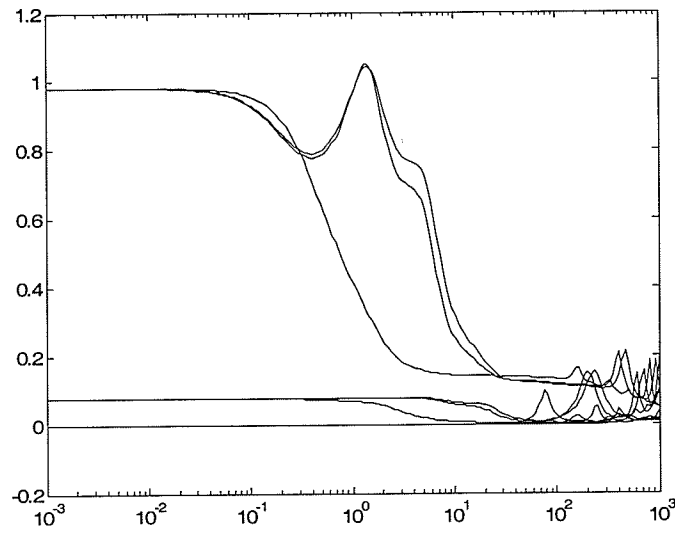


Figure 5.12: Eigenvalues of  $H(s)$  with Modified Functional Form method

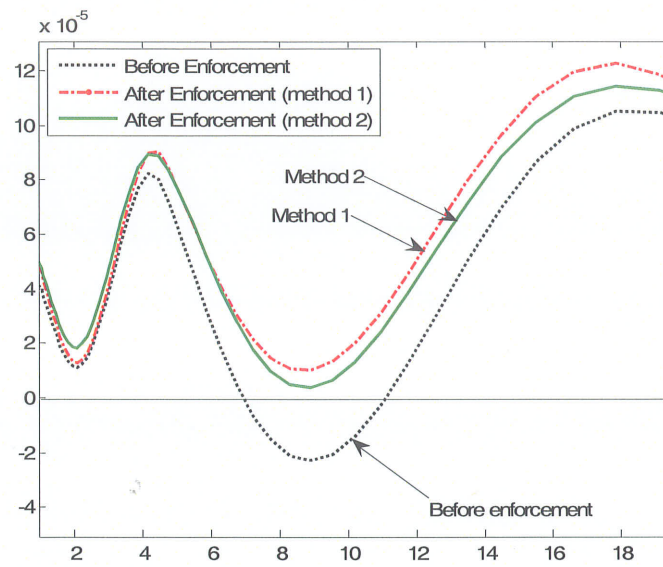


Figure 5.13: Second eigenvalue of  $H(s)$  before and after passivity enforcement

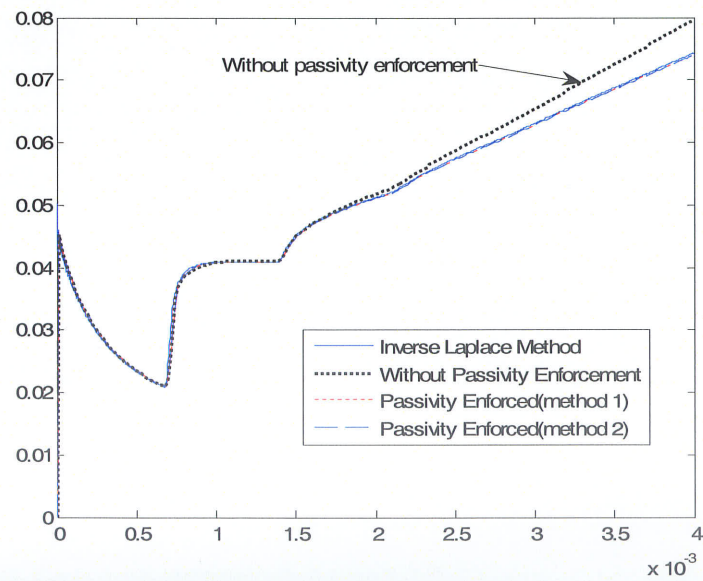


Figure 5.14: Sending-end current under short circuit conditions

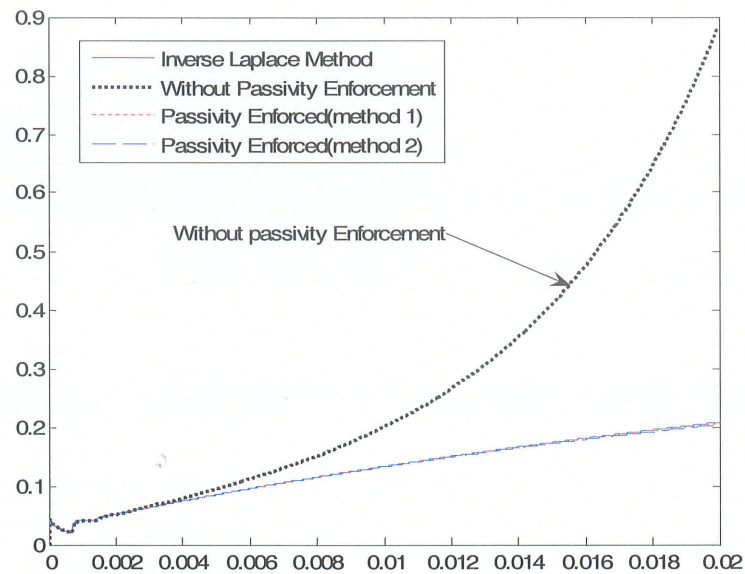


Figure 5.15: Sending-end current under short circuit conditions

	Perturbation of A(s)	Perturbation of Yc(s)
Construct time domain model		13.84 S
Generate matrices for CLS method	15.66 S	10.24 S
Execute CLS algorithm	2.35 S	1.15 S
Rms error before CLS	0.0938	0.0029
Rms error after CLS	0.1019	0.0071

Table 5.3: CPU time comparison and rms error before and after perturbation

## 5.8 Passivity enforcement using state variable approach

It is possible to apply eigenvalue perturbation to the state variable approach described in section 5.3.1. This is done by finding a suitable residue perturbations of characteristic admittance matrix such that the solution to equation (5.8) does not have any pure imaginary values for “s”. This approach is not described any further as the author did not use the state variable approach. For further details, the reader is referred to [65].

## 5.9 Chapter summary

In this chapter, it is demonstrated that time domain simulation methods for modeling transmission lines and cables, which are based on fitted transfer functions for admittance and propagation characteristics, can sometimes result in non-passive formulations. Such formulations have a potential hazard. For some passive terminations, they can lead to unstable simulations.

A new robust passivity enforcement algorithm is proposed to impose passivity on a non-passive transmission line model. The proposed, two-step method can be applied to detailed phase domain models, such as the Universal Line Model [44], which considers the frequency dependency of transformation matrices. This enforcement algorithm first uses a modified functional form method to remove large passivity violations, which are usually present at low frequencies. Then a constrained least squares method is employed to perturb diagonal elements of the propagation matrix (method 1) or characteristic admittance (method 2) eliminating any small passivity violations.

The accuracy of a time-domain simulation program, using either method, has been thoroughly validated by direct comparison with a numerical inverse-Laplace transform, applied to a frequency domain model with linearly terminating networks. An advantage of method 2 (perturbation of characteristic admittance matrix), compared with method 1 (perturbation of propagation matrix) is that the derivation is less complicated. However, for cases where length of the transmission line

model can be set to infinity, method 1 is recommended, as method 2 has a small risk of introducing non-passivity into the perturbed characteristic admittance matrix.

## Chapter 6

### Conclusions and Recommendations

In this Chapter, a summary of the contributions in this thesis is presented and some directions for future work are proposed. In the course of this thesis, several techniques were proposed to improve the accuracy and stability of electromagnetic transient simulations in overhead transmission lines and underground cable systems.

The thesis began by describing the basic theory of single-conductor transmission line modelling and then extended to multi-conductor modelling methods found in literature such as modal domain methods, phase domain methods etc. Modal domain methods employ transformation matrices to decouple transmission line matrices (e.g.  $Y_c(s)$  and  $A(s)$ ) in to modes. Some modal domain models assume constant transformation matrices. This assumption is not valid for highly asymmetrical overhead line configurations and for many underground cable systems leading to significant errors in time domain simulations. Modal domain models based on frequency dependent transformation matrices are numerically less efficient, since these models require additional convolutions involved between modal matrices and transformation matrices. Also there are difficulties in approximating some entries of transformation matrices using rational functions. Phase domain models have been developed to overcome the above problems. The downsides in direct (basic) phase domain modelling are difficulties in approximating rational functions and extracting transportation delays for some entries of phase domain matrices (e.g. phase  $A(s)$ ). Finally the use of frequency domain methods to obtain time domain responses was briefly described (Numerical Inverse Laplace Transform method). This method is traditionally used to validate time domain simulations for transmission line models. Based on the above observations the thesis made the following contributions.

## **6.1 Contributions towards improvements in accuracy and stability of transmission lines**

### **6.1.1 New cable model for accurate simulation of coaxial underground cables**

The third chapter proposed a new cable modelling method called mesh-domain method to simulate time-domain transients in underground cables accurately considering frequency dependent effects. The original phase domain transmission lines equations are converted into mesh equations using suitable transformation matrices. A noticeable advantage of this approach is that the resulting transformation matrix between phase and mesh domains is frequency independent. No additional convolutions are required as for the case of frequency dependent transformation matrices. These convolutions add complexity in TL modelling and the resulting model may be computationally expensive. Another benefit of mesh domain modeling is that mesh currents and voltages in co-axial cables are naturally decoupled at high frequencies hence the propagation function shows relatively smooth behaviour. Hence the rational function approximation and transportation delay estimation are relatively easier than in basic phase domain methods. Finally the mesh domain model was validated by comparing time domain simulation results with numerical inverse Laplace transform method for several cable examples.

### **6.1.2 Improvement in accuracy of TL models at low frequencies**

The fourth chapter introduced several techniques to increase accuracy at very low frequencies for existing TL models. The traditional TL modelling techniques using fitted admittance and propagation characteristics can result in significant errors at frequencies approaching dc. This is a crucial problem in modelling HVDC overhead lines and underground cable systems.

Methods traditionally used to address this problem include reducing the lower bound for fitting range or adding dc resistances to each phase. These approaches were shown to have serious drawbacks. In that they either required a significant increase in the fitting order or caused simulation errors at larger frequencies. Also there was no guarantee of passivity.



Two alternative approaches were introduced in this thesis to obtain accurate dc response by modifying the form of the fitted function. In the first approach, a suitable low frequency pole is added to the existing fitted function. The pole is carefully selected such that the resulting function gives correct dc value (at zero Hertz) and the other high frequency response is changed only insignificantly. In the second approach (Modified Functional Form method), the functional form of the fitted function is reformulated so that the modified function gives theoretical dc values at zero Hertz. The accuracy of time domain simulations are confirmed using numerical inverse Laplace transform over the entire frequency range from dc to higher frequencies. One important benefit of the Modified Functional Form method is that the resulting TL model is more likely to be passive; ensuring stable time domain simulations. The modified functional form method is recommended for the modelling of HVDC transmission systems in which correct reproduction of the very low frequency behavior is just as important as high frequency behavior.

In the early stages of implementing correction algorithms to obtain accurate response at low frequencies, one of the major difficulties encountered was that TL model sometimes gave unstable time domain simulations. This problem was later identified as, a result of non-passive formulation of TL models.

### **6.1.3 Passivity enforcement scheme for multi-conductor transmission line models**

The fifth Chapter demonstrated that the conventional approach to modelling cables and transmission lines in the time domain using fitted admittance and propagation characteristics can result in non-passive TL mode. The non-passive model may lead to unstable time domain simulations depending on the terminal conditions.

The existence of negative eigenvalues of a certain matrix ( $H(s)$  derived from fitted parameters such as  $A(s)$  and  $Y_c(s)$ ) indicates passivity violations of a TL model. A traditionally used method called frequency sweep method was used to identify passivity violations in a TL model. There are few drawbacks related to the frequency sweep method such as possible missing negative eigenvalues between frequency samples and also beyond the maximum frequency used for frequency sweep

method. This problem can be overcome by allocating more frequency samples where eigenvalues approach zero and by selecting a maximum frequency (e.g. 10 MHz) with the hope that negative eigenvalues are not present beyond that frequency. Once the passivity violations of a TL model are identified the next step is to enforce passivity.

A two-step robust passivity enforcement scheme for multi-conductor transmission line was presented to ensure passive TL model. Unlike traditional passivity correction algorithms, the proposed method can be applied to detailed phase domain models, which consider frequency dependency of transformation matrices.

In the first stage of the enforcement algorithm, the Modified Functional Form method with suitable conductance is used. As discussed earlier, this method not only improves accuracy at low frequencies but also removes large passivity violations usually present at these low frequencies. The value of the conductance can be selected by some experimentation; however, for most cable configurations it was observed that the conductance value of  $3 \times 10^{-9}$  S/m eliminates large passivity violations. Then constrained least squares method was employed to perturb diagonal elements of the propagation matrix or characteristic admittance to remove any remaining small passivity violations. As before the resultant model was validated for accuracy by comparing the simulated TD response with the numerical inverse Laplace transform method.

## **6.2 Directions for future research**

### **6.2.1 Identifying exact locations of passivity violations without frequency sampling**

An alternative method based on state variable approach can be used to identify passivity violations for delay free systems. In this method, the exact locations of passivity violations are analytically calculated and hence this technique does not require frequency sampling as for frequency sweep method. An extension of this method to delay based systems such as transmission line models can be found in recent literature work. The above methods can be used to check passivity for more simplified cable models (e.g. modal domain models which uses constant transformation matrices to convert phase to modal quantities), but share the drawback of frequency sweep method such as requirement of frequency sampling. Future research may need to enhance the above passivity identification method to identify exact locations of passivity violations (which is a critical requirement for a successful passivity enforcement scheme as discussed in the next paragraph) for detailed TL models such as ULM without frequency sampling.

### **6.2.2 Passivity enforcement scheme for detailed models based on state variable approach**

The alternative passivity identification method based on state variable approach has been extended recently to enforce passivity for multi-conductor transmission line models. However such methods are limited to modal TL models which use constant transformation matrices to convert phase to modal quantities and also need significant computational effort and frequency sampling as for the frequency sweep method.

Future research work may require to further enhance the above alternative passivity enforcement scheme to ensure global passivity without frequency sampling for detailed cable models such as Universal Line Model (ULM).

## Appendix A

### Modal Domain Equations

This section summarizes the modal domain equations for transmission lines [5], [69]. Consider  $n$ -conductor transmission line having length  $l$ .

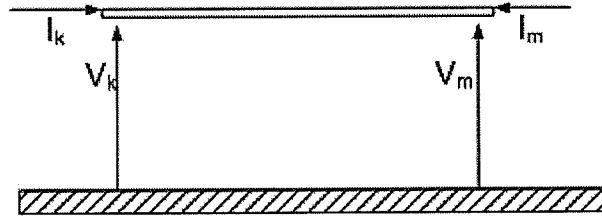


Figure A.1: Voltages and currents at sending-end and receiving-end of a TL

As discussed in Chapter 2, the frequency domain equations for the transmission line are,

$$I_m = Y_c V_m - A(Y_c V_k + I_k) \quad (\text{A.1})$$

$$I_k = Y_c V_k - A(Y_c V_m + I_m) \quad (\text{A.2})$$

Suffixes 'm' and 'k' denote receiving-end and sending-end respectively. The transformation from modal to phase involves transformation matrices [5], [69]. The current ( $E_I$ ) and voltage ( $E_V$ ) transformation matrices are,

$$I_{phase} = E_I I_{modal} \quad (\text{A.3})$$

$$V_{phase} = E_V V_{modal} \quad (A.4)$$

It can be shown that

$$E_I = (E_V^T)^{-1} \quad (A.5)$$

The useful transformations between modal and phase are summarized in the following table.

Modal to phase

Phase to modal

$$I_k = E_I I_k^m$$

$$I_k^m = E_V^T I_k$$

$$I_m = E_I I_m^m$$

$$I_m^m = E_V^T I_m$$

$$V_m = E_V V_m^m$$

$$V_m^m = E_I^T V_m$$

$$V_k = E_V V_k^m$$

$$V_k^m = E_I^T V_k$$

$$A = E_I A^m E_V^T$$

$$A^m = E_V^T A E_I$$

$$Y_c = E_I Y_c^m E_I^T$$

$$Y_c^m = E_V^T Y_c E_V$$

Note that the superscript letter 'm' denotes modal. With above conversions, the transmission line equations (A.1) and (A.2) in modal domain can be written as,

$$I_m^m = Y_c^m V_m^m - A^m (Y_c^m V_k^m + I_k^m) \quad (A.6)$$

$$I_k^m = Y_c^m V_k^m - A^m (Y_c^m V_m^m + I_m^m) \quad (A.7)$$

## Appendix B

### Cable Impedances and Admittances

This purpose of this appendix is to summarize the impedance formulae used in cable parameter calculations. The impedances of underground cables are basically functions of first and second kind modified Bessel functions. Alternatively accurate, robust and numerically efficient approximation formulae developed by Prof. Wedephol [17] are widely used in transmission line parameter calculations.

#### (1) Internal impedance of solid conductor

The skin effect impedance  $Z_{conductor}(\omega)$  of the inner solid conductor is expressed as a division of two first kind modified Bessel functions.

$$Z_{conductor}(\omega) = \frac{m\rho I_0(mr)}{2\pi r I_1(mr)} \quad (B.1)$$

where,

$\rho$  = resistivity of the conductor ( $\Omega\text{m}$ )

$m$  = reciprocal of complex depth of penetration

$$= \sqrt{\frac{j\omega\mu}{\rho}}$$

$\mu$  = permeability of the conductor (H/m)

$r$  = radius of the conductor (m)

In the standard notation,  $I_n(Z)$  represents the first kind modified Bessel function with order “n” and argument “Z”. Similarly, in the text to follow,  $K_n(Z)$  denotes the second kind modified Bessel

function with order “n” and argument “Z”. The approximation formula for conductor internal impedance ( $\Omega/m$ ) is given by [17],

$$Z_{conductor}(\omega) = \frac{\rho m \coth(0.777mr)}{2\pi r} + \frac{0.3565\rho}{\pi r^2} \quad (B.2)$$

(2) Impedance due to the time varying magnetic field in the  $i^{th}$  insulation layer [17],

$$Z_{insulator}(\omega) = \frac{j\omega\mu_i}{2\pi} \log_e \left( \frac{r_{i+1}}{r_i} \right) \quad (B.3)$$

where, for the  $i^{th}$  insulation layer

$\mu_i$  = magnetic permeability (H/m).

$r_i$  = inner radius (m) .

$r_{i+1}$  = outer radius (m).

(3) Inner sheath internal impedance

The surface impedance of the inner sheath is a function of first and second kind modified Bessel functions. It is the impedance related to the voltage difference on the inner surface of the sheath per unit current return through the inner conductor.

$$Z_{inner\_sheath}(\omega) = \frac{\rho m}{2\pi r_i D} \left[ I_0(mr_i) K_1(mr_{i+1}) + K_0(mr_i) I_1(mr_{i+1}) \right] \quad (B.4)$$

where, for the  $i^{\text{th}}$  cylindrical sheath

$$D = I_1(mr_{i+1})K_1(mr_i) - I_1(mr_i)K_1(mr_{i+1})$$

$\rho$  = resistivity of the sheath ( $\Omega \cdot \text{m}$ )

$r_i$  = inner radius (m)

$r_{i+1}$  = outer radius (m)

The approximate formula developed for inner sheath impedance [17] is,

$$Z_{\text{inner\_sheath}}(\omega) = \frac{\rho m}{2\pi r_i} \coth(m\Delta) - \frac{\rho}{2\pi r_i(r_i + r_{i+1})} \quad (\text{B.5})$$

where,  $\Delta = r_{i+1} - r_i$

#### (4) Sheath mutual impedance

This impedance is equal to the voltage drop outer surface of the sheath per unit current returning through the inner conductor or vice versa. The exact Bessel function solution and the approximate formula for the sheath mutual impedance are [17],

$$Z_{\text{sheath\_mutual}}(\omega) = \frac{\rho}{2\pi r_i r_{i+1} D} \quad (\text{B.6})$$

$$Z_{\text{sheath\_mutual}}(\omega) = \frac{\rho m}{\pi(r_i + r_{i+1})} \operatorname{cosech}(m\Delta) \quad (\text{B.7})$$

#### (5) Outer sheath impedance



This is given as the voltage drop along the outer surface of the sheath as the current returns through the outer conductor. The Bessel function solution and the approximate formula are given by,

$$Z_{outer\_sheath}(\omega) = \frac{\rho m}{2\pi r_{i+1} D} [I_0(mr_{i+1})K_1(mr_i) + K_0(mr_{i+1})I_1(mr_i)] \quad (B.8)$$

$$Z_{outer\_sheath}(\omega) = \frac{\rho m}{2\pi r_{i+1}} \coth(m\Delta) + \frac{\rho}{2\pi r_{i+1}(r_i + r_{i+1})} \quad (B.9)$$

(6) The admittance per unit length between two conducting layers,

$$y_i(\omega) = G_i + \frac{2\pi\epsilon_i\omega j}{\log_e\left(\frac{r_{i+1}}{r_i}\right)} \quad (B.10)$$

where, for the  $i^{th}$  insulation layer,

$G_i$  = conductivity (S)

$\epsilon_i$  = permittivity (F/m)

$r_{i+1}$  = outer radius (m)

$r_i$  = inner radius (m)

(7) Mutual earth return impedance

The analytical formulae for self and mutual earth impedances for buried cables were first derived by Pollaczek [25], [2]. The mutual earth return impedance between cables i and k is [27],

$$Z_{earth\_mutual}(\omega) = \frac{\rho m^2}{2\pi} [K_0(md) - K_0(mD) + \int_{-\infty}^{\infty} \frac{\exp(-(y_1 + y_2)\sqrt{\alpha^2 + m^2})}{|\alpha| + \sqrt{\alpha^2 + m^2}} \exp(j\alpha x) d\alpha] \quad (B.11)$$

where,

- $x$  = horizontal distance between cable i and k (m)
- $y_i, y_k$  = buried depths of cable i and k respectively (m)
- $d$  = direct distance between cables i and k (m)  
 $= \sqrt{x^2 + (y_i - y_k)^2}$
- $D$  = distance between cable i and image of cable k (m)  
 $= \sqrt{x^2 + (y_i + y_k)^2}$
- $\rho$  = resistivity of earth ( $\Omega \cdot m$ )
- $\mu$  = permeability of earth ( $H/m$ )
- $m$  = reciprocal of complex depth of penetration  
 $= \sqrt{\frac{j\omega\mu}{\rho}}$

The direct evaluation of formula (B.11) requires computation of Bessel functions using standard methods and the integral term using a numerical technique [42], [58]. A corresponding approximate formula for mutual earth return impedance developed by Wedepohl and Wilcox is [17],

$$Z_{earth\_mutual}(\omega) = \frac{j\omega\mu}{2\pi} \left[ -\log_e \left( \frac{\gamma md}{2} \right) + 0.5 - \frac{2mL}{3} \right] \quad (B.12)$$

where,

$\gamma$  = Euler's constant

$L = y_k + y_i$

$d$  = direct distance between cables  $i$  and  $k$  (m)

Another useful approximate formula developed by Saad, Caba and Ciroax is [35],

$$Z_{earth\_mutual}(\omega) = \frac{\rho m^2}{2\pi} \left[ K_0(md) + \frac{2e^{-(y_i+y_k)m}}{4+m^2x^2} \right] \quad (B.12)$$

where,

$x$  = horizontal distance between cable  $i$  and  $k$  (m)

The self earth return impedance can be easily derived by substituting  $y_k = y_i$  and  $x = r$  (*outer radius of cable*) in the above mutual impedance formulae.

## Appendix C

### Time Delay Calculation

As discussed in Chapter 2, rational function approximation of characteristic admittance and propagation function is an essential step in the time domain (TD) modelling. The propagation function (or entries of matrix A) can not be directly approximated with low order rational functions. Instead, time delay is extracted from the propagation function  $A(\omega)$  before approximation (curve-fitting), so that the rest of the function (after extraction,  $A_{uw}(\omega)$ ) can be fitted with low order rational functions. Hence the accurate delay estimation for entries of A is a critical step in TD modelling.

Physically time delay is the time required for travelling waves to reach the other end of the transmission line. In general, time delay is frequency dependent. But it is required to consider a single delay (or series of modal delays in some cable models) in order to develop a time domain equivalent circuit. In theory, time delay in time domain means phase shift in frequency domain. Phase shift in frequency domain can be written as,

$$A_{uw}(\omega)e^{-j\omega\tau} = A(\omega) \quad (\text{C.1})$$

Equivalent form in time domain,

$$a_{uw}(t - \tau) = a(t) \quad (\text{C.2})$$

In the above equations, lower case letters represent corresponding time domain form of upper case frequency domain functions.

There are several ways to extract delays from the propagation function.

(1) Based on the velocity of light

Time delay ( $\tau$ ) can be evaluated based on velocity of light ( $c = 3 \times 10^8 \text{ m/s}$ ). For a transmission line with length ( $l$ ), the propagation delay (time delay) is simply computed as  $\tau = l/c$ . This method is only successful for simple overhead lines configurations.

For underground cable systems, the travelling waves propagate with different velocities which are significantly different from velocity of light [17]. The propagation delay heavily depends on the values of permittivity and permeability of the insulations, hence significantly deviates from speed of light. In general, this method to calculate time delay (based on the speed of light) is not successful for underground cables.

(2) Based on Bode's Gain Phase relationship

A more accurate approach for time delay can be estimated using Bode's Gain Phase formula. For minimum phase functions, phase angle is uniquely defined by magnitude of the function. From the magnitude data, the phase angle of a minimum phase function can be determined by using the Bode's Gain Phase formula. It is assumed that unwound propagation function  $A_{uw}(\omega)$  is a minimum phase function.

$$A_{uw}(\omega) = A(\omega)e^{j\omega\tau} \quad (\text{C.3})$$

$$\text{let } A(\omega) = e^{a(\omega)+b(\omega)j}$$

then

$$\angle A_{uv}(\omega) = \angle A(\omega) + \angle \omega \tau$$

$$\angle A_{uv}(\omega) = \angle b(\omega) + \angle \omega \tau$$

$$\tau = \frac{\angle A_{uv}(\omega) - \angle b(\omega)}{\omega} \quad (\text{C.4})$$

The Bode's formula is shown in equation (C.5). The equation (C.5) is evaluated at some higher frequency  $\Omega$ , beyond which the magnitude of the function becomes very small [57]. The first term gives a good approximation to the angle of the minimum phase function  $A_{\min}(\omega)$ . If the second term is considered, a more accurate value for the angle can be computed. The integral is numerically evaluated typically taking frequency points limiting the integration from  $0.1\Omega$  to  $10\Omega$  Hz [57].

$$\angle A_{\min}(j\omega) = \frac{\pi}{2} \frac{d(\ln|A(j\omega)|)}{d(\ln(\omega))} \Big|_{\omega=\Omega} + \Delta(u) \quad (\text{C.5})$$

where,

$$\Delta(u) = \frac{1}{\pi} \int_{-\infty}^{\infty} \left\{ \left( \frac{d(\ln|A(j\omega)|)}{d(u)} - \frac{d(\ln|A(j\omega)|)}{d(u)} \right) \right\} \ln(\coth \frac{|u|}{2}) du$$

$$u = \ln \frac{\omega}{\Omega}$$

The propagation delay (time delay) can finally computed as,

$$\tau = \frac{\angle A_{\min} - \angle b}{\Omega} \quad (\text{C.6})$$

where,  $\Omega$  is the highest frequency point of interest.

It is experienced that delay estimation using Bode's formula is successful, if the magnitude response of the function is smooth (no oscillatory behaviour). For example, this method can be used to calculate delay for a modal propagation function, which has a smooth magnitude response, when plotted as a function of frequency. However, as discussed in Chapter 2, for underground cable systems and unsymmetrical overhead transmission lines, the magnitude response for elements of matrix  $A(\omega)$  shows oscillatory behaviour. In such cases, the delay evaluated using Bode's formula is not satisfactory.

From idempotent theory, it is reasonable to assume that entries of  $A(\omega)$  consist of series of modal delays instead of a single delay for multi-conductor systems [69], [44]. This may explain the difficulty in finding a single delay for entries of  $A(\omega)$  for some cable configurations using Bode's formula.

### (3) Optimization method

Alternatively an optimization method is developed to calculate the optimum delay for the propagation function. Contrast to the earlier method, there is no assumption of minimum phase functions and this technique can be applied for entries of  $A(\omega)$  and also for modal  $A(\omega)$ .

In this single dimensioned optimization problem (the only variable is the time delay  $(\tau)$ ), the time delay  $\tau \in [\tau_{\min}, \tau_{\max}]$ , which gives the minimum rms error between the fitted rational function

$A^{fitted}(\omega)$  and the actual function  $A_{uw}(\omega)$  is found.  $A_{uw}(\omega)$  is calculated as in (C.3). The order of the fitted function is kept constant (typical values for the order: 20 or 30). The minimum bound ( $\tau_{\min}$ ) is the delay calculated based on speed of light as discussed in section 2. The upper bound is  $\tau_{\max} = N\tau_{\min}$ , where  $N$  is selected by the user.

A simple approach is to use *golden section search method* to find the optimum delay. However these optimization techniques show several drawbacks such as significant increase in computational effort, possibility of convergence to a local minimum.



## Appendix D

### Rational function approximation using Vector Fitting

The Vector Fitting is a robust technique to approximate a frequency domain function using a rational function [43]. Rational function is a division of two polynomial functions with orders " $n$ " and " $m$ " as in (D.1).

$$f(s) \approx \frac{a_0 + a_1s + a_2s^2 + \dots + a_ns^n}{b_0 + b_1s + b_2s^2 + \dots + b_ms^m} \quad (D.1)$$

where,  $a_i, b_i$  are coefficients for upper and lower polynomials respectively and  $s = j\omega$ . This can be alternatively written as pole residue form as in (D.2).

$$f(s) \approx \sum_{n=1}^N \frac{c_n}{s - a_n} + d + sh \quad (D.2)$$

The frequency domain function to be approximated is  $f(s)$ . The unknowns terms yet to be found are  $a_n, c_n, d$  and  $h$ . This is a non linear problem, since denominator contains unknown poles. The Vector Fitting method solves the problem as a *linear problem* in two stages [43], [40], [41]. Assume the function  $\sigma(s)f(s)$  has the following form.

#### Stage 1

$$\sigma(s)f(s) = \sum_{n=1}^N \frac{c_n}{s - a_n} + d + sh \quad (D.3a)$$

$$\sigma(s) = \sum_{n=1}^N \frac{\bar{c}_n}{s - a_n} + 1 \quad (\text{D.3b})$$

Substituting  $\sigma(s)$  in (D.3b) to (D.3a),

$$\begin{aligned} \left( \sum_{n=1}^N \frac{\bar{c}_n}{s - a_n} + 1 \right) f(s) &= \sum_{n=1}^N \frac{c_n}{s - a_n} + d + sh \\ \sum_{n=1}^N \frac{\bar{c}_n f(s)}{s - a_n} - \sum_{n=1}^N \frac{c_n}{s - a_n} - d - sh &= -f(s) \end{aligned} \quad (\text{D.4})$$

Assume that starting poles  $a_n$ 's are known. Now equation (D.4) becomes an over-determined equation in the form  $Ax = B$ . where, "x" is the solution vector containing unknowns and,

$$\begin{aligned} A(s_0, :) &= \left[ \frac{f(s)}{s_0 - a_1} \dots \frac{f(s)}{s_0 - a_n} \quad \frac{-1}{s_0 - a_1} \dots \frac{-1}{s_0 - a_n} \quad -1 \quad -s_0 \right] \\ B(s_0, :) &= -f(s_0) \\ x &= \left[ \bar{c}_1, \bar{c}_n \quad c_1, c_n \quad d \quad h \right] \end{aligned}$$

For  $N_f$  frequency samples, the matrix  $A$  has a dimension  $(N_f \times (2N + 2))$  and  $B$  is a vector with dimension  $N_f$ .

### Stage 2

Once the unknown vector "x" is calculated, the next step is to compute the new set of poles ( $\bar{a}_n$ 's) for  $f(s)$  by calculating zeros of  $\sigma(s)$ . This can be done by evaluating eigenvalues of  $(A - bc^T)$  [40], [41].

where,

$A$  = diagonal matrix whose diagonal elements are starting poles

$b$  = column vector of ones

$c$  = column vector containing residues of  $\sigma^{fit}(s)$

The next step is to calculate the residues  $(\bar{c}_n \text{ in } D.5)$  for  $f(s)$ , using the new poles of  $f(s)$ . This can be also formulated as a least square problem in the form  $Ax = B$ .

$$f(s) = \sum_{n=1}^N \frac{\bar{c}_n}{s - \bar{a}_n} + d + sh \quad (D.5)$$

The unknowns in (D.5) are  $\bar{c}_n, d$  and  $h$ . The matrix  $A$  and the vectors  $B$  &  $x$  are,

$$\begin{aligned} A(s_0, :) &= \begin{bmatrix} \frac{1}{s_0 - \bar{a}_1} & \dots & \frac{1}{s_0 - \bar{a}_n} & 1 & s_0 \end{bmatrix} \\ B(s_0, :) &= f(s_0) \\ x &= \begin{bmatrix} \bar{c}_1 & \dots & \bar{c}_n & d & h \end{bmatrix} \end{aligned} \quad (D.6)$$

Finally, the rational function approximation for the  $f(s)$  is,

$$f(s) \approx \sum_{n=1}^N \frac{\bar{c}_n}{s - \bar{a}_n} + d + sh \quad (D.7)$$

## Appendix E

### Recursive Convolution

One of the typical problems in time domain modelling is to evaluate the time domain convolution. The recursive convolution is a numerically efficient technique used to compute convolutions. In theory, the product of two frequency domain functions ( $P(s)$  &  $Q(s)$ ) becomes convolution in time domain.

$$F(s) = P(s)Q(s) \quad (\text{E.1})$$

$$f(t) = p(t) \times q(t) \quad (\text{E.2})$$

Note that, lower case letters represent time domain form of corresponding upper case frequency domain functions and " $\times$ " denotes convolution. Assume one of the frequency domain functions in (E.1) can be written in the pole residue form as in (E.3), so that in time domain, this function can be expressed as a summation of exponentials (see (E.4)).

$$P(s) = \sum_{i=1}^n \frac{c_i e^{-s\tau}}{s - a_i} \quad (\text{E.3})$$

$$p(t) = \sum_{i=1}^n c_i e^{a_i(t-\tau)} \quad (\text{E.4})$$

The convolution can be written in the integral form,

$$f(t) = \int_{\tau}^{\infty} q(t-u)e^{a(u-\tau)} du \quad (E.5)$$

With discrete time domain with time step  $\Delta t$ , above integration can be written as,

$$\begin{aligned} f(t) &= \int_{\tau}^{\tau+\Delta t} q(t-u)e^{a(u-\tau)} du + \int_{\tau+\Delta t}^{\infty} q(t-u)e^{a(u-\tau)} du \\ &= \int_{\tau}^{\tau+\Delta t} q(t-u)e^{a(u-\tau)} du + e^{a(\Delta t)} f(t-\Delta t) \end{aligned} \quad (E.6)$$

Then discrete form of  $f(t)$  is shown in (E.7) in terms of past values of  $f(t)$  and  $q(t)$ , and the present value of  $q(t)$ .

$$f(t) = k_1 q(t-\tau) + k_2 q(t-\Delta t-\tau) + k_3 f(t-\Delta t) \quad (E.7)$$

The constants  $k_1$ ,  $k_2$ ,  $k_3$  in (E.7) are derived based on the assumption that  $q(t)$  has a linear variation between  $t-\tau-\Delta t$  and  $t-\tau$  and the constants are,

$$\begin{aligned} k_1 &= -\frac{c}{a} \left( 1 + \frac{1-e^{a\Delta t}}{a\Delta t} \right) \\ k_2 &= \frac{c}{a} \left( e^{a\Delta t} + \frac{1-e^{a\Delta t}}{a\Delta t} \right) \\ k_3 &= e^{a\Delta t} \end{aligned} \quad (E.9)$$

### Stability of the Recursive Convolution

The BIBO stability of any discrete recursive formula can be predicted using Z transform [29]. As for any transfer function, the poles of the denominator should be within unit circle for stability. Lets assume the delay is approximately an integer multiple of time step (as required for discrete simulations). i.e  $\tau = N\Delta t$  and  $N$  is a integer ( $N > 0$ ). After applying Z transform to (E.7),

$$F(z) = k_1 z^{-N} Q(z) + k_2 z^{-(N+1)} Q(z) + k_3 z^{-1} F(z) \quad (\text{E.10})$$

Then (E.10) becomes,

$$\frac{F(z)}{Q(z)} = \frac{z^{-N} (zk_1 + k_2)}{z - k_3} \quad (\text{E.11})$$

The stability is guaranteed, if  $k_3$  lies inside a unit circle in the complex plane. For recursive convolution,  $k_3 = e^{a\Delta t}$  and for stable poles ( $a < 0$ ),  $k_3 < 1$  and the simulation is stable (BIBO).

## Appendix F

### Numerical Inverse Laplace Transform

This section is based on references [43], [15], [69] and the discussion with L.M. Wedepohl in preparing this section is greatly appreciated. In many engineering applications, one of the common problems is to find the time domain function from a known frequency domain functions and vice versa. A widely used technique is the Fourier transform method. The Fourier integral and inverse Fourier integral are defined as,

$$H(\omega) = \int_{-\infty}^{\infty} h(t) e^{-j\omega t} dt \quad (\text{F.1})$$

$$h(t) = \frac{1}{2\pi} \int_{-\infty}^{\infty} H(\omega) e^{j\omega t} d\omega \quad (\text{F.2})$$

where,  $h(t)$ ,  $H(\omega)$ ,  $\omega = 2\pi f$  are the time domain function, corresponding frequency domain function and the angular frequency respectively. One drawback in (F.1) is that if  $h(t)$  is an unstable function of time and then  $H(\omega)$  does not exist. This difficulty can be avoided by multiplying  $h(t)$  by an exponential function as shown below.

$$h_1(t) = h(t) e^{-ct} \quad (\text{F.3.})$$

The proper selection of constant "c" ensures that always  $h_1(t)$  tends to zero as time tends to infinity, hence (F.1) gives meaningful result. This guarantee that  $h_1(t)$  is a stable function of time even if  $h(t)$  is unstable. Substituting  $h_1(t)$  in (F.2) to (F.1),

$$H_1(\omega) = \int_{-\infty}^{\infty} h(t) e^{-(c+j\omega)t} dt \quad (\text{F.4})$$

The new transform is called the Laplace transform and mathematically it is same as the Fourier transform with complex frequency  $s = c + j\omega$ . The Laplace transform and inverse Laplace transform formulae are,

$$H(s) = \int_0^{\infty} h(t) e^{-st} dt \quad (\text{F.5})$$

$$h(t) = \frac{1}{2\pi j} \int_{c-\infty}^{c+\infty} H(s) e^{st} ds \quad (\text{F.6})$$

It may not be always possible to obtain the analytical solution directly using Laplace transform method. As an example,  $H(s)$  in (F.5) may be calculated in discrete form at given frequency samples. In such cases, numerical methods are used to evaluate the inverse Laplace integration and hence to find  $h(t)$ . Numerical techniques are subjected to two types of errors namely truncation error and step length error.



(a) Truncation error

In discrete sampling, the upper limit for integration in (F.6) is limited to some maximum value  $\omega = \Omega$  instead of infinity. This introduces a significant error and causes oscillations on time domain solution  $h(t)$  (called Gibb's oscillations). The frequency of the oscillations is given by  $f_\sigma = \frac{2\pi}{\Omega}$ .

The Laplace transform is restated below with upper frequency  $\omega = \Omega$  for integration.

$$h_\Omega(t) = \frac{e^{-ct} + \Omega}{2\pi} \int_{-\Omega}^{+\Omega} H(c + j\omega) e^{j\omega t} d\omega \quad (F.7)$$

This undesirable effect can be effectively removed by Lanczos filter. The averaging of (F.7) only for the integral over period  $2\pi f_\sigma$  gives,

$$h_\sigma(t) = \frac{e^{-ct}}{2\pi} \left[ \frac{\Omega}{2\pi} \int_{t-\frac{\pi}{\Omega}}^{t+\frac{\pi}{\Omega}} \left\{ \int_{-\Omega}^{+\Omega} H(c + j\omega) e^{j\omega t'} d\omega \right\} dt' \right] \quad (F.8)$$

$$h_\sigma(t) = \frac{e^{-ct} + \Omega}{2\pi} \int_{-\Omega}^{+\Omega} \sigma H(c + j\omega) e^{j\omega t} d\omega$$

where, the Lanczos filter  $\sigma(\omega)$  defined as

$$\sigma(\omega) = \frac{\sin\left(\frac{\pi\omega}{\Omega}\right)}{\frac{\pi\omega}{\Omega}} \quad (A.1)$$

The convolution between the time domain form of  $\sigma(\omega)$  and  $h(t)$  reveals a non-causal function and hence  $h_\sigma(t)$  becomes non-causal too. This drawback However  $\sigma(\omega)$  in (F.9) is non-causal and modified Lanczos filter  $\sigma'(\omega)$  overcomes this drawback by multiplying  $\sigma(\omega)$  with an exponential term, hence becomes causal.

$$\sigma'(\omega) = \frac{\sin\left(\frac{\pi\omega}{\Omega}\right)}{\frac{\pi\omega}{\Omega}} e^{-\frac{j\omega\pi}{\Omega}} \quad (\text{F.10})$$

(b) Step Length error

In evaluating the integral in (F.6) numerically, the frequency domain function  $H(\omega)$  is sampled at constant finite frequency steps  $\omega_0 = 2\pi f_0$  and then integral is approximated as a finite series. Thus time domain solution  $h(t)$  is valid only between  $[0, T]$  s, and  $T$  is called the *time of validity*  $\left(T = \frac{2\pi}{\omega_0}\right)$ .

The selection of the constant term “c” for complex frequency  $s = c + j\omega$

The effect on sampling can be represented by a function  $G(\omega)$  and now equation (A.6) becomes,

$$h(t) = \frac{e^{ct}}{2\pi} \int_{-\infty}^{+\infty} G(\omega) H(c + j\omega) e^{j\omega t} d\omega \quad (\text{F.11})$$

where,

$$G(\omega) = \sum_{n=-\infty}^{\infty} e^{-jn\omega T} \quad (\text{F.12})$$

$$T = \frac{2\pi}{\omega_0}$$

$$s = c + j\omega$$

To demonstrate the error due to sampling, it is assumed,

$$H(\omega) = \frac{1}{c + j\omega}$$

The corresponding correct time domain function is,  $h(t) = e^{-ct}$ . However, consider the product

$H'(c + j\omega) = G(\omega)H(c + j\omega)$  in (F.11). In time domain,

$$h'(t) = g(t) \times h(t) \quad (\text{F.13})$$

where,

$$g(t) = \sum_{n=1}^{\infty} \delta(t - nT)$$

$$h(t) = e^{-ct}$$

$\times = \text{time domain convolution}$

Then (F.13) now becomes,

$$h'(t) = \frac{e^{-ct}}{1 - e^{-cT}} \quad (\text{F.14})$$

Compared with actual time domain function  $h(t)$  with the function  $h'(t)$  affected by sampling, the error introduced by sampling is  $\frac{1}{1 - e^{-cT}}$ . An increase in the constant "c" reduces Gibbs aliasing errors, but increases the magnitude of the Gibbs oscillations. Prof. L.M. Wedepohl has proposed the following compromised value for "c".

$$c = \frac{\log_e N_f}{T} \quad (\text{F.15})$$

#### The selection of the time step

The time step in time domain ( $t_0$ ) and the frequency domain ( $f_0$ ) are unrelated. However the rise time of the Gibbs oscillations impose a constrain to a minimum useful time step and is

$$\tau = t_{0,\min} = \frac{2\pi}{\Omega} = \frac{1}{f_{\max}} \text{ s.}$$

#### *Example*

To demonstrate the numerical inverse Laplace transform method (NILT), the following frequency domain function is selected. The frequency domain response is shown in figure (F.1).

$$H(s) = \frac{1}{s} \quad (\text{F.16})$$

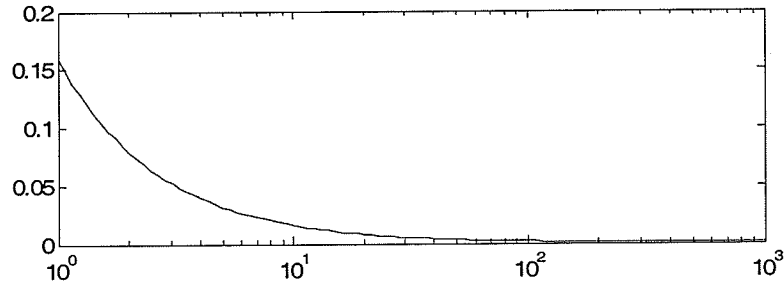


Figure F.1:  $H(s)$  as a function of frequency

The corresponding time domain function  $h'(t)$  is the unit step function (theoretical solution),

$$h'(t) = u(t) \quad (\text{F.17})$$

The numerical evaluation of the integral in (F.6) requires the sampling of the frequency domain function  $H(s)$  at regular frequency steps  $f_0$ . In this example, the frequency step ( $f_0$ ) and the number of samples ( $N_f$ ) are selected as 1 Hz and 1000 respectively. The maximum frequency ( $\Omega$ ) considered for the integration is  $1000 \times 1 = 1 \text{ kHz}$ .

The time of validity ( $T$ ) for the time domain simulation is  $\frac{1}{f_0} = \frac{1}{1} = 1$  s. The compromised value for

the constant term is  $c = \frac{\log_e N_f}{T} = 6.9078$ . Figure F.2 shows the time domain function obtained via

NILT for a period of  $[0, 1]$  s. A noticeable observation is the oscillations in the vicinity of the end of the time period. Figure F.3 displays the expanded plot for the circled section in figure F.2. It can be

readily seen that the period of the oscillations is 0.01 s, which is exactly equal to  $\frac{1}{f_{\max}} = \frac{1}{1000} = 0.01$

s. Earlier discussion reveals that these are Gibb's oscillations with period  $\frac{1}{f_{\max}}$  s. (The time step used

in the simulation is  $\frac{\tau}{10}$  to observe the Gibbs oscillations clearly, since minimum useful time step

( $\tau$ ) is equal to the period of the Gibbs oscillations,)

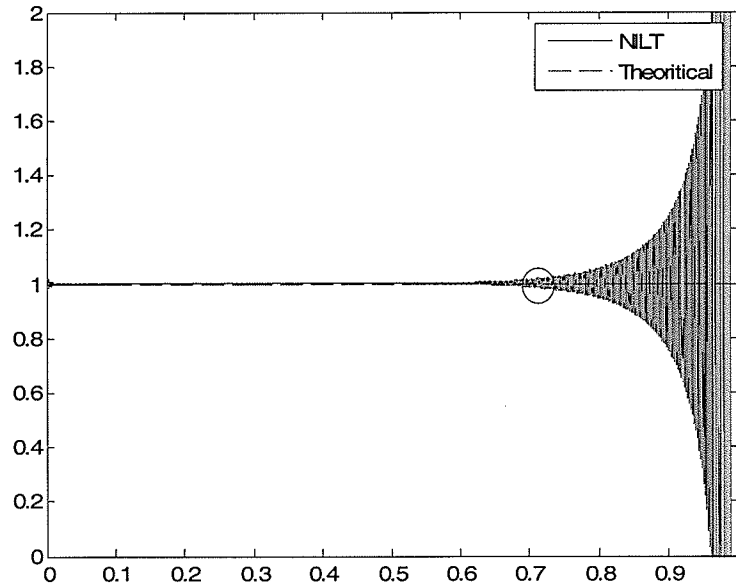


Figure F.2: Plot of time domain function  $h(t)$  for  $[0,1]$  s

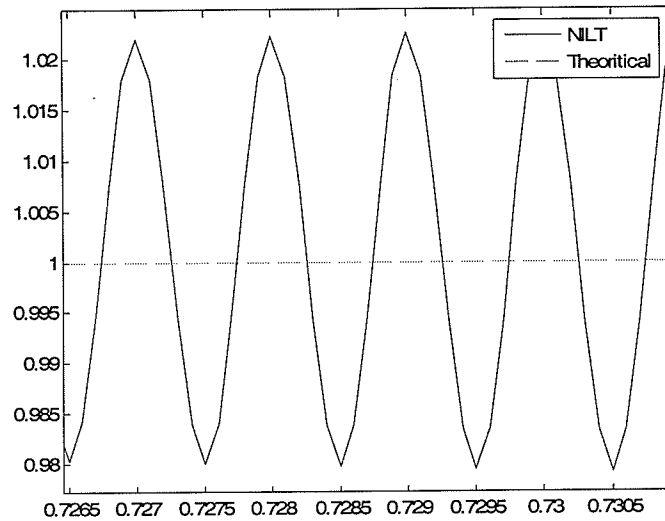


Figure F.3: Expanded section of figure F.2

In order to minimize these undesirable oscillations, the modified Lanczos filter is implemented. Figure F.4 show the time domain simulation with the filter, indicating that the oscillations are significantly reduced. The time domain function is in a close agreement with the theoretical solution.

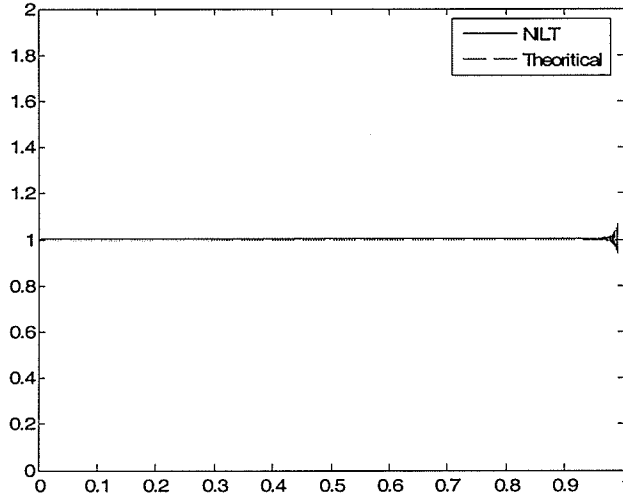


Figure F.4: Plot of time domain function  $h(t)$  with filter

Time domain simulations with different constant terms (“c” in F.15) are carried out to see the effect of “c” on simulation. Figure F.5 displays the expanded section of the tail portion of the time domain simulation (e.g. between [0.9, 1.0] s), where Gibbs oscillations are clearly seen. Note that the constant

term used in the NILT is  $c = \frac{\log_e N_f}{T} = 6.9078$ . With  $c = \frac{\log_e \frac{N_f}{10}}{T} = 4.6052$ , the magnitude of the

Gibbs oscillations are reduced compared with F.5 (see figure F.6). However a noticeable error

between theoretical and simulation result can be observed. With  $c = \frac{\log_e N_f \times 10}{T} = 9.2103$ , the

Gibbs oscillations are magnified as in figure F.7. This confirms that the magnitude of the Gibbs oscillations is amplified with large values of c. However the error due to sampled data decreases with increased values of “c” (as seen from equation F.14). For example, the corresponding aliasing errors are 1%, 0.1%, 0.01% for  $c = 4.6052, 6.9078, 9.2103$  respectively.

Hence this confirms that the value of the constant term  $c = \frac{\log_e N_f}{T} = 6.9078$  gives a compromise between aliasing error and magnitude of Gibbs Oscillations.



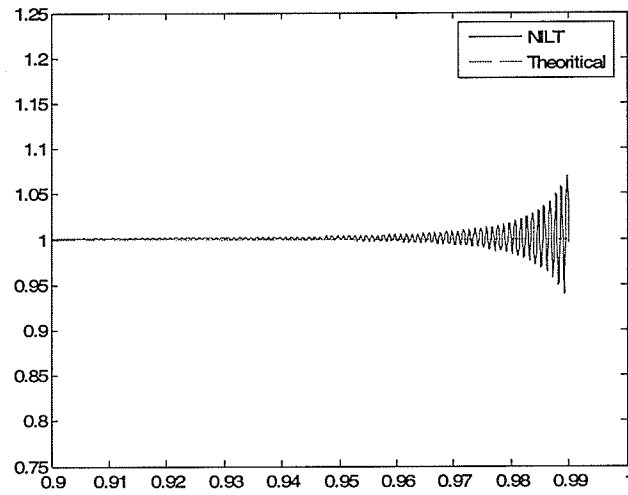


Figure F.5: Plot of time domain function  $h(t)$  with  $c = 6.9078$

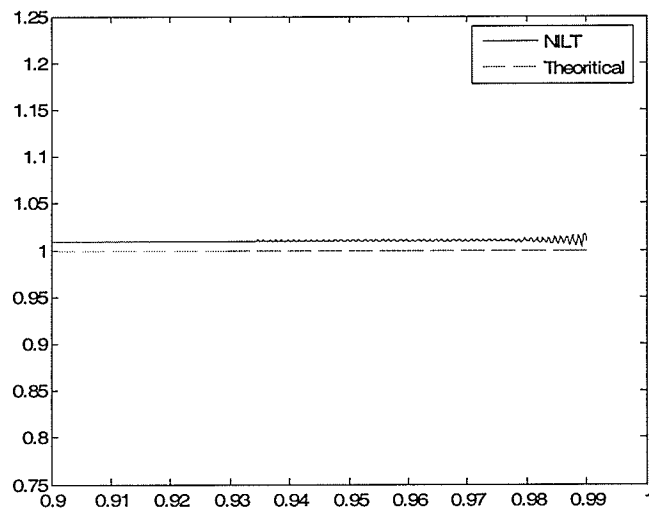


Figure F.6: Plot of time domain function  $h(t)$  with  $c = 4.6052$

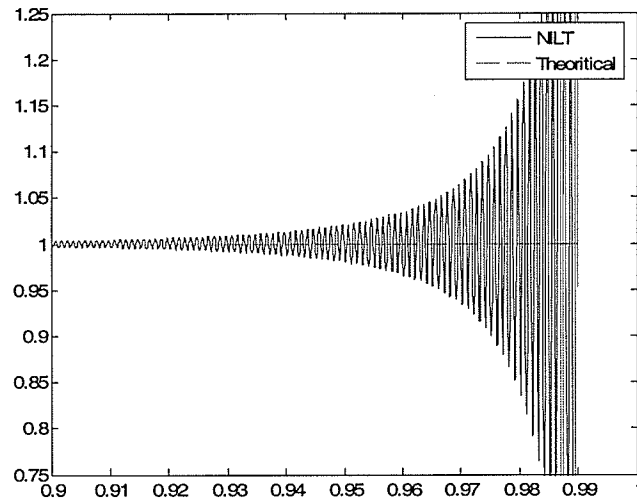


Figure F.7: Plot of time domain function  $h(t)$  with  $c = 9.2103$

## Appendix G

### Constrained Least Squares Method

This appendix describes the constrained least squares method used to eliminate the small error at high frequencies for a two-conductor case. The equation (G.1) shows the actual functional form used for the propagation function. In comparison to (4.9) in Chapter 4, the only difference is the additional constant terms ( $d_i's$ ), that offer better accuracy. In general, for Q distinctive delays there can be Q-1 such additional terms.

$$A_{i,j}^{fun}(s) \approx \sum_{n_1=1}^{N_1} \frac{c_{n_1}'' s e^{-s\tau_1}}{s - a_{n_1}} + \sum_{n_2=1}^{N_2} \frac{c_{n_2}'' s e^{-s\tau_2}}{s - a_{n_2}} + \dots + \sum_{n_Q=1}^{N_Q} \frac{c_{n_Q}'' s e^{-s\tau_Q}}{s - a_{n_Q}} \quad (G.1)$$

$$+ d_{dc,theoretical} e^{-s\tau_1} + d_1 (e^{-s\tau_2} - e^{-s\tau_1}) + d_1 (e^{-s\tau_3} - e^{-s\tau_1}) \dots d_{Q-1} (e^{-s\tau_Q} - e^{-s\tau_1})$$

The unknown coefficients ( $c_n''$ 's and  $d_i's$ ) are calculated first (see Appendix H for details), using Vector Fitting method. The terms  $d_i's$  and  $d_{dc,theoretical}$  are real. Although  $A_{i,j}^{fun}(s)$  gives the exact dc value at  $s = 0$ , at very high frequencies the function may slightly deviate from zero-which is contrary to the physical laws for propagation functions. At very high frequencies (as  $s \rightarrow j\infty$ ) (G.1) becomes,

$$A_{i,j}^{fun}(s = j\infty) \approx e^{-s\tau_1} \sum_{n_1=1}^{N_1} c_{n_1}'' + e^{-s\tau_2} \sum_{n_2=1}^{N_2} c_{n_2}'' + \dots + e^{-s\tau_Q} \sum_{n_Q=1}^{N_Q} c_{n_Q}'' \quad (G.2)$$

$$+ d_{dc,theoretical} e^{-s\tau_1} + d_1 (e^{-s\tau_2} - e^{-s\tau_1}) + d_2 (e^{-s\tau_3} - e^{-s\tau_1}) - d_{Q-1} (e^{-s\tau_Q} - e^{-s\tau_1}) \neq 0$$

This error can be eliminated by perturbing some parameters ( $c_n''$ 's and  $d_i's$ ) of (G.1) without significantly affecting the fitting error. The perturbation of the fitted function in (G.1) is,

$$\begin{aligned}
A_{i,j}^{\text{mod}}(s) \approx & e^{-s\tau_1} \sum_{n_1=1}^{N_1} \frac{(c''_{n_1} + \Delta c''_{n_1})s}{s - a_{n_1}} + e^{-s\tau_2} \sum_{n_2=1}^{N_2} \frac{(c''_{n_2} + \Delta c''_{n_2})s}{s - a_{n_2}} + \dots + e^{-s\tau_Q} \sum_{n_Q=1}^{N_Q} \frac{(c''_{n_Q} + \Delta c''_{n_Q})s}{s - a_{n_Q}} \\
& + d_{dc,theoretical} e^{-s\tau_1} + (d_1 + \Delta d_1)(e^{-s\tau_2} - e^{-s\tau_1}) + (d_2 + \Delta d_2)(e^{-s\tau_3} - e^{-s\tau_2}) + \dots \\
& + (d_{Q-1} + \Delta d_{Q-1})(e^{-s\tau_Q} - e^{-s\tau_{Q-1}})
\end{aligned} \tag{G.3}$$

To fulfill high frequency requirement (i.e.  $A_{i,j}^{\text{mod}}(s = j\infty) \rightarrow 0$ ), the following conditions ((G.4a) ... (G.4c)) should be met.

$$\sum_{n_1=1}^{N_1} (c''_{n_1} + \Delta c''_{n_1}) - \sum_{i=1}^{Q-1} (d_i + \Delta d_i) + d_{dc,theoretical} = 0 \tag{G.4a}$$

$$\sum_{n_2=1}^{N_2} (c''_{n_2} + \Delta c''_{n_2}) + (d_1 + \Delta d_1) = 0 \tag{G.4b}$$

.....

$$\sum_{n_Q=1}^{N_Q} (c''_{n_Q} + \Delta c''_{n_Q}) + (d_{Q-1} + \Delta d_{Q-1}) = 0 \tag{G.4c}$$

In general, for Q-distinctive modes, there are Q numbers of equality constraints. Only real parts of  $c''_{n_i}$ 's are required to perturb and the dc response of the perturbed function remains undisturbed ( $= d_{dc,theoretical}$ ). The unknown coefficients ( $\Delta c''_n$ 's and  $\Delta d_i$ 's) in equation (G.3) are calculated by solving the Equality Constrained Least Square problem. The fitting error in (G.3) is minimized subjected to the equality constraints ((G.4a)... (G.4c)) to eliminate the high frequency error.

Minimize the least square error,

$$\left\| A_{i,j}^{actual}(s) - \left( A_{i,j}^{mod}(s) \right) \right\|^2 \quad (G.5)$$

Subjected to the equality constraints ((G.4a).....(G.4c)). Matlab function (lsqlin) is used to solve the constraint least square problem. The detail matrix formulation is described next for an entry of the propagation matrix  $A_{i,j}(s)$ .

In matrix form, the problem is formulated as minimize the least square error  $\left\| \tilde{A}x - \tilde{B} \right\|$  subjected to the equality constrain  $\tilde{C}x - \tilde{D} = 0$ . The first row of the matrix  $\tilde{A}$  is,

$$\tilde{A}(s_1,:) = \begin{bmatrix} \frac{s_1 e^{-s_1 \tau_1}}{s_1 - a_1} & \frac{s_1 e^{-s_1 \tau_1}}{s_1 - a_2} & \dots & \frac{s_1 e^{-s_1 \tau_Q}}{s_1 - a_N} & (e^{-s_1 \tau_2} - e^{-s_1 \tau_1}) & (e^{-s_1 \tau_3} - e^{-s_1 \tau_1}) & \dots & (e^{-s_1 \tau_Q} - e^{-s_1 \tau_1}) \end{bmatrix} \quad (G.6)$$

Similar expressions can be written for other frequency samples. For  $N_f$  number of frequency samples, matrix  $\tilde{A}$  has a dimension  $(N_f \times (N + Q - 1))$ .  $N$  is the total number of poles (or residues) in the transfer function  $N = \sum_{i=1}^Q N_i$ .  $\tilde{B}$  is a  $N_f$  dimensioned vector. The first element is,

$$\tilde{B}(s_1) = \left[ A_{i,j}(s_1)^{actual} - A_{i,j}(s_1)^{fun} \right] \quad (G.7)$$

The real matrix  $\tilde{C}$  has a dimension  $(Q \times (N + Q - 1))$ .

$$\tilde{C} = \begin{bmatrix} V_{1,1} & V_{1,2} & \dots & V_{1,Q} & V_{1,Q+1} \\ V_{2,1} & V_{2,2} & \dots & V_{2,Q} & V_{2,Q+1} \\ \vdots & \vdots & \dots & \vdots & \vdots \\ V_{Q,1} & V_{Q,2} & \dots & V_{Q,Q} & V_{Q,Q+1} \end{bmatrix} \quad (\text{G.8})$$

$V_{i,j}$  denotes  $N_j$  dimensioned vectors. ( $N_j$  is the order of the  $j^{\text{th}}$  mode).

$$V_{i,i} = [1 \quad 1 \quad \dots \quad 1] \quad (\text{G.9})$$

$$V_{i,j} = [0 \quad 0 \quad \dots \quad 0] \quad (i=1, Q \quad j=1, Q \quad i \neq j)$$

$$V_{1,Q+1} = [-1 \quad -1 \quad \dots \quad -1]$$

$$V_{2,Q+1} = [1 \quad 0 \quad \dots \quad 0]$$

$$V_{3,Q+1} = [1 \quad 1 \quad \dots \quad 0]$$

.....

$$V_{Q,Q+1} = [0 \quad 0 \quad \dots \quad 1]$$

The  $Q$  dimensioned vector  $\tilde{D}$  has the form,

$$\tilde{D} = \begin{bmatrix} -\sum_{n_1=1}^{N_1} c''_{n_1} + \sum_{i=1}^{Q-1} d_i - d_{dc,theoretical} \\ -\sum_{n_2=1}^{N_2} c''_{n_2} - d_1 \\ \vdots \\ -\sum_{n_Q=1}^{N_Q} c''_{n_Q} - d_{Q-1} \end{bmatrix} \quad (\text{G.10})$$

The unknown coefficient vector (solution vector,  $x$ ) contains the increments in residues ( $\Delta c''_i$ 's) and constant terms ( $\Delta d_i$ 's).

$$x = [\Delta c_1'' \quad \Delta c_2'' \quad \dots \quad \Delta c_N'' \quad \Delta d_1 \quad \Delta d_2 \quad \dots \quad \Delta d_{Q-1}] \quad (\text{G.11})$$

The above matrices are generated assuming that poles (and hence residues) are purely real. Care must be taken in dealing with complex conjugate pairs. The number of unknown variables in the  $x$  vector reduces in the presence of complex conjugate pairs. To explain this, consider the following complex conjugate pair,

$$f(s) \approx \frac{(c_1 + c_2 j) s e^{-s\tau_1}}{s - (a_1 + a_2 j)} + \frac{(c_1 - c_2 j) s e^{-s\tau_1}}{s - (a_1 - a_2 j)} \quad (\text{G.12})$$

It is assumed that the first two poles belonging to the first mode are complex. (G.13) shows the corresponding entry of  $\tilde{A}$  matrix and although there are two terms in the function in (G.12), only one entry is constructed. Because, only the real part of the residue is required to perturb the function in order to attain correct high frequency response. (If the poles in (G.12) are real (two distinctive poles), then there are two corresponding entries for  $\tilde{A}(s_1, 1)$ ).

$$\tilde{A}(s_1, 1) = \left[ \frac{s e^{-s\tau_1}}{s - (a_1 + a_2 j)} + \frac{s e^{-s\tau_1}}{s - (a_1 - a_2 j)} \right] \quad (\text{G.13})$$

The first entry of the vector  $x$  is  $\Delta c_1$ . ( $x = [\Delta c_1, \dots, \dots]$ ). In matrix  $\tilde{D}$ , the first element of the  $V_{1,1}$  vector should be 2.

$$V_{1,1} = [2, \dots, \dots] \quad (\text{G.14})$$

## Appendix H

### Modified Functional Form method in ULM

A detailed description of the actual implementation of the modified functional form method is described in this section. As discussed in Chapter 2, the Universal Line Model assumes a common set of poles in approximating rational functions for characteristic admittance  $Y_c(s)$  and propagation  $A(s)$  functions. For example, the trace of the characteristic admittance matrix is first curve-fitted to identify the common set of poles. With this common set of poles, the residues for the entries of matrix are then calculated.

In the Modified Functional Form method, the procedure for the identification of the common set of poles either for  $Y_c(s)$  or  $A(s)$  remains unaltered. Next pace is to calculate residues with this common set of poles. The function should depict the correct zero frequency response (i.e. function value at zero Hertz equals to the exact theoretical value by Modified Functional Form as in (H.1)).

$$Y_{c_{i,j}}^{fun}(s) = \sum_{m=1}^M \frac{c_m s}{s - a_m} + d_{dc,theoretical} \quad (H.1)$$

Since the poles are known, the unknown coefficients in the equation (H.1) are  $c_m$ 's. The error between the fitted function and the actual function is minimized in the least squares sense.

$$\min \left\| Y_{c_{i,j}}(s)^{actual} - Y_{c_{i,j}}(s)^{fitted(fun)} \right\| \quad (H.2)$$



In matrix form, this can be formulated as a linear least square problem as follows.

$$\min \|\tilde{A}x - B\| \quad (\text{H.3})$$

The matrix  $\tilde{A}$  has a dimension  $(N_f \times M)$ , where  $N_f$  is the number of frequency samples. B is a  $N_f$  dimensioned vector. The M-dimensioned vector  $x$  contains the  $c_m$ 's in (H.1).

$$\tilde{A} = \begin{bmatrix} \frac{s_1}{s_1 - a_1} & \frac{s_1}{s_1 - a_2} & \cdot & \frac{s_1}{s_1 - a_M} \\ \frac{s_2}{s_2 - a_1} & \frac{s_2}{s_2 - a_2} & \cdot & \frac{s_2}{s_2 - a_M} \\ \cdot & \cdot & \cdot & \cdot \\ \frac{s_{N_f}}{s_{N_f} - a_1} & \frac{s_{N_f}}{s_{N_f} - a_2} & \cdot & \frac{s_{N_f}}{s_{N_f} - a_M} \end{bmatrix} \quad (\text{H.4})$$

$$B = \begin{bmatrix} Yc_{i,j}(s_1)^{actual} - d_{dc,theoretical} \\ Yc_{i,j}(s_2)^{actual} - d_{dc,theoretical} \\ \cdot \\ Yc_{i,j}(s_{N_f})^{actual} - d_{dc,theoretical} \end{bmatrix} \quad (\text{H.5})$$

$$x = [c_1 \quad c_2 \quad \cdot \quad c_M] \quad (\text{H.6})$$

The actual formula for the propagation function is slightly different from (4.9) in Chapter 4. It has additional constant terms for better degree of freedom.

$$\begin{aligned}
 A_{i,j}^{fun}(s) \approx & \sum_{n_1=1}^{N_1} \frac{c_{n_1} s e^{-s\tau_1}}{s - a_{n_1}} + \sum_{n_2=1}^{N_2} \frac{c_{n_2} s e^{-s\tau_2}}{s - a_{n_2}} + \dots + d_{dc,theoretical} e^{-s\tau_1} \\
 & + d_1 (e^{-s\tau_2} - e^{-s\tau_1}) + d_2 (e^{-s\tau_3} - e^{-s\tau_1}) + \dots \\
 & + d_{Q-1} (e^{-s\tau_Q} - e^{-s\tau_1})
 \end{aligned} \tag{H.6}$$

Where,  $Q$  is the number of different delays terms (delay groups). In general for  $Q$  number of delay groups, there are additional  $Q-1$  numbers of constant terms ( $d_i$ 's). Note that the additional terms do not change the value of the function at zero Hertz. The matrices are,

$$\tilde{A} = \begin{bmatrix} \frac{s_1 e^{-s_1 \tau_1}}{s_1 - a_1} & \frac{s_1 e^{-s_1 \tau_1}}{s_1 - a_2} & \dots & \frac{s_1 e^{-s_1 \tau_Q}}{s_1 - a_N} & (e^{-s_1 \tau_2} - e^{-s_1 \tau_1}) & (e^{-s_1 \tau_3} - e^{-s_1 \tau_1}) & \dots & (e^{-s_1 \tau_Q} - e^{-s_1 \tau_1}) \\ \frac{s_2 e^{-s_2 \tau_1}}{s_2 - a_1} & \frac{s_2 e^{-s_2 \tau_1}}{s_2 - a_2} & \dots & \frac{s_2 e^{-s_2 \tau_Q}}{s_2 - a_N} & (e^{-s_2 \tau_2} - e^{-s_2 \tau_1}) & (e^{-s_2 \tau_3} - e^{-s_2 \tau_1}) & \dots & (e^{-s_2 \tau_Q} - e^{-s_2 \tau_1}) \\ \vdots & \vdots & \ddots & \vdots & \vdots & \vdots & \ddots & \vdots \\ \frac{s_{N_f} e^{-s_{N_f} \tau_1}}{s_{N_f} - a_1} & \frac{s_{N_f} e^{-s_{N_f} \tau_1}}{s_{N_f} - a_2} & \dots & \frac{s_{N_f} e^{-s_{N_f} \tau_Q}}{s_{N_f} - a_N} & (e^{-s_{N_f} \tau_2} - e^{-s_{N_f} \tau_1}) & (e^{-s_{N_f} \tau_3} - e^{-s_{N_f} \tau_1}) & \dots & (e^{-s_{N_f} \tau_Q} - e^{-s_{N_f} \tau_1}) \end{bmatrix} \tag{H.7}$$

$$B = \begin{bmatrix} A_{i,j}(s_1)^{actual} - d_{dc,theoretical} e^{-s_1 \tau_1} \\ A_{i,j}(s_2)^{actual} - d_{dc,theoretical} e^{-s_2 \tau_1} \\ \vdots \\ A_{i,j}(s_{N_f})^{actual} - d_{dc,theoretical} e^{-s_{N_f} \tau_1} \end{bmatrix} \quad (H.8)$$

$$x = [c_1 \quad c_2 \quad \dots \quad c_N \quad d_1 \quad d_2 \quad \dots \quad d_Q] \quad (H.9)$$

Finally, the equations in the Modified Functional Form ( (H.1) and (H.6) ) can be transformed in to a traditional pole residue form, so that recursive convolution technique (as described in Chapter 2) can be readily used to evaluate the time domain convolution. As an example (H.1) can be converted as,

$$Y_{C_{i,j}}^{fun}(s) = \sum_{m=1}^M \frac{\tilde{c}_m}{s - a_m} + \tilde{d} \quad (H.10)$$

where,

$$\begin{aligned} \tilde{c}_m &= a_m c_m \\ \tilde{d} &= \sum_{m=1}^M c_m + d_{dc,theoretical} \end{aligned} \quad (H.11)$$

In a similar approach, (H.6) can be written as,

$$A_{i,j}^{fum}(s) \approx \sum_{n_1=1}^{N_1} \frac{\tilde{c}_{n_1} e^{-s\tau_1}}{s - a_{n_1}} + \sum_{n_2=1}^{N_2} \frac{\tilde{c}_{n_2} e^{-s\tau_2}}{s - a_{n_2}} + \dots + \tilde{d}_1 e^{-s\tau_1} + \tilde{d}_2 e^{-s\tau_2} \dots \tilde{d}_Q e^{-s\tau_Q} \quad (\text{H.12})$$

where,

$$\tilde{c}_{n_1} = c_{n_1} a_{n_1} \quad (\text{H.13})$$

$$\tilde{c}_{n_2} = c_{n_2} a_{n_2}$$

.....

$$\tilde{d}_1 = d_{dc,theoretical} - \sum_{i=1}^Q d_i + \sum_{n_1=1}^{N_1} c_{n_1}$$

$$\tilde{d}_2 = d_2 + \sum_{n_2=1}^{N_2} c_{n_2}$$

....

$$\tilde{d}_Q = d_Q + \sum_{n_Q=1}^{N_Q} c_{n_Q}$$

The equation (H.12) has a minor drawback. It is contrary to the fact that as frequency approaches infinity, the propagation function tends to zero (i.e.  $\tilde{d}_1 = 0, \tilde{d}_2 = 0, \dots, \tilde{d}_Q = 0$ ). This drawback is overcome by an Equality Constrained Least Square Method (ECLS method discussed in Chapter 4).

## Appendix I

### Passivity identification using state variable approach

The State variable approach is an alternative method to identify the passivity violations of a given system. This is a purely algebraic method and contrast to the traditional frequency sweep method, this method identifies the exact locations of passivity violations analytically.

#### *(A) State variable approach to identify exact passivity violations in electrical networks*

##### (A.1) The state variable formulation of transfer functions

As an example, assume that the admittance of a single-port electrical network is given by the following rational function.

$$G(s) = \sum_{k=1}^N \frac{c_k}{s - a_k} + d \quad (I.1)$$

where, the terms  $c_k, a_k, d, N, s$  are  $k^{\text{th}}$  residue,  $k^{\text{th}}$  pole, order of the transfer function, constant term and the complex frequency ( $s = j\omega$ ). The state space form of (I.1) can be written with state variable vector  $x(t)$  as [31],

$$\begin{aligned} \dot{x}(t) &= Ax(t) + Bu(t) \\ y(t) &= Cx(t) + Du(t) \end{aligned} \quad (I.2)$$

where,

$$A = \begin{bmatrix} a_1 & 0 & . & 0 \\ 0 & a_2 & . & 0 \\ 0 & 0 & . & 0 \\ 0 & 0 & . & a_N \end{bmatrix} \quad (I.3)$$

$$B = \begin{bmatrix} 1 & 1 & . & 1 \end{bmatrix}$$

$$C = \begin{bmatrix} c_1 & c_2 & . & c_N \end{bmatrix}$$

$$D = d$$

$$x(t) = \begin{bmatrix} x_1(t) & x_2(t) & . & x_N(t) \end{bmatrix}^T$$

The transfer function of the system is,

$$G(s) = C(sI - A)^{-1} B + D \quad (I.4)$$

#### (A.2) passivity criteria for the admittance G(s)

The next phase is to determine the passivity criteria for  $G(s)$ . It is assumed that the complex poles (and residues) are always in conjugate form and  $G(s)$  does not have poles in the right-half s-plane so that the first two conditions for passivity are met (see (5.5) in Chapter 5 for the definition of passivity). The Vector fitting algorithm ensures that the poles are in the right-half-s-plane. An analytical solution can be found to fulfill the third condition for passivity (all eigenvalues of Hermitian matrix ( = real( $G(s)$ ) ) are positive at every frequency) , which leads to the following theorem, hence states the passivity criteria for (I.4) [61].

#### Theorem 1

The state space system is passive if the following Hamiltonian matrix (M) has no pure imaginary eigenvalues [61].

$$M = \begin{bmatrix} A - B(D + D^T)^{-1}C & -B(D + D^T)^{-1}B^T \\ C^T(D + D^T)^{-1}C & -A^T + C^T(D + D^T)^{-1}B^T \end{bmatrix} \quad (I.5)$$

The presence of imaginary eigenvalues indicates that the system is not passive, the next pace is to identify the exact locations of the passivity violations (the frequencies at which the eigenvalues of Hermitian matrix  $(= \text{real}(G(s)))$  cross the frequency axis,  $f_1$  and  $f_2$  as shown in figure I.1. The following theorem helps to identify those locations [61].

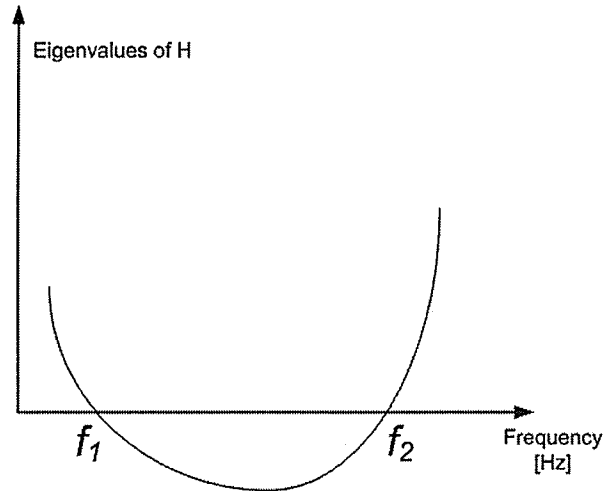


Figure I.1: An eigenvalue of Hermitian matrix (H) crossing frequency axis

### Theorem 2

The real part of the symmetric admittance matrix  $G(j\omega_0)$  is singular, if  $j\omega_0$  is an eigenvalue of the corresponding Hamiltonian matrix  $M$ , provided  $D + D'$  is a positive definite matrix.

The above theorem can be generalized to unsymmetrical admittance matrices. In that case, real part of the symmetric admittance matrix in second theorem is replaced with Hermitian matrix

$([G(j\omega_0) + G(-j\omega_0)]/2)$ . The second theorem states that the imaginary eigenvalues (say  $j2\pi f_1, j2\pi f_2$ ) of M (Hamiltonian matrix) corresponding to the frequency at which eigenvalues of H (Hermitian matrix (= real(G(s))) cross the frequency axis at frequencies  $f_1$  and  $f_2$ . Hence using this method, the exact location of passivity violations can be identified (i.e.  $f_1$  and  $f_2$  in figure I.1).

### (A.3) Example

Let's assume that the admittance of a single-port network is given by,

$$G(s) = \frac{s + k_1}{s + k_2}, s = j2\pi f \text{ and } k_1, k_2 \in \Re \quad (1.6)$$

The first objective is to construct a state space model of the transfer function. The  $G(s)$  can be written in pole residue form,

$$G(s) = \frac{k_1 - k_2}{s + k_2} + 1 \quad (1.7)$$

Let  $Y(s)$  is the response for the arbitrary input  $U(s)$ .

$$G(s) = \frac{Y(s)}{U(s)} = \frac{k_1 - k_2}{s + k_2} + 1 \quad (1.8)$$

The new state variable  $X(s)$  is defined as,



$$X(s) = \frac{U(s)}{s + k_2} \quad (I.9)$$

or

$$sX(s) = -k_2X(s) + U(s)$$

The equation (I.7) can be rearranged with state variable  $X(s)$ ,

$$Y(s) = (k_1 - k_2)X(s) + U(s) \quad (I.10)$$

The time domain equivalents of (I.9) and (I.10) (hence the state space representation) are,

$$\begin{aligned} \dot{x}(t) &= -k_2x(t) + u(t) \\ y(t) &= (k_1 - k_2)x(t) + u(t) \end{aligned} \quad (I.11)$$

In the next step, the passivity of the system (I.11) is investigated as discussed in section (b) by checking the eigenvalues of the Hamiltonian matrix  $H$  defined in (I.5).

$$H = \begin{bmatrix} -k_2 - 0.5(k_1 - k_2) & -0.5 \\ 0.5(k_1 - k_2)^2 & k_2 + 0.5(k_1 - k_2) \end{bmatrix} \quad (I.12)$$

The eigenvalues of  $H$  are calculated by finding the solution of the equation,

$$\lambda^2 - 4k_1k_2 = 0 \quad (I.13)$$

then

$$\lambda = \pm 2\sqrt{k_1k_2}$$

Note that the eigenvalues are purely imaginary and independent of frequency. If both  $k_1$  and  $k_2$  are positive (or both negative) the eigenvalues are real and according to section (b), the electrical network

is passive. If one of  $k_1$  or  $k_2$  are negative and other one is positive then the eigenvalues are imaginary and the electrical network is non-passive.

Case 1

Consider the transfer function,

$$G(s) = \frac{s+2}{s+8} \quad (\text{I.14})$$

The eigenvalues of the H matrix are,

$$\lambda_1 = \pm 4 \quad (\text{I.15})$$

The real eigenvalues indicate a passive system. The real part of the admittance function  $G(j\omega_0)$  in (I.14) remains positive throughout the frequency range as in Figure(I.1). Hence confirm that the electrical system defined in (I.14) is passive.

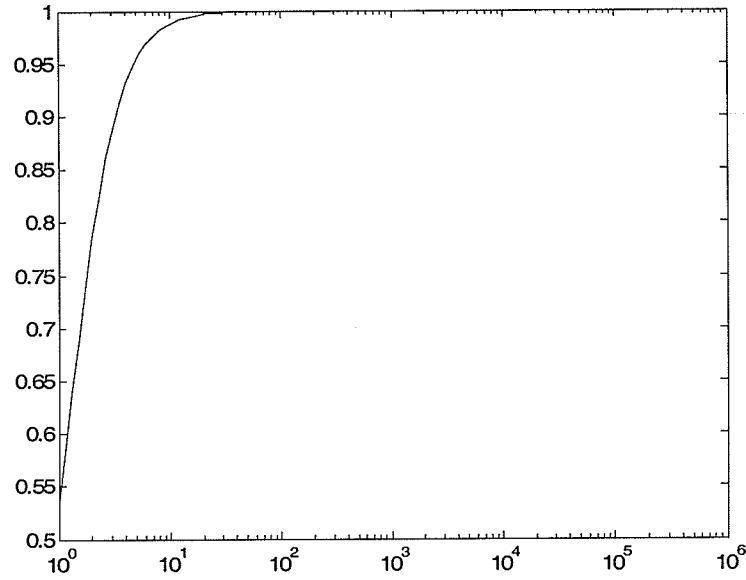


Figure I.1: Real part of the admittance function  $G(j\omega_0)$

### Case 2

Consider the transfer function,

$$G(s) = \frac{s+5}{s-3} \quad (\text{I.16})$$

The eigenvalues of the H matrix are,

$$\lambda_1 = \pm 3.8730j \quad (\text{I.17})$$

The pure imaginary eigenvalues indicate a non-passive system. The next step is to identify the exact locations of passivity violations in the frequency axis. As discussed in section (A.b), the locations where real part of the admittance function crosses the frequency axis are given by,

$$f_0 = \pm \frac{3.8730}{2\pi} = \pm 0.6164 \text{ Hz} \quad (\text{I.18})$$

The real part of the admittance function  $G(j\omega)$  in (I.14) crosses the frequency axis at  $f_0$  Hz as in Figure (I.2) and Figure (I.3) (an enlarged view of circled section of Figure (I.2)). The  $\text{real}(G(j\omega))$  is being negative below  $f < f_0$  and hence confirm that the electrical system defined in (I.16) is non-passive.

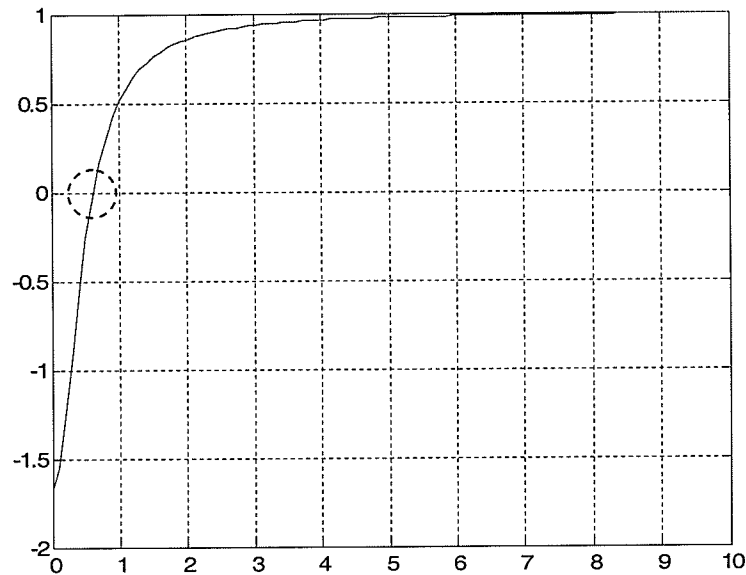


Figure I.2: Real part of the admittance function  $G(j\omega_0)$

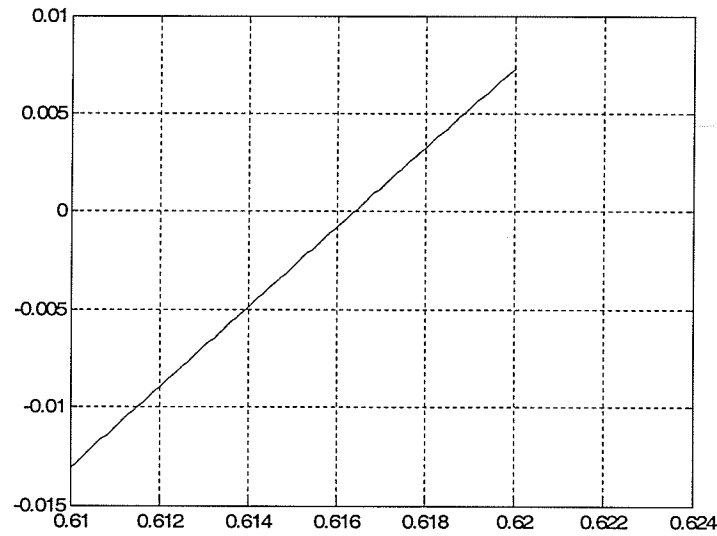


Figure I.3: Real part of the admittance function  $G(j\omega_0)$

### ***(B) State variable approach to identify exact passivity violations in transmission lines***

A similar passivity identification method in section (1) can be used to verify the passivity of the transmission line model treating as an electrical network. However since the transmission line model contains transportation delays, a straightforward application of the above method is not feasible. The identification of exact passivity violations using state variable approach for delay based transmission lines (TL) is an ongoing research topic. Recent advances can be found in [61], [59]. This section briefly explains the approach used in the paper [61] using a simple example, a single conductor transmission line model.

#### **(B.1) Passivity criteria for transmission line models.**

As discussed in detail in Chapter 5 (section 5.2), passivity of a transmission line model is guaranteed, if and only if the eigenvalues of Hermitian matrix  $H(s)$  defined in (I.5) are all positive at any frequency  $\omega$  (with  $s = j\omega$ ). The Hermitian matrix is related to the transfer admittance  $\tilde{Y}(s)$  of a transmission line. The transfer admittance  $\tilde{Y}(s)$ , relating sending and receiving-end voltages to the currents, is shown below in (I.6) in terms of  $A$  and  $Y_c$ .

$$H(s) = \tilde{Y}^T(s^*) + \tilde{Y}(s) \quad (\text{I.5})$$

$$\tilde{Y} = \begin{bmatrix} (I - A^2)^{-1}(I + A^2)Y_c & (I - A^2)^{-1}(-2A)Y_c \\ (I - A^2)^{-1}(-2A)Y_c & (I - A^2)^{-1}(I + A^2)Y_c \end{bmatrix} \quad (\text{I.6})$$

The matrices  $\tilde{Y}(s)$ ,  $A$  and  $Y_c$  are functions of frequency and for simplicity, “s” term is removed in (I.6).

In this method, above passivity a criterion is restated in a simplified form: The passivity of a transmission line is guaranteed, if and only if both  $\left[ Y_1(s) + Y_1(s^*)^T \right]$  and  $\left[ Y_2(s) + Y_2(s^*)^T \right]$  have real positive eigenvalues for any frequency. The functions  $Y_1(s)$  and  $Y_2(s)$  are defined as,

$$Y_1(s) = (1 + A)^{-1}(1 - A)Y_c \quad (\text{I.7})$$

$$Y_2(s) = (1 - A)^{-1}(1 + A)Y_c \quad (\text{I.8})$$

The proof is given below.

Define the matrix  $\Phi(s)$  as,

$$\Phi(s) = \begin{bmatrix} Y_1(s) + Y_1^T(s^*) & 0 \\ 0 & Y_2(s) + Y_2^T(s^*) \end{bmatrix} \quad (\text{I.9})$$

It can be easily shown that the Hermitian matrix  $H(s)$  is related to  $\Phi(s)$  in (I.9) using a constant transformation matrix  $J$ .

$$H(s) = J^{-1}\Phi(s)J \quad (\text{I.10})$$

where,

$$J = \begin{bmatrix} 1 & 1 \\ -1 & 1 \end{bmatrix} \quad (\text{I.11})$$

Therefore, the eigenvalues of  $H(s)$  ( $\lambda\{H(s)\}$ ) in (I.10) are the set of eigenvalues of both  $[Y_1(s) + Y_1^T(s^*)]$  and  $[Y_2(s) + Y_2^T(s^*)]$  matrices as in (I.12).

$$\begin{aligned} \lambda\{\Phi(s)\} &= \lambda\{H(s)\} \\ &= \lambda\{Y_1(s) + Y_1^T(s^*)\} \cup \lambda\{Y_2(s) + Y_2^T(s^*)\} \end{aligned} \quad (\text{I.12})$$

In the traditional approach, the passivity is ensured by checking all positive eigenvalues of Hermitian matrix  $H(s)$  for any frequency. However in this definition, the passivity is guaranteed by checking all positive eigenvalues of simplified matrices  $[Y_1(s) + Y_1^T(s^*)]$  and  $[Y_2(s) + Y_2^T(s^*)]$  for any frequency.

We may now explain the similar method discussed in section (A) to detect passivity violations for transmission line models. In section (A), the network admittance  $G(s)$  is first expressed in state

variable form and the passivity is verified by checking the presence of pure imaginary eigenvalues of Hamiltonian matrix, derived by coefficients of state variable formulation of  $G(s)$ .

Analogously, for the case of transmission line models, two matrices  $Y_1(s)$  and  $Y_2(s)$  are first expressed in state variable form and passivity is verified by checking the presence of pure imaginary generalized eigenvalues of certain matrix derived from coefficients of state variable formulation of  $Y_1(s)$  and  $Y_2(s)$ .

### (B.2) State variable representation of $Y_1(s)$ and $Y_2(s)$

In this section, the state variable representation of  $Y_1(s)$  is described. To ease the derivation, the sub matrices of  $Y_1(s)$ , namely  $\Pi_1(s)$ ,  $\Pi_2(s)$  and  $\Pi_3(s)$  are defined as follows.

$$\Pi_1(s) = (1 + A) \quad (I.13)$$

$$\Pi_2(s) = (1 - A) \quad (I.14)$$

$$\Pi_3(s) = Y_s \quad (I.15)$$

Then the matrix  $Y_1(s)$  is,

$$Y_1(s) = \Pi_1^{-1}(s) \Pi_2(s) \Pi_3(s) \quad (I.16)$$

It is assumed that  $A$  and  $Y_c$  functions are expressed as rational functions with orders  $N$  and  $M$  as stated in (I.17) and (I.18).



$$Y_c(s) = \sum_{k=1}^N \frac{c_k}{s - a_k} + d \quad (\text{I.17})$$

$$A(s) = \sum_{k=1}^M \frac{\bar{c}_k e^{-s\tau}}{s - \bar{a}_k} \quad (\text{I.18})$$

By substituting  $A(s)$  in (I.18) to  $\Pi_1(s)$  in (I.13), function  $\Pi_1(s)$  can be converted in to the state variable form as in (I.19) [31]. The unknown matrices  $(K_1, A_1, B_1, C_1, D_1)$  are derived from the coefficients of  $A(s)$  in (I.18) and  $x_1(t)$  is the state variable vector. The state variable representation for such systems is straightforward and hence not repeated here. The more information can be found in reference [31] .

$$\begin{aligned} K_1 \dot{x}_1(t) &= A_1 x_1(t) + B_1 u_1(t) \\ y_1(t) &= C_1 x_1(t - \tau) + D_1 u_1(t) \end{aligned} \quad (\text{I.19})$$

A similar set of equations can be derived for the function  $\Pi_2(s)$  and has the same form in (I.19). The state variable formulation for  $\Pi_3(s)$  can be constructed after substituting  $Y_c(s)$  in (I.17) to (I.15) as shown in (I.20) with state variable vector  $x_2(t)$ .

$$\begin{aligned} K_2 \dot{x}_2(t) &= A_2 x_2(t) + B_2 u_2(t) \\ y_2(t) &= C_2 x_2(t) + D_2 u_2(t) \end{aligned} \quad (\text{I.20})$$

Then the functions,  $\Pi_1(s)$  can be written as,

$$\Pi_1(s) = C_1 e^{-s\tau} (sK_1 - A_1)^{-1} B_1 + D_1 \quad (\text{I.21})$$

The function  $\Pi_2(s)$  has the same form in (I.21). The function  $\Pi_3(s)$  is,

$$\Pi_3(s) = C_2(sK_2 - A_2)^{-1} B_2 + D_2 \quad (\text{I.22})$$

### (B.3) Derivation of formula to identify passivity violations

Let's assume that the transmission line model has passivity violations. As discussed in section (a), passivity violations are identified as presence of negative eigenvalues in set of eigenvalues of both  $[Y_1(s) + Y_1^T(s^*)]$  and  $[Y_2(s) + Y_2^T(s^*)]$  matrices. The objective is to identify the locations of passivity violations, where eigenvalue crosses the frequency axis (e.g.  $f_1$  and  $f_1$  in Figure I.1, at frequency  $f = f_1$  or  $f = f_2$ , the eigenvalue become zero and hence the corresponding matrix becomes singular). Let's assume that there exists such frequency  $f = f_0$  for the matrix  $[Y_1(s) + Y_1^T(s^*)]$ . Since the matrix is singular, there exists a vector  $\eta$ , which satisfy,

$$[Y_1(s_0) + Y_1^T(s_0^*)]\eta = 0, \quad s_0 = j2\pi f_0 \quad (\text{I.23})$$

If (I.23) is written in terms of  $\Pi_i(s)$ ,

$$[\Pi_1(s_0)^{-1} \Pi_2(s_0) \Pi_3(s_0) + \Pi_3^T(s_0^*) \Pi_2^T(s_0^*) \Pi_1^T(s_0^*)^{-1}]\eta = 0, \quad s_0 = j2\pi f_0 \quad (\text{I.24})$$

By pre-multiplying  $\Pi_1(s_0)$  and substituting  $\varphi(s) = \Pi_1^T(s_0^*)^{-1} \eta$

$$[\Pi_2(s_0) \Pi_3(s_0) \Pi_1^T(s_0^*) + \Pi_1(s_0) \Pi_3^T(s_0^*) \Pi_2^T(s_0^*) \Pi_2^T(s_0^*)^{-1}]\varphi = 0, \quad s_0 = j2\pi f_0 \quad (\text{I.24})$$

Substituting  $\Pi_1(s)$  in (I.21),  $\Pi_3(s)$  in (I.22) and similar expression for  $\Pi_2(s)$  and some mathematical manipulation yields the following form.

$$s_0 \tilde{K}_1 \xi_1 = H_1(s_0) \xi_1 \quad (I.25)$$

Hence, the solution  $(s_0)$  for the equation (I.25) is the frequency in which the eigenvalue of the matrix  $[Y_1(s) + Y_1^T(s^*)]$  crosses the frequency axis. If such a frequency is found that means the eigenvalue becomes negative crossing the frequency axis at  $f_0 = \frac{s_0}{j2\pi}$ .

A similar expression can be derived for the matrix  $[Y_2(s) + Y_2^T(s^*)]$ .

$$s_0 \tilde{K}_2 \xi_2 = H_2(s_0) \xi_2 \quad (I.26)$$

Hence, the transmission line model is passive if and only if there does not exist any purely imaginary values for “s” that satisfy the following set of equations.

$$s \tilde{K}_1 \xi_1 = H_1(s) \xi_1 \quad (I.27)$$

$$s \tilde{K}_2 \xi_2 = H_2(s) \xi_2 \quad (I.28)$$

#### (B.4) Solution to equations (I.27) and (I.28)

The procedure to solve (I.27) is same as for (I.28), hence only the solution method to (I.27) is described below. It can be shown that  $H_1(s)$  is a periodic function of frequency  $s (= j\omega)$  and hence

the solution to (1.27) is periodic (i.e. if  $s = j\omega_0$  is a solution to (1.27) and then  $s = j\omega_0 + j\frac{2n\pi}{\tau}$  is also a solution. where,  $n$  is an integer ( $n = 0, \pm 1, \pm 2, \dots$ )).

The equation (1.27) is solved by sampling in frequency domain and then solving via generalized eigenvalue problem (GEP) as stated in the form in (1.29).  $\sigma(s), \xi_1$  are generalized eigenvalues and eigenvectors. Due to the periodic nature of the solution, GEP is solved for  $N$  number of frequency samples in the frequency range  $s \in \left( j0, j\frac{2\pi}{\tau} \right)$ . In each frequency, the generalized eigenvalues of  $H_1(s)$  are calculated and check the presence of any eigenvalue/values with zero real part (pure imaginary eigenvalues). The pure imaginary eigenvalues (if exist) satisfy the equation (1.27) [59].

$$\sigma(s)\tilde{K}_1\xi_1 = H_1(s)\xi_1 \quad (1.29)$$

In practice, it may not be able to identify exact location of the eigenvalues with zero real part, since finite number of frequency points are considered for computation. The strategy used in [59] is that the eigenvalues with diminishing real values are checked for each frequency between zero and  $\frac{2\pi}{\tau}$ . If

such eigenvalue at frequency  $f'_0 = \frac{2\pi}{\tau n}$  is found for some integer  $n$  then, equation (1.29) is linearized

over  $f'_0$  and using an iterative technique, a close approximation for the frequency  $f_0$  at which eigenvalue becomes purely imaginary is found.

## Appendix J

### Matrix formulation in passivity enforcement

This section describes the derivation of matrices used in the linearization method to eliminate small passivity violations for Chapter 5. First consider the derivation of coefficient matrix  $K_1(f_k)$  (equation (5.12) in Chapter 5), which gives the relationship between increments of some parameters of the fitted propagation matrix to the matrix itself. The functional form of the fitted function for propagation function can be found in (5.10) in Chapter 5. However, in actual implementation, a slightly modified version is used as in (J.1) with additional constant terms ( $d_i$ 's) for better accuracy. Note that at zero Hz,  $A_{i,j}^{fun}(s=0)$  gives theoretical solution ( $d_A^{dc\_theoretical}$ ).

$$\begin{aligned}
 A_{i,j}^{fun}(s) \approx & \sum_{n_1=1}^{N_1} \frac{c_{n_1} s e^{-s\tau_1}}{s - a_{n_1}} + \sum_{n_2=1}^{N_2} \frac{c_{n_2} s e^{-s\tau_2}}{s - a_{n_2}} + \dots + d_A^{dc\_theoretical} e^{-s\tau_1} \\
 & + d_1 (e^{-s\tau_2} - e^{-s\tau_1}) + d_2 (e^{-s\tau_3} - e^{-s\tau_1}) + \dots \\
 & + d_{Q-1} (e^{-s\tau_Q} - e^{-s\tau_1})
 \end{aligned} \tag{J.1}$$

where,  $Q$  is the number of different delays terms (delay groups). In general, for  $Q$  number of delay groups, there are additional  $Q-1$  numbers of constant terms ( $d_i$ 's). Only residues ( $c_{n_i}$ 's) and constant terms ( $d_i$ 's) are slightly changed so that the perturbation does not alter correct dc response ( $d_A^{dc\_theoretical}$ ). The increment in the function is,

$$\begin{aligned}
 \Delta A_{i,j}^{fun}(s) \approx & \sum_{n_1=1}^{N_1} \frac{\Delta c_{n_1} s e^{-s\tau_1}}{s - a_{n_1}} + \sum_{n_2=1}^{N_2} \frac{\Delta c_{n_2} s e^{-s\tau_2}}{s - a_{n_2}} + \dots \\
 & + \Delta d_1 (e^{-s\tau_2} - e^{-s\tau_1}) + \Delta d_2 (e^{-s\tau_3} - e^{-s\tau_1}) + \dots \\
 & + \Delta d_{Q-1} (e^{-s\tau_Q} - e^{-s\tau_1})
 \end{aligned} \tag{J.2}$$

At some frequency point  $s_k (= j2\pi f_k)$ , this can be written in matrix form as,

$$\Delta A_{i,j}(f_k) = \tilde{K}_1(f_k) \Delta C_{i,j} \quad (\text{J.3})$$

The coefficient matrix  $\tilde{K}_1(f_0)$  is,

$$\tilde{K}_1(s_k) = \begin{bmatrix} \frac{s_k e^{-s_k \tau_1}}{s_k - a_1} & \frac{s_k e^{-s_k \tau_1}}{s_k - a_2} & \dots & \frac{s_k e^{-s_k \tau_Q}}{s_k - a_N} & (e^{-s_k \tau_2} - e^{-s_k \tau_1}) & (e^{-s_k \tau_3} - e^{-s_k \tau_1}) & \dots & (e^{-s_k \tau_Q} - e^{-s_k \tau_1}) \end{bmatrix} \quad (\text{J.4})$$

where,  $s_k = j2\pi f_k$ ,  $\Delta C_{i,j} = [\Delta c_1 \quad \Delta c_2 \quad \dots \quad \Delta c_N \quad \Delta d_1 \quad \Delta d_2 \quad \dots \quad \Delta d_{Q-1}]^T$  and  $N = \sum_{i=1}^Q N_i$ . Since only the diagonal elements of propagation matrix are subjected to change, the total increment of the matrix in vector form (i.e. stacking diagonal entries of matrix into a single vector  $\Delta A^v(f_k)$ ) is,

$$\Delta A^v(f_k) = K_1(f_k) \Delta C^v \quad (\text{J.5})$$

where,

$$\Delta A^v(f_k) = [\Delta A_{1,1}(f_k) \quad \Delta A_{2,2}(f_k) \quad \dots \quad \Delta A_{M,M}(f_k)]^T \quad (\text{J.6})$$

$$\Delta C^v = [\Delta C_{1,1} \quad \Delta C_{2,2} \quad \dots \quad \Delta C_{M,M}]^T$$

$$K_1(f_k) = \begin{bmatrix} \tilde{K}_1(f_k) & 0 & 0 & 0 \\ 0 & \tilde{K}_1(f_k) & 0 & 0 \\ 0 & 0 & \dots & 0 \\ 0 & 0 & 0 & \tilde{K}_1(f_k) \end{bmatrix}$$

M is the total number of conductors (i.e. dimension of the square matrix A). The next step is to find a linear relationship between increments in transfer admittance  $\tilde{Y}(f_k)$  to increments in  $\Delta A(f_k)$ . The transfer admittance  $\tilde{Y}(f_0)$  is restated here (equation (5.4b) in Chapter 5).

$$\tilde{Y} = \begin{bmatrix} (I - A^2)^{-1}(I + A^2)Y_c & (I - A^2)^{-1}(-2A)Y_c \\ (I - A^2)^{-1}(-2A)Y_c & (I - A^2)^{-1}(I + A^2)Y_c \end{bmatrix} \quad (\text{J.7})$$

Define sub-matrices for  $\tilde{Y}(f_k)$  as follows,

$$\tilde{Y}_{1,1} = (I - A^2)^{-1}(I + A^2)Y_c \quad (\text{J.8})$$

$$\tilde{Y}_{1,2} = (I - A^2)^{-1}(-2A)Y_c \quad (\text{J.9})$$

The perturbation of (J.8) is,

$$(I - (A + \Delta\tilde{A})^2)(\tilde{Y}_{1,1} + \Delta\tilde{Y}_{1,1}) = (I + (A + \Delta\tilde{A})^2)Y_c \quad (\text{J.10})$$

Note that in matrix form, the expansion of  $(A + \Delta\tilde{A})^2 = A^2 + (\Delta\tilde{A})A + A(\Delta\tilde{A}) + (\Delta\tilde{A})^2$ . Neglecting higher order terms, (J.10) can be written as,

$$\Delta\tilde{Y}_{1,1} = (I - A^2)^{-1} \left\{ (\Delta\tilde{A})AY_c + A(\Delta\tilde{A})Y + (\Delta\tilde{A})A\tilde{Y}_{1,1} + A(\Delta\tilde{A})\tilde{Y}_{1,1} \right\} \quad (\text{J.11})$$

Also (J.11) can be rearranged by staking entries of  $\Delta\tilde{Y}_{1,1}$  and  $\Delta\tilde{A}$  into vectors,

$$\Delta Y_{1,1}^v = G_1 \Delta A^v \quad (\text{J.12})$$

where,  $\Delta Y_{1,1}^v$  is a vector containing the entries of the matrix  $\Delta \tilde{Y}_{1,1}$  (i.e. by stacking the columns of  $\Delta \tilde{Y}_{1,1}$ ).  $\Delta A^v$  is a vector containing the diagonal entries of the matrix  $\Delta \tilde{A}$ .  $G_1$  is a complex matrix. The Kronecker matrix product is a useful tool in deriving (J.12). Same procedure is followed to derive the increments for the other sub-matrix  $(\tilde{Y}_{1,2})$  and finally the following relationship is derived.

$$\Delta \tilde{Y}_v = K_2 \Delta A_v \quad (\text{J.13})$$

where,  $\Delta \tilde{Y}_v$  is a vector (dimension  $(2M)^2$ ) containing increments of the matrix  $\tilde{Y}$  and the  $K_2$  is a complex coefficient matrix.

The third step is to develop a relationship between increments of the Hamiltonian matrix to the increments of the transfer admittance (equation (5.5b) in Chapter 5). The formula is restated as,

$$H = \tilde{Y} + \tilde{Y}^{*T} \quad (\text{J.14})$$

The perturbation of (J.14) gives,

$$\begin{aligned} H + \Delta H &= (\tilde{Y} + \Delta \tilde{Y}) + (\tilde{Y} + \Delta \tilde{Y})^{*T} \\ \Delta H &= \Delta \tilde{Y} + \Delta \tilde{Y}^{*T} \end{aligned} \quad (\text{J.15})$$

It is required to convert (J.15) into a vector form, so that later it can be combined into other equations. To explain the conversion, it is assumed  $\Delta \tilde{Y}$  is a two-dimensioned square matrix as in (J.16).

$$\Delta \tilde{Y} = \begin{bmatrix} y_1^r + y_1^i j & y_3^r + y_3^i j \\ y_2^r + y_2^i j & y_4^r + y_4^i j \end{bmatrix} \quad (\text{J.16})$$



Suffixes  $r$  and  $j$  denote real and imaginary parts. The increment in  $\Delta H$  from (J.15) is,

$$\Delta H = \begin{bmatrix} 2y_1^r & y_3^r + y_2^r + y_3^i j - y_2^i j \\ y_2^r - y_3^r + y_2^i j - y_3^i j & 2y_4^r \end{bmatrix} \quad (\text{J.17})$$

$\Delta H$  and  $\Delta \tilde{Y}$  is then converted into vector form as in (J.18),

$$\Delta H^v = G_2 \Delta \tilde{Y}^v \quad (\text{J.18})$$

where,

$$\begin{aligned} \Delta H^v &= [\Delta H_{1,1}^r \quad \Delta H_{1,1}^i \quad \Delta H_{2,1}^r \quad \Delta H_{2,1}^i \quad \Delta H_{1,2}^r \quad \Delta H_{1,2}^i \quad \Delta H_{2,2}^r \quad \Delta H_{2,2}^i] \\ \Delta \tilde{Y}^v &= [\Delta y_1^r \quad \Delta y_1^i \quad \Delta y_2^r \quad \Delta y_2^i \quad \Delta y_3^r \quad \Delta y_3^i \quad \Delta y_4^r \quad \Delta y_4^i] \\ G_2 &= \begin{bmatrix} 2 & 0 & 0 & 0 & 0 & 0 & 0 & 0 \\ 0 & 0 & 0 & 0 & 0 & 0 & 0 & 0 \\ 0 & 0 & 1 & 0 & 1 & 0 & 0 & 0 \\ 0 & 0 & 0 & 1 & 0 & -1 & 0 & 0 \\ 0 & 0 & 1 & 0 & 1 & 0 & 0 & 0 \\ 0 & 0 & 0 & -1 & 0 & 1 & 0 & 0 \\ 0 & 0 & 0 & 0 & 0 & 0 & 2 & 0 \\ 0 & 0 & 0 & 0 & 0 & 0 & 0 & 0 \end{bmatrix} \end{aligned} \quad (\text{J.19})$$

Similarly, this procedure can be extended for any dimension of  $\tilde{Y}$ . Finally the derivation of equation (5.15) in Chapter 5 is considered. The relationship between the eigenvalue  $\lambda(f_k)$  to corresponding right eigenvalue  $E_R(f_k)$  (column vector) of a matrix  $H(f_k)$  is given by,

$$(H - \lambda I) E_R = 0 \quad (\text{J.20})$$

where,  $I$  is the identity matrix. For simplicity, the term  $f_k$  is dropped in writing (J.20). The perturbation of (J.20) gives,

$$(H - \lambda I)\Delta E_R + (\Delta H - \Delta\lambda I)E_R = 0 \quad (\text{J.21})$$

By pre-multiplying (J.20) with corresponding left (row) eigenvector  $E_R$ , the first term disappears and (J.21) becomes,

$$E_L(\Delta H - \Delta\lambda I)E_R = 0 \quad (\text{J.22})$$

i.e.

$$\Delta\lambda = \frac{E_L \Delta H E_R}{E_L E_R} \quad (\text{J.23})$$

Note that  $E_L E_R$  is a scalar. By considering all eigenvalues of the matrix  $H(f_k)$ , the equation (J.23) can be rearranged as,

$$\Delta\lambda^V = K \Delta H^V \quad (\text{J.24})$$

where,  $\Delta H^V$  and  $\Delta\lambda^V$  are vectors containing columns of  $\Delta H$  and eigenvalues of  $H(f_k)$ .  $K$  is a coefficient matrix.

## References

- [1]. J.R Carson, "Wave propagation in overhead wires with ground return", Bell Syst. Tech, Vol 5, pp. 539-554, 1926.
- [2]. F. Pollaczek, "Sur le champ produit par un conducteur simple infiniment long parcouru par uncourant alternatif", Revue Gén. Elec, vol. 29, pp. 851-867, 1931.
- [3]. S.A Schelkunoff, "The electromagnetic theory of coaxial transmission lines and cylindrical sheaths", The Bell system technical journal, Vol XIII, 1934.
- [4]. L. Weinberg, "Network Analysis and Synthesis", McGraw Hill Book Company, ISBN: 978-0070690370, 1962.
- [5]. L.M Wedepohl, "Application of Matrix Methods to the Solution of Traveling Wave Phenomena in Polyphase Systems", Proc IEE, 110, pp. 2200-2212, 1963.
- [6]. R.H. Galloway, W.B. Shorrock, L.M Wedepohl, "Calculation of electrical parameters for short and long polyphase transmission lines", Proc, IEE, Vol. 111, No. 12, December 1964.
- [7]. D.E. Hedman, "Propagation on Overhead Transmission Lines, I - Theory of Modal Analysis and II - Earth Conduction Effects and Practical Results", Trans IEEE, Power Apparatus and Systems, p200, 1965.
- [8]. L.M. Wedepohl, R.G. Wasley, "Wave propagation in polyphase transmission systems- Resonance effects due to discretely bonded earth wires", Proc. IEE, Vol 112, No 11, November 1965.
- [9]. L.M. Wedepohl, "Electrical characteristics of polyphase transmission systems with special reference to boundary value calculations at power line carrier frequencies", Proc. IEE, Vol. 112, No 11, November 1965.
- [10]. L.M. Wedepohl, R.G. Waseley, "Wave Propagation in Polyphase Transmission Systems - Resonance Effects due to Discretely Bonded Earth Wires," Proc. IEE, Vol. 112, No. 11, pp. 2113-2119, 1965.

- [11]. S. Karni, "Network Theory: Analysis and Synthesis", The Allyn and Bacon Series in Electrical Engineering, ASIN: B0007DOYG6, 1966.
- [12]. L.M. Wedepohl, R.G. Wasley, "Propagation of carrier signals in homogeneous, nonhomogeneous and mixed conductor systems", Proc. IEE, Vol 115, No 1, January 1968.
- [13]. M.Ronald, "Lumped and Distributed Passive networks, A generalized and Advanced Viewpoint", Academic Press, 1969.
- [14]. L.M. Wedepohl, S.E.T. Mohamed, "Multiconductor transmission lines- Theory of natural modes and Fourier integral applied to transient analysis", Proc. IEE, vol. 116, No. 9, September 1969.
- [15]. L.M. Wedepohl, S.E.T. Mohamed, "Transient analysis of multiconductor transmission lines with special reference to nonlinear problems", Proc. IEE, vol. 117, No. 5, May 1970.
- [16]. L.M. Wedepohl, D.J. Wilcox, "Estimation of transient sheath overvoltages in power-cable transmission systems", Proc. IEE, Vol. 120, No 8, August 1973.
- [17]. L.M. Wedepohl, D.J. Wilcox, "Transient Analysis of Underground Power Transmission Systems", Proc. IEE, Vol. 120, No 2, February 1973.
- [18]. L.M. Wedepohl, C.S. Indulkar, "Switching Overvoltages in Long Crossbonded Cable Systems Using the Fourier Transform", IEE Transactions on Power Apparatus and Systems", Vol. PAS-98, No 4 July/August, 1974.
- [19]. L. Weinberg, "Network Analysis and Synthesis", McGraw Hill Book Company, ISBN: 0070690375, 1975.
- [20]. A. Semlyen and A. Dabuleanu, "Fast and Accurate Switching Transient calculations on Transmission Lines With Ground Return Using Recursive Convolutions", IEE Trans. on Power Apparatus and Systems, Vol. PAS-94, pp. 561-571, March/April 1975.
- [21]. A. Ametani, "A highly efficient method for calculating transmission line transients", IEEE transactions on PAS, PAS-95, No 05, Sept/Oct 1976.

- [22]. L.M. Wedepohl, D.J. Wilcox, "Transient pilot-cable induction from underground power-transmission systems", Proc. IEE, Vol. 126, No 12, December 1979.
- [23]. A. Ametani, "A General Formulation of Impedance and Admittance of Cables", IEEE transactions on power delivery, Vol. 99, No. 1, May 1980.
- [24]. A. Semlyen, "Contributions to the Theory of Calculation of Electromagnetic Transients on Transmission Lines with Frequency dependent Parameters", IEEE Trans. on Power Apparatus and Systems, Vol. PAS-100, pp. 848-856, February 1981.
- [25]. A. Deri, G. Tevan, A. Semlyen, and A. Castanheira, "The Complex Ground Return Plane: A Simplified Model for Homogeneous and Multi-Layer Earth Return", IEEE Transactions on Power Apparatus and Systems, Vol. PAS-100, pp. 3686-93, August 1981.
- [26]. J.R Marti, "Accurate modeling of frequency dependent transmission line in electromagnetic transient simulations", IEEE Transactions on Power Apparatus and Systems, Vol 3, PAS - 101, No 01, January 1982.
- [27]. H.W. Dommel, "Electromagnetic Transients Program Reference Manual (EMTP Theory Book)", Prepared for Bonneville Power Administration, Dept. of Electrical Engineering, University of British Columbia, August 1986.
- [28]. Charles L. Lawson, Richard J. Hanson, "Solving least squares problems", Society for Industrial Mathematics; New Ed edition, ISBN 0898713560, January 1987.
- [29]. C.R Paul, "Analysis of Multi-conductor Transmission lines", Wiley Interscience, ISBN 047102080x, 1994.
- [30]. S.S. Sastry, "Introductory Methods of Numerical Analysis", Second Edition, Prentice Hall of India Private Ltd, 1995, ISBN 8120306112, 1995.
- [31]. K. Ogata, "Modern Control Engineering", Prentice Hall, ISBN 0-13-227307-1, 1996.

- [32]. T. Noda, N. Nagaoka, A. Ametani, "Phase Domain Modelling of Frequency Dependent Transmission lines by means of ARMA model", IEEE transactions on power delivery, Vol. 11, No. 1, January 1996.
- [33]. L.M Wedepohl, H.V Nguyen , G.D Irwin, " Frequency Dependent Transformation Matrices for Un-transposed Transmission lines using Newton- Raphson method", IEEE Transactions on Power Systems, Vol 11, No 3, August 1996.
- [34]. A. Bjorck, "Numerical Methods for Least Squares Problems", SIAM: Society for Industrial and Applied Mathematics; 1 edition, ISBN 0898713609, April 1996.
- [35]. O. Saad, G. Gaba, M. Giroux, "A closed-form approximation for ground return impedance of underground cables", IEEE Transactions on Power Delivery, Vol. 11, Issue 3, pp. 1536-1545, July 1996.
- [36]. H.V. Nguyen, H.W. Dommel, J.R. Marti, "Direct Phase Domain Modelling of Frequency Dependent Overhead Transmission lines", IEEE Transactions on Power Delivery, Vol. 12, No 03, July 1997.
- [37]. L. Marti, "Simulation of transients in underground cables with frequency dependent modal transformation matrices", IEEE transactions on Power delivery, Vol. 03, No 03, July 1998.
- [38]. T. Noda, N. Nagaoka, A. Ametani, "Further improvements to a ARMA line model in terms of convolution, steady state initialization and stability", IEEE Transactions on Power Delivery, Vol. 12, No 3, July 1997.
- [39]. B. Gustavsen, A. Semlyen, "Calculation of Transmission Line Transients Using Polar Decomposition", IEEE Transactions on Power Delivery, Vol. 13, No 3, July 1998.
- [40]. B. Gustavsen, A. Semlyen, "Combined Phase and Modal domain calculation of transmission line transients based on Vector fitting", IEEE Transactions on Power Delivery, Vol. 13, No 2, April 1998.

- [41]. B. Gustavsen, A. Semlyen, "Simulation of transmission line transients using Vector fitting and modal decomposition", IEEE trans., Power Delivery, Vol. 13, No 2, April 1998.
- [42]. T.T. Nguyen, "Earth-return path impedance of underground cables. Part 1: Numerical integration of infinite integrals", Proc IEE, Vol. 145, No. 6, pp. 621-626, November 1998.
- [43]. B. Gustavsen and A. Semlyen, "Rational approximation of frequency domain responses by vector fitting", IEEE Trans. Power Delivery, Vol. 14, no. 3, pp. 1052-1061, July 1999.
- [44]. A. Morched, B. Gustavsen, M. Tartibi, "A Universal Model for Accurate Calculation of Electromagnetic Transients on Overhead Lines and Underground cables", IEEE Transactions on Power Delivery, Vol. 14, No 3, July 1999.
- [45]. Y. Wang. S. Liu, "A Review of Methods for Calculation of Frequency-dependent Impedance of Overhead Power Transmission Lines", Proc. Natl. Sci. Coun. ROC(A), Vol. 25, No. 6, pp. 329-338, 2001.
- [46]. T.T. Nguyen, H.Y. Chan, "Evaluation of modal transformation matrices for overhead transmission lines and underground cables by optimization method", Vol 16, Issue 5, pp 694-701, Sept. 2001.
- [47]. B. Gustavsen, "Enforcing Passivity for Admittance Matrices Approximated by Rational Functions", IEEE Transactions on Power Systems, Vol. 16, No 1, February 2001.
- [48]. J.R. Marti, "zCable model for frequency dependent modelling of Cable Transmission systems", International Conference on Power Systems Transients, IPST 2001.
- [49]. T.C. Yu, J.R Marti, "A Robust phase coordinates frequency dependent Underground cable model (z Cable) for the EMTP", IEEE Transactions on Power Delivery, Vol. 18, No 1, January 2003.
- [50]. Uribe.F, "Assessing closed-form approximations for underground cable earth impedances", Power Engineering Society General Meeting, IEEE, Vol 2, pp 654, July 2003

- [51]. D. Saraswat, R. Achar, M. Nakhla, "Enforcing passivity for rational function based macromodels of tabulated data", *Electrical Performance of Electronic Packaging*, pp. 295 – 298. October 2003
- [52]. D. Saraswat, M. Achar and M. Nakhla, "On Passivity Check and Compensation of Macromodels from Tabulated Data", in *Proc. 7th IEEE workshop on Signal Propagation on Interconnects*, pp 25-28, 2003.
- [53]. S. Grivet-Talocia, "The passivity enforcement of linear time-invariant multiport systems in state-space form", *IEEE trans., Circuits and Systems*, Vol. 51, No 9, September 2004.
- [54]. S. Grivet-Talocia, "Passivity Enforcement via perturbation of Hamiltonian Matrices' *IEEE Trans. Circuit Syst.* 1,vol 51, no 9,pp 1755-1769, September 2004.
- [55]. A. B. Fernandes, W. L. A. Neves, E. G. Costa, and M. N. Cavalcanti, "Transmission Line Shunt Conductance From Measurements", *IEEE Transactions on Power Delivery*, Vol. 19, No. 2, April 2004.
- [56]. C.P.Coelho, J. Phillips, L.M. Silveira, "A convex programming approach for generating guaranteed passive approximations to tabulated frequency-data", *Computer-Aided Design of Integrated Circuits and Systems*, *IEEE Trans*, Volume 23, Issue 2, pp 293 – 301, February 2004.
- [57]. B. Gustavsen, "Time delay identification for transmission line modeling", *Signal Propagation on Interconnects*, 2004. *Proceedings. 8th IEEE Workshop*, 9-12 , pp. 103 – 106, May 2004.
- [58]. G. K. Papagiannis, D. A. Tsiamitros, D. P. Labridis, P. S. Dokopoulos, "Direct Numerical Evaluation of the Earth Return Path Impedances of Underground Cables", *IEE Proceedings on Generation, Transmission and Distribution*, Vol. 152, No. 03, pp. 321-328, May 2005.
- [59]. E. Gad, C. Chen, R. Achar, "Passivity Verification in Delay-Based Macromodels of Electrical Interconnects", *IEEE Trans. Circuit and systems*, vol. 52, October 2005.



- [60]. C. Chen , E. Gad, R. Achar, "Passivity Verification in Delay-Based Macromodels of Multi-conductor Electrical Interconnects", IEEE Trans. Circuit and systems, vol. 52, October 2005.
- [61]. D. Saraswat, R. Achar, M. S. Nakhla, "Global Passivity Enforcement Algorithm for Macromodels of Interconnect Subnetworks Characterized by Tabulated Data", IEEE Trans. VLSI Syst., pp. 819-832, 2005.
- [62]. B. Gustavsen, "Computer Code for Passivity Enforcement of Rational Macromodels by Residue Perturbation", IEEE Transactions on Advanced Packaging, Volume 30, Issue 2, pp 209 – 215, May 2007.
- [63]. C. Chen, D. Saraswat, E. Gad, M. Nakhla, R. Achar, M.C.E. Yagoub, "Passivity Enforcement for Method of Characteristics-based Multiconductor Transmission Line Macromodels", Signals, Systems and Electronics, 2007. ISSSE '07. International Symposium, pp. 25 – 28 July 30 2007-August 2 2007.
- [64]. C. Chen, D. Saraswat, E. Gad, M. Nakhla, R. Achar and M. C. E. Yagoub, "Passivity Enforcement for Method of Characteristics-based Macromodels", Proc. International Symposium on Signals, Systems and Electronics (ISSSE), Montreal, Canada, July 2007.
- [65]. A. Chinea, S. Grivet-Talocia, "A Passivity Enforcement Scheme for Delay-Based Transmission Line Macromodels", Microwave and Wireless Components Letters, IEEE Volume 17, Issue 8, pp. 562 – 564, August. 2007.
- [66]. H.M.J. De Silva, A.M. Gole and L.M. Wedepohl, "Accurate Electromagnetic Transient Simulations of HVDC Cables and Overhead Transmission Lines", IPST 2007.
- [67]. B. Gustavsen.; J. Nordstrom, "Pole Identification for the Universal Line Model Based on Trace Fitting", IEEE Transactions on Power Delivery, Volume 23, Issue 1, pp. 472 – 479, Jan. 2008
- [68]. Y. Ting-Chung, "Influences of Frequency-Dependent Shunt Admittances on Underground Cable Systems", IEEE Transactions on Power Delivery, Vol. 23, No. 4, October 2008.

- [69]. L.M Wedepohl, "Transmission Line Theory", Course Notes, Faculty of Electrical and Computer Engineering, University of Manitoba.
- [70]. Webpage Reference, <http://pageperso.aol.fr/binoushousam/index.html>
- [71]. PSCAD/EMTDC Library example, "VSC Transmission with AC Transmission Characteristics".